REPORT

Review of the Seismic Hazard and Risk Protocol for induced seismicity related to gas production from small gas fields in the Netherlands

I. Grigoratos, R. Schultz, J. van Ginkel, T. Gunatilake, S. Wiemer

Swiss Seismological Service, ETH Zürich

commissioned by the Dutch State Supervision of Mines (SodM)

Version 4.2
October 4, 2023

[blank page]

1 Summary

This report has been compiled by researchers of the Swiss Seismological Service (SED) of ETH Zurich as commissioned by the State Supervision of Mines (SodM), who are the supervisor of mining activities in the Netherlands and an advisor to the Dutch ministry of Economic Affairs and Climate Policy (both in regard to the safety of people and the protection of the environment). This is a preparatory study for the development of a new protocol for Seismic Hazard and Risk Assessments (SHRA) of induced seismicity related to the production of small gas fields in the Netherlands. The report is organized as follows: sections 2 to 4 contain a literature review of the state-of-the-art regarding seismic hazard and risk assessment of induced seismicity, section 5 includes a critical review of the current Dutch SHRA protocol, and in section 6 a list of recommendations for a future updated version of the protocol is provided. We benefitted from frequent interaction with the Dutch State Supervision of Mines and an external review panel of three experts during this process.

The literature review of the state-of-the-art of scientific research involved all relevant components of the current Dutch SHRA (and of similar SHRAs adopted in other jurisdictions), with special focus on gas extraction. Both the cited literature in the current guidelines and new relevant publications that have emerged in the past 7 years have been considered for review. The field of induced seismicity has seen prolific writing since 2015 and thus many new methodologies have been introduced. Because of the attention paid to the situation in Groningen, many Dutch-specific models have been published and could now be considered and compared. Any recent publications related to datasets or core methods employed in the existing protocol were also considered for review. To that end, a significant portion of the literature review was devoted to (1) past global case-studies of fluid-extraction induced earthquakes, (2) the estimation of the seismicity rates via geomechanical modeling, (3) suitable ground-motion prediction models (4) updated site-amplification functions for the country, (5) recent relevant fragility and vulnerability functions and (5) modeling frameworks for seismic risk assessment.

The strengths and weaknesses of the new approaches in relation to the current ones are documented and justified in our critical review of the existing protocol. Finally, we identified and outlined detailed suggestions for improving or fully replacing components of the current SHRA protocol. Specific recommendations are made for all the components of the SHRA protocol with justifications from the cited literature. The overall 3-step design of the protocol remains the same. However, we recommend refinement of the procedures followed for Step 1 (DHAIS), and replacement of the procedure followed for Step 2 (SRA). The improvements proposed for Step 1 are methodological, rather than conceptual, while the new version of Step 2 is much more quantitative and in line with the latest regulatory framework. Practical considerations were made to render Step 2 easily enforceable by practitioners without specialized scientific or computational background. Furthermore, we recommend a much more structured layout for the risk management plan submitted by the operators.

Table of Contents

2 Case studies of induced seismicity related to fluid extraction

In this section, we provide a literature review of induced seismicity cases caused by fluid extraction, primarily focusing on operations such as groundwater withdrawal and petroleum production. Lessons learned from historical cases could inform both prevention and mitigation protocols. They may provide clues on the triggering mechanisms, on the maximum expected magnitudes and on the interplay between overlapping human activities. We should acknowledge the bias of published research towards cases where the earthquakes were most impactful; in other words, there are many undocumented areas where fluid extraction did not cause any detectable levels of seismicity. There could also be areas where low-magnitude seismicity was triggered but remained undetected from the existing (sparse) seismic networks. Our search initiated from past literature reviews (including references within) [Suckale, 2009; Wilson et al., 2017; Foulger et al., 2018] and the HiQuake database (https://inducedearthquakes.org/). We expanded our search for recent papers (after 2018) that had either cited these works or included terms such as "production/extraction" and "earthquake/seismicity", via a Google Scholar search. Upon examining each basin/case, we expanded our search in these areas for additional relevant information.

First, it would be good to clarify that the terms "induced" and "triggered" seismicity are often used interchangeably in the literature, despite not being identical. "Induced" seismicity refers to earthquakes that are directly caused by a human activity, remain largely contained within the perturbed rock volume, and release a minority amount of accumulated tectonic strain. On the other hand, "triggered" seismicity refers to ruptures linked to a human activity, which propagated outside the perturbed rock volume, releasing mostly tectonic strain. "Triggered" earthquakes were likely to eventually occur naturally, but were brought forward in time by a human activity. What is more confusing, is that naturally occurring aftershocks are also called "triggered" seismicity. As far as the Netherlands is concerned, the situation is more clear, because the tectonic activity in the country is very low and thus it is reasonable to assume that any magnitudes close to the ones observed so far are "induced".

Our intention here is to focus on extraction and ignore subsurface injection, with the latter being often understood as one of the primary drivers of induced earthquakes. Despite this intention, there are cases with mixed operations – such as secondary recovery in oil production fields, which uses fluid injection to manage reservoir pressures and increase resource productivity. These ambiguities are unavoidable, since the literature has noted examples that were initially reported as solely production related but have since been recognized as having influences from injection/disposal [e.g., Grasso et al., 2021]. Unambiguously distinguishing between the two would require a close statistical examination of the underlying data of each case [Grigoratos et al 2022]. Thus, we ultimately chose to expand our literature review to include secondary recovery cases too (Figure 1). We also note that studies on production induced earthquakes were sparse in the past, as a reflection of the sparse and sporadic monitoring networks in intraplate regions. Thus, the reporting of production induced earthquakes will be incomplete and inconsistent.

Here, we organize the details of our literature review into subsections, starting from the operational cause and then further subdividing into geological basins or geographical locations. Each location is written

in a parallel style that answers pertinent questions such as the targeted formation and field, tectonic regime, baseline seismicity, (induced) earthquake proximity to reservoir/aquifer, temporal relationship/lag, largest magnitude, style of reactivated fault slip, triggering mechanism, strength of evidence, and reported consequences of the events. We exhaustively cite all the literature found, as relevant for each case. While we aim to address all these topics, each case will differ in the amount and depth of preexisting literature – which in some cases significantly restricts the scope of case examinations. Comprehensive reviews of induced seismicity that cover extraction/production cases can be found in prior works [Nicholson & Wesson, 1992; McGarr et al., 2002; Suckale, 2009; Grünthal, 2014; Foulger et al., 2018; Chen et al., 2023].

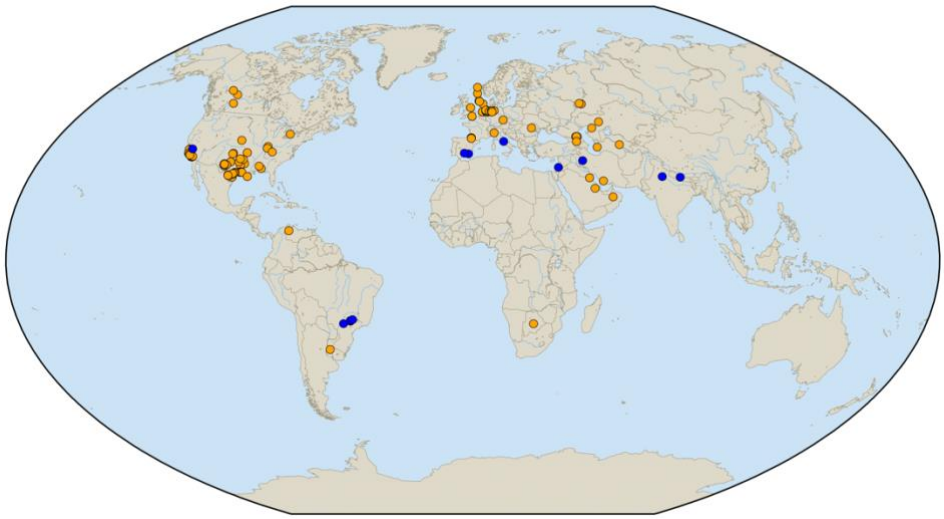

Figure 1. Global locations of case studies. Case studies (circles) are separated by anthropogenic type: either from oil and gas production (orange) or groundwater extraction (blue).

2.1 Oil and gas production (including secondary recovery)

2.1.1 Groningen gas field

The Groningen gas field (~900 km²) was first discovered in 1959 with the drilling of the Slochteren No. 1 well, and production began in 1963 [Stauble & Milius, 1970]; it is the largest gas field in Western Europe and among the largest in the world [Whaley, 2009]. The target reservoir is the Permian aged sandstones of the Upper Rotliegend Group at 2600-3200 m depth (~100-300 m thick) [de Jager & Visser, 2017]. The underlying Carboniferous strata are coal-bearing and is thought to be the main gas source-rock. Over the extent of the entire field, the gas is sealed by the Permian aged Zechstein evaporites overlying the reservoir.

In the Netherlands, seismicity is primarily concentrated within the Roer Valley Graben, which is an active rift [Dost & Haak, 2007]. There, normal faulting and strike-slip events predominate, with the largest documented earthquakes being M_L 5.8. On the other hand, the northeast of the Netherlands is thought to be stable and essentially tectonically aseismic [Muntendam-Bos et al., 2022].

The idea that the northeast Netherlands was aseismic was first challenged in 1986, when a M_L 2.8 earthquake was recorded at the Eleveld gas field near Assen. Following this, a small array was installed in

1988 – recordings there discerned that seismicity in the area was more widespread than originally thought [Dost & Haak, 2007]. Northeastern Dutch earthquakes located in or around existing gas fields were eventually recognized as induced by gas extraction [Gussinklo et al., 2001; Dost & Haak, 2007; Dost et al., 2012; Thienen-Visser & Breunese, 2015; Muntendam-Bos et al., 2022]. The first event associated with the Groningen gas field was M_L 2.4 on 5 December 1991. The largest magnitude earthquake was the 16 August 2012 M_L 3.6 Huizinge event [Dost & Kraaijpoel, 2013]. The Groningen gas field is the most well studied extraction induced seismicity case: events are typically located within the production reservoir [Spetzler & Dost, 2014; Willacy et al., 2019], focal mechanisms are predominantly normal with some strike-slip [Dost et al., 2020], with events concentrated along mappable faults [NAM, 2015]. Significant subsidence (~10s centimeters) has also been noted above the Groningen gas field: partly due to shallower compaction of clay, oxidation of shallow peat, and artificially modified groundwater levels, alongside deeper reservoir compaction from gas depletion [Thienen-Visser & Breunese, 2015]. This reservoir compaction process is thought to drive the Groningen seismicity [NAM, 2015]. Notably, extensive efforts have been placed towards better understanding the hazards and risks from these events via maximum magnitude estimates [e.g. NAM, 2022], local site amplification [e.g. Kruiver et al, 2022], ground motion models [e.g. Bommer et al., 2017], hazard analysis [e.g. Bourne et al., 2015], fragility studies [e.g. Crowley et al., 2017], and risk frameworks [e.g. van Elk et al., 2017]. We note that the literature discussed here is a high-level overview and thus is not comprehensive.

Seismicity at the Groningen gas field is arguably certainly induced, with numerous studies reaching similar conclusions. Most of the current literature is now aimed at understanding or managing the hazards/risks from these earthquakes. Groningen events here have been widely felt and have caused limited structural and extensive non-structural damages; in fact, these induced events have caused significant public outrage that eventually spurred the decision to completely abandon gas extraction [van der Voor & Vanclay, 2015]. Decisions to abandon the field first attempted to reduce production, following the (largest so far) M_L 3.6 Huizinge event [Muntendam-Bos et al., 2022]. Comparatively speaking, Dutch regulations have been more comprehensive than most jurisdictions: including a three-tiered approach that consists of a priori screening protocols, hazard/impact assessment, and a (rather generic) risk management plan [Muntendam-Bos et al., 2015; van Thienen-Visser et al., 2017].

2.1.2 Small gas fields in the Netherlands and Germany

While the Groningen gas field is the largest in Western Europe, there are also other smaller gas fields in the adjacent regions: stretching from England, through the Netherlands, into Poland. The fields in the Netherlands have been developed since the 1960s, following the success at Groningen, while the German fields were developed decades later. Many of the operational fields target the same gas-bearing Rotliegend Group, which is typically deeper in the North German Basin. Other targets have also included the overlying Buntsandstein sandstones, underlying Carboniferous strata, carbonate reservoirs in the Zechstein evaporite layer, and reservoirs in the shallow Vlieland sandstones.

These gas fields are situated in the Central European Basin, which is composed of several sub-basins of defined by ~N-S horst and graben structures [Uta, 2017]. Tectonic seismicity in northeastern Netherlands and the North German Basin is largely quiescent, with some records of historical events in the North German Basin – correspondingly, many of the events exhibit normal or strike-slip motions [Uta, 2017].

The first extraction induced earthquake (M_L 2.8) was recorded in 1986 at the Eleveld gas field near the town of Assen [Dost & Haak, 2007]. Subsequent monitoring noted cases in Hooghalen and Noord-Holland. In the Netherlands, 38 out of 450 gas fields are now associated with induced seismicity, with two having larger events (M_L>3: Bergermeer & Roswinkel) and only four fields recording more than ten events [Muntendam-Bos et al., 2022]. Studies have suggested statistical links to gas fields and seismicity, based on geological and operational factors [van Eijs et al., 2006]. Similarly, seismicity (M_W 4.4, 20 October 2004) has also been noted in the North German Basin, with normal slip that is consistent with depletion induced stress changes and the ambient stress field [Dahm et al., 2007; Gudehus et al., 2023]. Geomechanical studies have been assessing the potential for German gas fields to reactivate fault slip [Haug et al., 2018; Hergert et al., 2022; Gudehus et al., 2023], partly motivated by worries of future Groningen-like scenarios.

The evidence that events are induced varies on a case-by-case basis. Most assessments are made solely based on spatial association (since very few events have been observed), bolstered by the relatively aseismic background and the analogy to the Groningen case. However, unambiguous indentification for some cases in the North German Basin have been hampered by records of historical seismicity [Dahm et al., 2007; Uta, 2017]. Many of the larger events in the Netherlands have noted felt reports and damage, while the German cases have not [Hergert et al., 2022]. Gas fields in the Netherlands are subject to specific seismic regulations, while German gas fields do not have official seismic regulations, although special working groups do insist on independent hazard/risk assessments and monitoring [FKPE, 2022].

2.1.3 Fields throughout the North Sea

The North Sea was one of the most prolific hydrocarbon basins in the world, hosting a variety of oil and gas fields typically within Permian-Cretaceous aged strata [Glennie, 1998]. For example, the Dan field targets a Cretaceous Maastrichtian chalk, structured as a dome split into two blocks; it is the oldest oil field in the North Sea [Ovens et al., 2008]. Production from the North Sea is declining.

The North Sea has a low-intermediate rate of seismicity, where most events are within the passive margins of the Viking and Central grabens [Jerkins et al., 2020; Ottemöller et al., 2005]. Correspondingly, strike slip and normal fault motion dominate the natural seismicity [Hicks et al., 2000]. Much of the purported induced seismicity is within the ongoing background seismicity [Musson, 2007].

Potential cases of induced seismicity in the North Sea have been reported in disparate fields [Wilson et al., 2015]. Notable examples include the Dan [Ovens et al., 1998], Visund [Wiprut & Zoback, 2000], Valhal [Zoback & Zinke, 2002], and Ekofisk [Ottemöller et al., 2005] fields. Typically, events are found to spatially correlate with fields, although temporal correlations are not noted/documented [Wilson et al., 2015]. Depth of events is typically difficult to constrain due to the offshore location; however, cases with

downhole geophones had located microseismic events just above the producing reservoir at Valhall [Zoback & Zinke, 2002]. The largest reported event in the literature was M_W 4.3 on 7 May 2001 at Ekofisk [Ottemöller et al., 2005; Selby et al., 2005; Cesca et al., 2011]. Events are typically noted as normal fault motion [Zoback & Zinke, 2002; Cesca et al., 2011], which is consistent with the background stress field [Hicks et al., 2000]. Many cases have also noted surface subsidence overlying the producing fields [Zoback & Zinke, 2002; Cesca et al., 2011]. Reported triggering mechanisms have been varied, suggesting influences from post glacial rebound and elevated pore pressure from accumulating/trapped hydrocarbons [Wiprut & Zoback, 2000]. Most cases have suggested a pressure decline model [Segall, 1989]. For example, the events in the Ekofisk field are consistent with a pressure decline model, but also had (unintentional) water injection occurring [Ottemöller et al., 2005; Borges et al., 2020].

Much of the potential for induced seismicity in the North Sea is confounded by the ongoing natural seismicity [Wilson et al., 2015; Musson, 2007], although this is likely hampered by the poorer offshore seismological resolution. Overall, there appears to be some evidence of a relationship between operations and seismicity. The largest event (M_W 4.3) was felt at the Ekofisk offshore platform, no damage was reported [Ottemöller et al., 2005].

2.1.4 The Lacq field (France)

The Lacq field is an anticline structure of ~10 km in lateral extent [Grasso & Wittlinger, 1990], located in the Pyrenees in France. Production is subdivided into two compartments: 1) a shallower Upper Cretaceous aged (fractured) dolomites/limestones oil field and 2) a deeper Lower Cretaceous through Upper Jurassic aged dolomitic sandstone and limestone gas field [Grasso & Wittlinger, 1990]. Both gas and oil have been produced from this region since 1957 and 1955, respectively, with disposal/injection ongoing contemporaneously [Bardainne et al., 2008; Grasso et al., 2021]. Gas extraction ended in 2013 [Aocia & Brunol, 2018]. Injection has maintained reservoir pressure in the oil field, while the gas field has had significant reservoir pressure decline with production [Grasso et al., 2021].

The Lacq field is near the western edge of the Pyrenean chain, ~30 km north of the orogenically associated natural seismicity along the North Pyrenean Fault [Bardainne et al., 2008]. The exact state of stress in the Pyrenees is debated, with focal mechanisms showing a variety of results [Lacan & Ortuño, 2012]. The Lacq seismic swarm is well separated from this natural seismicity.

The induced earthquakes of the Lacq seismic swarm started in November of 1969 and has been ongoing through at least 2016 [Grasso et al., 2021]. Seismicity generally correlates with production and injection data. The first seismic event (~M3-4) was felt in 1969, after 30 MPa of gas reservoir pressure decline [Maury et al., 1992]. Seismicity generally trends within a few kilometers above/below the anticlinal reservoir depth [Bardainne et al., 2008]. The largest event was M_L 4.2 on 18 September 1978 [Aocia & Brunol, 2018]. More recently, another notable event (M_W 3.9) occurred in 2016, ~60 years after extraction began, and ~3 years after gas extraction ended [Aocia & Brunol, 2018]. The focal mechanism of this event was normal slip on an ~E-W oriented fault. Surface subsidence (on the order of centimeters) was also documented overlying this field, with a linear relationship between pressure decline and subsidence amount

[Maury et al., 1992]. Generally, the mechanism triggering seismicity here is thought to be a poroelastic response to the gas reservoir pressure decline [Segall et al., 1994], which is consistent with the hypocentral depths and mechanisms [Bardainne et al., 2008]. However, recent seismological studies have begun to implicate the nearby disposal/injection of wastewater as a potential contributor [Grasso et al., 2021].

The evidence that this Lacq case was induced is strong: the swarm's beginning marks a change in the local rate of seismicity, it responds temporally to the ongoing production/injection, it is spatially coincident with the oil/gas fields, and plausible amounts of stress change were inferred. Consequentially, these induced events were large enough to be felt by the local communities. No reports of damage are known. France has no official regulation (or traffic-light system) for earthquakes caused by petroleum operations, except for earthquake monitoring requirements [Grasso et al., 2021].

2.1.5 Fields in the Western Canada Sedimentary Basin, Canada

The Western Canada Sedimentary Basin is a large petroleum basin spanning multiple western Canadian provinces. Industry has targeted numerous strata throughout its history of hydrocarbon exploitation. Two noteworthy fields are Strachan [Wetmiller, 1986] and Eagle [Horner et al., 1994]. The Strachan field targeted the Leduc Formation, a Devonian aged carbonate, for gas extraction. The Eagle field targeted the Belloy Formation, a Permian aged carbonate interspersed with sandstone, for secondary oil extraction. Gas production started at the Strachan field in 1971. Oil production started at the Eagle field in 1977, with waterflood injection following shortly after in 1980.

Seismicity within the Western Canada Sedimentary Basin is quiescent, with natural seismicity concentrated along the Cordillera [Stern et al., 2013]. Focal mechanisms within the basin are predominantly reverse and strike slip [Wang et al., 2018]. Each of these cases (Strachan & Eagle) are located basinward (east) of the Cordillera seismicity and appear as isolated clusters.

The Western Canada Sedimentary Basin has a long history of induced seismicity [Milne & Berry, 1976]. Unfortunately, station geometry in the basin was historically sparse, so some older cases are only speculative [Milne, 1970]. Despite this, there were previous cases that were well instrumented, with local array deployments installed [Wetmiller, 1986; Horner et al., 1994]. At the Strachan field, seismicity started in ~1975, with an approximate 5-year delay following production. Earthquakes generally correlate well with gas production showing a decreasing rate associated with declining production [Stern et al., 2013]. Events at this field are located underneath the Leduc Formation carbonate reservoir with thrust mechanisms [Wetmiller, 1986; Schultz & Wang, 2020]. At the Eagle field, seismicity was first noticed in 1984, several years after operations began; declining production was followed by declining seismicity rates [Horner et al., 1994]. Events were roughly at the reservoir depth and within the footprint of the oil field. In both cases, events just above M4 were noted throughout their history of production. Notably, models of poroelaleastic stress change from declining reservoir pressure were developed for the basin, largely modelled from the Strachan case [Baranova et al., 1999].

In both the Strachan and Eagle cases, there is strong evidence that the events were induced: the swarms appear above prior baseline seismicity, trend spatiotemporally with operations, and have plausible

stress changes inferred. Although, the relative importance of injection and extraction for fault reactivation here are debatable. In both cases, the ~M4 events were felt locally, with cases of damage and shaking impacts noted [Horner et al., 1994]. No regulations were developed to manage seismicity caused by (secondary) production, in either Alberta or British Columbia.

2.1.6 Fields in Texas, USA

The state of Texas hosts a series of petroleum basins that have been exploited by industry as early as the late 1800s. Targets have included the Permian Basin, Fort Worth Basin, and the Western Gulf Basin.

Seismicity within Texas is quiescent and largely restricted to west Texas and the panhandle [Davis et al., 1989; Petersen et al., 2008]. Here, earthquake slip on faults transitions between normal to strike-slip, depending on the location [Lund Snee & Zoback, 2016].

The state of Texas also has a long history of induced seismicity following industry development [Davis et al., 1989; Frohlich et al., 2016; Grigoratos et al 2022]. In fact, the first ever documented case of extraction induced seismicity was in the Goose Creek oil field of Texas [Pratt & Johnson, 1926; Yerkes and Castle, 1976]. There, subsidence of ~1 m was noted [Pratt & Johnson, 1926] alongside accompanying normal faulting and intensity III-IV earthquakes in 1925 [Yerkes and Castle, 1976]. Other cases include Goldsmith (M 3.4, 1966) [Yerkes and Castle, 1976], South Houston (M 1.5, 1969) [Yerkes and Castle, 1976], East Texas (intensity V, 1957) [Yerkes and Castle, 1976], Gladewater (M 4.7, 1957) [Frohlich et al., 2016], War-Wink (M 3.9, 1976) [Rogers & Malkiel, 1979; Keller et al., 1987; Doser et al., 1992], Imogene oil and gas fields (M 3.9, 1984) [Pennington et al., 1986; Davis et al., 1995], Fashing gas field (M 3.6, 1983; M 4.3, 1991; M 4.6, 2011) [Pennington et al., 1986; Davis et al., 1995; Frohlich & Brunt, 2013], Alice (M 3.9, 1997; M 3.9, 2010) [Bilich et al., 2012; Frohlich et al., 2012], and Falls City (M 3.6, 1991; M 4.3, 2008) [Olson & Frohlich, 1992; Frohlich et al., 2016]. These cases represent operations targeting disparate basins throughout the state of Texas; notably, the implicated oil fields had often produced ~10^6 m^3 at the time of felt events [Frohlich et al., 2016]. While many of these cases are hampered by poorer resolution, models of poroelastic stressing from reservoir pressure decline are thought to be responsible for fault reactivation in these cases. When reported, earthquakes exhibit strike-slip or normal faulting [Doser et al., 1991], which is consistent with the ambient stress field [Lund Snee & Zoback, 2016].

Cases in Texas appear likely to be induced by extraction of oil in the past. Many of the older cases were inferred solely based on spatial associations, sometimes in the absence of seismographic records [Pratt & Johnson, 1926; Yerkes and Castle, 1976]. Despite past limitations, more recent analogous examinations of a plethora of cases would suggest a likely induced origin for these cases [Frohlich et al., 2016]. Certainly, many of these events were felt [Yerkes and Castle, 1976; Olson & Frohlich, 1992; Bilich et al., 2012], with some reporting surface ruptures [Yerkes & Caste, 1976]. No regulatory system to manage extraction induced seismicity was implemented in Texas [Frohlich et al., 2016].

2.1.7 Fields in California, USA

The state of California also hosts a series of petroleum basins that have been exploited by industry as early as the late 1800s. Target basins in the state have been numerous, but the most relevant and well-studied cases primarily focus on the Los Angeles Basin. Production here started in 1903 and was most prolific during 1920-1930 [Hough & Page, 2016].

Natural seismicity within California is significant, owing to the continental transform that separates the North American and Pacific plates [Toppozada & Branum, 2004]. Here, earthquakes are predominantly strike-slip and concentrated along major faults like the San Andreas, San Jacinto, and Hayward.

The state of California has had a surprisingly under-studied history of induced seismicity, given the dense instrumentation and prevalence of petroleum industry. Cases have likely been obscured by the ongoing natural seismicity, and thus require more elaborate methods to discern [Goebel & Shirzaei, 2020]. Historical studies have pointed to the Wilmington Oil Field in the Los Angeles Basin [Kovach, 1974; Yerkes & Caste, 1976]. There, subsidence on the order of ~10 m had been observed by 1967 [Yerkes & Caste, 1976; Hough & Bilham, 2018], alongside linear trends between net fluid extraction, reservoir pressure decline, and cumulative reservoir compaction [Yerkes & Castle, 1976]. Earthquakes as large as M3.3 occurred in 1955 and 1961 [Yerkes & Caste, 1976]. Following the abandonment of production at Wilmington, no clear correlation with earthquakes in the Los Angeles Basin has been observed [Hauksson et al., 2015]. More recent re-examinations of seismicity in the Los Angeles Basin have suggested interesting relationships: such as correspondence of production with coincident earthquakes [Hough & Page, 2016], Coulomb stress changes on the order of 1 MPa within 2 km of the active oil fields [Hough & Bilham, 2018], and an M_L 4.2 event in 2001 below the Beverly Hills Oil Field [Hauksson et al., 2015]. Other larger events have been noted near oil fields in the Los Angeles Basin [Hough & Page, 2016; Hough & Bilham, 2018], but their causal relationship is less clear [Hauksson et al., 2015]. We note that within California, cases of oil production near Coalinga (M_L 6.7) have also been highlighted [McGarr, 1991], but ultimately ruled as tectonic [Rymer & Ellsworth, 1999].

The case near the Wilmington Oil Field of California appears likely to have been induced by extraction of oil in the past. Many of the older cases were inferred solely based on spatial associations [Kovach, 1976; Yerkes and Castle, 1976], but recent re-examinations have shown some temporal relationships too [Hough & Page, 2016]. Many of these events were felt [Yerkes and Castle, 1976; Olson & Frohlich, 1992; Bilich et al., 2012], with some reporting damage [Hauksson et al., 2015] – likely due to the highly populous setting of the Los Angeles Basin.

2.1.8 Fields in the Middle East (Kuwait, Saudi Arabia, Oman, & Iran)

The first commercial oil well in the Middle East was drilled in 1908 in the Masjid-i-Sulaiman Field of Iran [Alsharhan & Nairn,1997]. The Middle East hosts some of the most productive wells in the world throughout its numerous basins that include: the Greater Arabian Basin, Zagros Basin, and Oman Basin.

The seismotectonic state of the Middle East includes significant natural seismicity along the margins of the corresponding tectonic Arabian Plate [Bou-Rabee, 2000]. The northward motion of this

minor plate is related to features such as rifting of the Red Sea from the African Plate, contributing to the Persia–Tibet–Burma orogeny from collision with the Eurasian Plate, and strike-slip motion along the East Anatolian Fault and the Dead Sea Transform Fault Zone. Most cases of induced seismicity have been noted at the plate interior, distant from ongoing natural seismicity.

Cases of induced seismicity have been noted throughout the Middle East, with Kuwait being the most well studied with events up to M 4.7 [Bou-Rabee, 1994; Bou-Rabee & Nur, 2002]. Earthquakes here have shown a spatial correspondence with oil fields [Bou-Rabee & Abdel-Fattah, 2004; Al-Enezi et al., 2008], as well as a hints of a temporal relationship. For example, two M 4.7 events in June 1993 followed the super-fast uncontrolled depletion from the Kuwait oil fires in southern Kuwait [Bou-Rabee & Nur, 2002]; here, 504 out of 770 wells were ablaze, with depletion at quadruple the typical production rates between 22 February 1991 to 6 November 1991. Similarly, shallow events (up to M_L 4.2) in the eastern province of Saudi Arabia have noted a spatial correspondence with the Ghawar oil & gas field [Mukhopadhyay et al., 2018]. A well-resolved case with a long-standing local array suggested events were induced within the north-central group of petroleum fields in the Fahud Salt Basin of Oman [Sarkar, 2008; Sarkar et al., 2008; Zhang et al., 2009]. The extraction operations target the Lower Cretaceous aged Shuaiba chalk for oil production, and the shallower Natih Formation for gas production [Sarkar, 2008]. Here, events are well located in the footprint of the field, delineated at depths above and below the reservoir along previously known faults, and temporally correlate with production operations with a lag on the order of months. Last, a study in the Shanul Gas Field of the Zagros Basin in Iran suggested a potential link with reverse slip events up to M_W 5.7 on 9 June 2020 [Jamalreyhani et al., 2021] – although this interpretation is somewhat hampered by the relatively active tectonic setting of these earthquakes. Here, gas extraction started in 2006 with 18 wells targeting anticlines from the Permo-Triassic aged Dehram Group carbonates at 3-4 km depth.

Several cases of seismicity in the Middle East appear likely to have been induced; they are purportedly in previously quiescent regions and spatiotemporally related to oil field operations. That said, many of the cases have been obscured by poorer resolution and could benefit from modern examinations that systematically compare production data alongside earthquake catalogues. Many of the larger events were felt.

2.1.9 Fields in Central Asia & Russia

The regions of Central Asia and Russia host petroleum basins (e.g., West Siberian Basin) that have been exploited by industry. The Samotlor and Romashkino are two supergiant oil fields that were discovered in 1964 and 1949 respectively.

The seismotectonic state of Central Asia and Russia is predominantly controlled by the margins of the Eurasian Plate. Most relevant for our focus areas is the collision with the African, Arabian and Indian plates – and the corresponding seismicity [Mikhailova et al., 2015]. While cases of induced seismicity have been distant from ongoing natural seismicity, many cases have been in seismically active areas.

Cases of induced seismicity, from various anthropogenic sources, have been variously noted throughout Central Asia and Russia [Adushkin, 2016]. The most notable extraction case took place in the Romashkino Oil Field near Almetyevskaya, Russia. This is the biggest oil field in Russia, extending for ~70 km laterally, and targeting Devonian aged sandstones and carbonates [Adushkin et al., 2000]. Production began in 1948, with water injection starting in 1954, by 1963 the total injected/extracted fluid volumes had balanced, and by 1974 ~10^9 m^3 of fluid had been injected. This region is seismically quiescent, with events first being felt by residents in 1982-1983 – following this, a local seismic network was installed in 1985 and recorded shallow events up to M 4.0 within the footprint of the oil field [Adushkin et al., 2000]. Near the Gazli Gas Field of Uzbekistan, three (M_S ~7.0) earthquakes (8 April 1976; 17 May 1976; 19 March 1984) were first argued to be induced by Simpson & Leith [1985]. Here, operations target a series of stacked Cretaceous aged anticlinal sandstones at shallow depth (~2km). The Gazli Gas Field was first discovered in 1956, production began in 1962, and ~10^9 m^3 of water was injected by 1976 [Adushkin et al., 2000]. Other cases that have been noted in the literature include the 1971 M 4.7 event in the Starogroznenskoe Oil Field of Russia [Kouznetsov et al., 1994], the 1984 M 6.0 earthquake in the Barsa-Gelmes-Vishka Oild Field of Turkmenistan [Kouznetsov et al., 1994], and the 2005 M_W 5.6 earthquake in the vicinity of the Piltun-Astokh offshore oil and gas field of Sakhalin [Konovalova et al., 2015].

From the literature, it seems most likely that the Romashkino case was induced: events are both spatially coincident and temporally correlated to the oil extraction and water injection [Ognev & Stepanov, 2021]. The Gazli events were contentious: alternatively argued to be induced in some studies but tectonic in others [Suckale et al., 2009]. Like the Coalinga M_L 6.7 event in California, the Gazli events don't fit the typical observations for cases of extraction induced seismicity – being at significant (mid-deep) crustal depths, having limited spatiotemporal association, and anomalously large magnitudes. Other cases of induced seismicity were simply noted, based on their spatial proximity to ongoing operations – here, further studies would be required to make more confident statements on their anthropogenic origin.

2.1.10 Miscellaneous cases (Kentucky, Ontario, Argentina, Alabama, Indiana, Nebraska, Italy, UK, Botswana)

Here, we summarize information from petroleum extraction cases that were not well-studied, which were discussed in only 1-2 publications. Each of the following paragraphs covers a unique region that discussed the potential for induced events.

In the Seventy-Six Oil Field in the Appalachian Basin of Clinton County, Kentucky, USA, downhole geophones monitored seismicity from 1993-1995, recording events up to M_W 0.9 [Rutledge et al., 1998]. There, oil was produced from structurally-controlled Indian Creek syncline that targeted Ordovician aged carbonates of the Lexington Limestone to the Knox Group at shallow depths (300-490 m). Events were temporally correlated to the ongoing production, with a lag of 2-3 weeks [Rutledge et al., 1998]. Events were also spatially correlated with ongoing production, occurring at depths slightly above and below the production zone – and even delineated fault planes extending from the production wells to ~200 m deeper. Composite focal mechanisms for deeper events were thrust [Rutledge et al., 1998], which

is consistent with poroelastic stressing models that anticipated ~0.02 MPa of stress change promoting fault slip. Despite the limited scope of this study, there is strong evidence that these small events were induced by contemporaneous oil production.

From 1980-1984, a temporary network observed moderate magnitude events (up to M ~3.4) that were felt by residents near the town of Gobles, Ontario, Canada [Mereu et al., 1986]. The installation of the array was triggered by a M 2.8 event that was felt by residents of Gobles on 30 December 1979. The nearby oil and gas production targets a pinchout from the Algonquin Arch, within the Upper Cambrian aged Au Clair Sandstone, at a depth of 884 m. Production here started in 1960, with ~70 producing wells drilled by 1986; secondary recovery began in 1969 due to low reservoir initial pressures, with water from shallower Silurian strata being pumped into the deeper oil reservoir [Mereu et al., 1986]. Event locations are clustered into two regions that fall within the footprint of the drilled wells, mostly along the margins of the producing area. Depths of events are also near the producing reservoir at 800-1000 m. Focal mechanisms were constrained for the two clusters using a composite mechanism, supporting the idea that two separate faults were reactivated as normal and reverse [Mereu et al., 1986]. Events also temporally correlated with operations, where seismicity stopped following the cessation of pumping in this field [Mereu et al., 2002]. Overall, it is most likely that the seismicity near Gobles was induced by oil field production.

Within Argentina, most of the hydrocarbon producing basins are within Patagonia. In particular, the Neuquén Basin and Golfo de San Jorge Basin were the focus of a recent study [Tamburini-Beliveau et al., 2022]. Two notable events have ocurred recently: the 17 October 2019 M_L 5.0 earthquake near the town of Las Heras in the Golfo de San Jorge Basin, and the 7 March 2019 M_L 4.9 event near the village of Sauzal Bonito in the Neuquén Basin. Both events were felt by nearby residents. Both basins have undergone significant conventional hydrocarbon extraction, with the Neuquén Basin also having undergone unconventional development from hydraulic fracturing since 2011. In both basins, subsidence has been well correlated with net-extraction volumes [Tamburini-Beliveau et al., 2022]. Furthermore, in the Neuquén Basin, shows that seismicity is lagging hydraulic fracturing development; seismic energy release is roughly correlated with production data. These cases could have been potentially induced, however, additional studies that better quantify the uncertainties of the earthquake catalogue and confounding operations would be beneficial.

On 24 October 1997, a M_W 4.9 earthquake occurred in the nearly aseismic Gulf Coast Plain of Alabama, USA [Gomberg & Wolf, 1999]. The normal focal mechanism of the mainshock was consistent with north-south extensional stress field of the region. Operations in the Big Escambia Creek, Little Rock, and Sizemore Creek production fields targeted the Smackover Formation limestone and Norphlet Formation sandstone at depths of up to 4.5 km [Gomberg & Wolf, 1999]. The main shock depth was estimated to be 4.5 km [Chang et al., 1998], with a temporary array delineating aftershocks between 2-6 km [Gomberg & Wolf, 1999]. No significant changes were noted in nearby production/injection operations. The limited temporal scope of this study makes it difficult to discern if this case was induced or not – although the reports are consistent with better resolved induced cases.

During November 1995 to June 1996, a temporary seismic network detected earthquakes up to M_W 1.8 near the town of New Harmony in Indiana, USA (near the Indiana-Illinois border) [Eager et al., 2006]. Events here were clustered in both time, space, and waveform similarity; with most event depths near 4-5 km and some near 2 km. Earthquake epicentres were in the Wabash Valley Seismic Zone, which is also within the Illinois Basin that had ongoing secondary recovery at oil fields [Eager et al., 2006]. Again, the limited temporal scope of this study makes it hard to decide if this case truly was triggered or induced – with the reported observations being consistent with better resolved induced cases.

During 1979-1980 [Rothe & Liu, 1983] and 1982-1984 [Evans & Steeples, 1987], earthquakes up to M 2.9 were recorded on temporary arrays over the Sleepy Hollow Oil Field near the Nebraska-Kansas border. Earthquakes were felt by residents at intensities of III-IV, within the ~10 km limits of the Sleepy Hollow Oil Field [Rothe & Liu, 1983]. Delineated focal mechanisms suggested strike-slip fault motion. Events were well located within the footprint of the oil field, with depths widely distributed around the production interval [Evans & Steeples, 1987]. The Sleepy Hollow Oil Field is located at the southern edge of the Cambrian Arch, with the Pennsylvanian aged Sleepy Hollow sandstone being the primary oil target. This oil field was discovered in 1960, with secondary recovery starting in 1966. The limited temporal scope of these studies limits discerning if events were induced. However, the reported observations are consistent with better resolved induced cases.

Mid-May of 1951, two moderately sized earthquakes (M_W 5.4 & 4.5) occurred close to the Italian town of Caviaga. Initially, these earthquakes were thought to be induced based on an assumption of an aseismic setting and proximity to nearby gas extraction [Caloi et al., 1956]. Certainly, significant extraction since 1944 has occurred from the Caviaga gas field that targets the anticline of Plioene aged Strati di Caviaga [Caciagli et al., 2015]. However, this event occurs in a region of historical seismicity – with some events (1786) of similar magnitude occurring nearby the 1951 event at comparable lower-crustal depths [Caciagli et al., 2015]. Generally, the natural tectonic seismicity in Italy is complex and can obscure the identification of induced seismicity cases [Lavecchia et al., 2021]. Similarly, regional Italian studies have suggested that the evidence for hydrocarbon-extraction induced seismicity is currently speculative [Braun et al., 2018]. Recently, regulations governing induced seismicity in Italy have been implemented, with a red-light set at M 3.0 [Braun et al., 2020].

During 2018-2019, an earthquake swarm (up to M_L 3.2) occurred in the Weald Basin of southern UK [Hicks et al., 2019]. Strike slip events here occurred at shallow depths (~2.3 km) and were associated with the Newdigate Fault. Approximately 3 km away from this swarm, the Horse Hill well was completed in 2014 and targets the Jurassic aged Portland sandstone. Some studies have suggested that this event may have been induced [Westaway et al., 2020]. On October 2018, the Oil and Gas Authority hosted a workshop on the Horse Hill earthquake swarm (https://www.nstauthority.co.uk/news-publications/news/2018/oga-newdigate-seismicity-workshop-3-october-2018/). This working group found that the events here were unlikely to be induced by the ongoing and nearby extraction operations.

This assessment was based on a lack of temporal correlation (e.g., events started before operations began) and the swarm being comparable to baseline seismicity for the Weald Basin.

On 3 April 2017 a M_W 6.5 earthquake occurred in Botswana – one of the largest events ever recorded regionally [Albano et al., 2017]. This event was deep (~20 km), had normal slip on a NW-SE fault, was widely felt, and caused injuries. The event is located within a region of active rifting with extensional motion. Nearby to this event, the Lesedi project has been targeting the lower Morupule Coal Seam for coal bed methane extraction: a process that must dewater the coal for gas extraction [Albano et al., 2017]. Overall, this event appears to be unlikely to be induced: the reactivated fault is deep within crust, the mechanism is incompatible with expected stress changes, and no temporal relationship was reported – the event only happens to be laterally coincident with the ongoing operation.

2.2 Groundwater withdrawal

2.2.1 The Central Valley of California

In the San Joaquin Valley of California, continued extraction of groundwater for irrigation (since 1860) has resulted in significant subsidence [Amos et al., 2014]. The loss of mass has also impacted the surrounding region, by creating uplift on the order of 1-3 mm/year over distances of 100s of kms from the valley. The uplift rates vary periodically with the seasons, peaking in the summer months, which is out of phase with the water recharge that occurs during the winter season. Simple elastic models suggest that stress changes transmitted to the subparallel San Andreas fault could cause unclamping at a rate of ~0.1 kPa/year – with ~10 kPa of unclamping accumulating over the history of extraction, at locations like Coalinga. The study of Amos et al., [2014] further suggested that this unclamping of faults could be responsible for the seasonality of earthquakes at Parkfield.

2.2.2 The Alto Guadalentin Basin of Spain

At the Alto Guadalentin Basin of Spain, long-term groundwater pumping has caused subsidence on the order of 10 cm/year [González et al., 2012]. Here, extraction induced unloading stress changes on the order of ~10 kPa were suggested to have been transmitted to nearby faults, like the Alhama de Murcia fault. There, the 11 May 2011 M_W 5.1 Lorca earthquake may have been triggered by groundwater extraction that promoted fault slip. This earthquake was significant, in that it caused both damage to buildings and fatalities. Coseismic ground deformation constraints placed this thrust event at shallow depths (2-4 km) [González et al., 2012]. Following this, studies began linking swarms of seismic activity in southern Spain with the hydrologic cycle and groundwater extraction [Doblas et al., 2014].

2.2.3 The Gran Sasso Basin of Italy

At one of the largest aquifers in central Italy, a construction project tunneled through the Gran Sasso chain from 1970-1986. Following this project, earthquakes up to M 3.9 began at the north-west margins of the basin [Bella et al., 1998]. It is thought that a combination of increased snow melting on the

mountain and groundwater flow redirection from the tunnelling are thought to have caused the increase in nearby seismicity rates.

2.2.4 The Dead Sea Transform Fault of Jordan

At the Lake Kinneret Basin in the northern section of the Dead Sea Transform Fault of Jordan, a series of seismic swarms occurred in 2013, 2018, and 2022 [Wetlzer et al., 2019; Shalev et al., 2023]; the single largest event was M_W 4.5. The earlier events (2013 & 2018) reactivated with normal slip, while the later events (2022) reactivated as strike-slip motion. To the west of the earlier swarms (~10 km), ongoing groundwater extraction targets the Cretaceous aged Judea Group aquifer at ~1 km depth. The extraction process has resulted in subsidence of ~10 mm/year and a decrease in groundwater level of 50 m [Wetzler et al., 2019]. Poroelastic stress changes on the order of 0.1 MPa, transmitted from extraction at the aquifer to the swarm location, has been suggested as responsible for triggering these events. Similarly, to the east of the later swarms (~4 km), groundwater extraction from the Wadi Al-Arab Basin is thought to have triggered these events [Shalev et al., 2023]. This area has hosted very large tectonic earthquakes in the past [Grigoratos et al 2020].

2.2.5 The Zagros fold-and-thrust belt of Iran

At the Zagros fold-and-thrust belt of Iran, an oblique thrust event of M 7.3 event occurred on 12 November 2017 [Kundu et al., 2019]. Groundwater extraction for irrigation, from the nearby Euphrates and Tigris River plains is thought to have contributed to triggering this event. Ground water extraction has noted subsidence on the order of ~7 mm/year and a decrease in ground water level of 20 cm. More information would be needed to conclude if this event was induced or not.

2.2.6 Indo-Ganga Basin of India

In the Delhi region of India, an ongoing swarm of seismic activity has been tied to the ongoing groundwater extraction [Tiwari et al., 2021]. Earthquakes largely occur within the footprint of the greatest groundwater depletion rate and are temporally related to the groundwater level over a period of ~10 years. Groundwater pumping in the Indo-Ganga Basin near Delhi is thought to have decreased the storage levels by up to ~1.6 cm/year and corresponded with centimeters of subsidence. Stress changes on the order of ~10 kPa were also suggested to have been transmitted to underlying basement faults [Tiwari et al., 2021]. Similar arguments have been made for the triggering of the M_W 7.8 Gorkha earthquake, where groundwater extraction from the Indo-Ganga Basin is thought to have played a role in promoting fault slip [Kundu et al., 2015].

3 Guidelines

Due to the limited amount of literature specific to extraction-related induced seismicity guidelines, we have expanded our search to all categories of induced seismicity. Guidelines have been discussed in the context of geothermal systems [Majer et al., 2012; Trutnevyte & Wiemer, 2017; Wiemer et al., 2017; Kraft et al., 2020], wastewater disposal [Zoback, 2012; NRC, 2013; GWP, 2021], carbon sequestration [Nicol et al., 2013; White & Foxall, 2016; IEAGHG, 2022; Templeton et al., 2021; 2023], hydraulic fracturing [CAPP, 2012; Shipman et al., 2018; Schultz et al, 2020a; 2021a], and hydrocarbon extraction [Muntendam-Bos et al., 2015; van Thienen-Visser et al., 2018; Vlek, 2018]. These guidelines begin to outline how to avoid, mitigate, or minimize risks [Pate-Cornell, 2002] within a seismic context [Bommer et al., 2015; Walters et al., 2015; Wiemer et al., 2015; van Elk et al., 2019]. Typically, this risk reduction process has been subdivided into steps, including: a pre-screening of anticipated hazards/risks [Davis & Frohlich, 1993; TNO, 2021], selection of risk metrics and tolerances, design of traffic light systems [Bommer et al., 2006], real-time monitoring, quantifying the observed seismic hazards/risks, developing mitigation plans, and outreach/communication with all the affected stakeholders.

3.1 Pre-screening of anticipated hazards/risks

In many induced seismicity cases, the risks of earthquakes were only recognized in hindsight – with risk management steps being taken afterwards, in an *ad hoc* manner. However, following the recent increase in recognition of these earthquakes, jurisdictions have begun outlining the pre-screening step more rigorously [Majer et al., 2012; Muntendam-Bos et al., 2015; Walters et al., 2015; Trutnevyte & Wiemer, 2017; Shipman et al., 2018; van Thienen-Visser et al., 2018]. Pre-screening risk assessments are understandably uncertain, due to the lack of concrete input data. For this reason, many guidelines suggest using a risk matrix approach to qualitatively categorize the degree of risk [Thomas et al., 2013], for example, by delineating between likelihood and severity of risk. We note that this pre-screening process can be used to assess candidate-site risk, in order to guide choices for suitable project locations.

Spurred on by the need to better quantify the *a priori* likelihood of induced seismicity, assessing where and why induced seismicity can occur has emerged as a recent research theme. Case studies of induced events have shown that only a subset of injection/extraction wells induce events, exhibiting spatial biases towards susceptible regions [Schultz et al., 2016; Eaton & Schultz, 2018; Skoumal et al., 2018; Galloway et al., 2018; Hincks et al., 2018]. This susceptibility has been interpreted as due to a spatial bias in the underlying geological, tectonic, and geomechanical factors that are needed to induce earthquakes: faults that are well-oriented in the ambient stress field, a means of communicating anthropogenic stress changes to the fault, and sufficient stress changes for fault reactivation. A combination of these insights was first used to distinguish between the seismogenic/aseismic gas fields in the Netherlands via a Bayesian model [van Eijs et al., 2006]: in this study, factors like fault density, reservoir-seal stiffness contrast, and reservoir pressure drop were combined to estimate the likelihood of encountering extraction induced earthquakes. Machine learning techniques have since been utilized to inform regions susceptible to earthquakes [Pawley et al., 2018], where the availability of input data and the methodological approach can

vary the output estimates [Wozniakowska & Eaton, 2020; Hicks et al., 2021; Amini et al., 2021; Wang et al., 2022]. In the context of hydraulic fracturing, expert panels have recommended the quantification of susceptibility as an important regulatory tool [SHFRP, 2019].

Other approaches have also begun to quantify the likelihood of induced seismicity though more geophysically motivated analysis. For example, fault slip potential quantifies both the likelihood and amount of fluid overpressure required to reactivate a fault [Walsh & Zoback, 2016]. Here, these quantities are defined from knowledge of the *in situ* state of stress, inventory of fault geometries, the Mohr-Coulomb failure criteria, and (often assumed) information about fault frictional properties. This approach can rank the criticality of faults, even before operations have commenced. Addressing fault slip potential has now been used in a wide variety of regions and operational settings [Shen et al., 2019; Hennings et al., 2019; 2021; Zhu et al., 2022; Nantanoi et al., 2021]. In fact, software to perform this analysis has been publicly released [Walsh et al., 2017]. That said, the predictive power of this method has not been empirically validated [Hennings et al., 2021] and is still under debate. We note that other studies have also begun case-specific geomechanical quantifications of the seismogenic potential [Haug et al., 2018; Hergert et al., 2022; Gudehus et al., 2023].

3.2 Selection of risk metrics and tolerances

The first step in reducing the severity of a risk is to agree on a definition of an unacceptable risk (i.e., the tolerance to risk). Prior guidelines have suggested that multiple metrics of risk (e.g., nuisance, damage, fatality) will likely be important for successfully managing induced seismicity [Majer et al., 2012; Bommer et al., 2015; Templeton et al., 2021]. Sometimes studies have also suggested using hazard metrics (e.g. PGV or PGA thresholds) instead of magnitude, as these parameters are more closely linked to risk.

One consideration is the risk of fatality or personal harm, because of the importance of ensuring personal safety of nearby residents. This is especially important to consider, since in extremely rare cases induced seismicity has caused injuries or even loss of life [Lei et al., 2019; Grigoli et al., 2018]. The discussion of likelihood of fatality has previously been described for earthquakes in a tectonic setting [Marzocchi et al., 2015], where likelihoods of 10^{-4}-10^{-6} are typically accepted as standards due to their use in health/safety guidelines. In fact, Dutch law has enshrined a mean-value likelihood of 10^{-5} for local personal risk at the Groningen, based on the recommendations of an expert committee [Meijdam, 2015]. Correspondingly, studies have begun building frameworks to manage fatality risks [Crowley et al., 2017], exploring the use fatality tolerances in TLS red-light design [Schultz et al., 2022b] and quantification of the potential for brick chimney collapse [Edwards et al., 2021].

The consideration of damage is an important risk due to the potential for direct and indirect economic consequences. In fact, cases of induced seismicity have caused noteworthy damage [Yeck et al., 2017; Muntendam-Bos et al., 2022], in some cases up to millions of dollars' worth of (often uninsured) damage [Grigoratos et al 2021]. Risk-based frameworks for damage need to consider the hazard source, fragility of structures, and their exposure to shaking [Bommer et al., 2015; Crowley et al., 2019]. While damage is likely an important consideration, little has been agreed upon or put into application for

tolerances to this risk metric. Generally, guidelines have discussed the consideration of this factor through magnitude or ground motion-based proxies. Likely, these tolerances should be agreed upon at a regional level, by all the impacted stakeholders, before operations begin. We note that these tolerances can potentially also depend on the infrastructure in question, where critical infrastructure (e.g., hydroelectric dams or nuclear powerplants) will require lower tolerances to damage. One example of a damage management system is the case of the Groningen gas field, where the operator is legally required to pay the costs of all earthquake damages and building retrofitting [Bal et al., 2019].

The use of nuisance as a risk metric is a nascent research field, despite fairly early recommendations of its consideration [Majer et al., 2012]. Likely, research here has been underappreciated because of the relative severity of its consequences compared to fatality and damage risks. From a legal perspective, this risk factor is important to consider since many jurisdictions often have nuisance liabilities [Cysper & Davis, 1998], where landowners are entitled to a 'quiet enjoyment' of their property that is free from vibrational 'trespass'. More practically, this factor is important considering induced seismicity cases which have come under regulatory scrutiny or caused project abandonment/moratoriums without any damage or injuries reported (e.g., hydraulic fracturing in North America and the UK) – purely because of social anxieties, arguably triggered by felt events. In this way, nuisance can be linked to the 'social license to operate'. Persistent nuisance can also lead to decreased evaluation-prices for the exposed buildings [Koster & van Ommeren, 2015; Cheung et al 2018]. Some recent studies have quantified the potential for nuisance risks [Cremen et al., 2020; Schultz et al., 2021b], used them to design TLS red-lights [Schultz et al., 2021a], or inferred tolerances to these risks (Figure 2) [Schultz et al., 2021c; Schultz et al., 2022b].

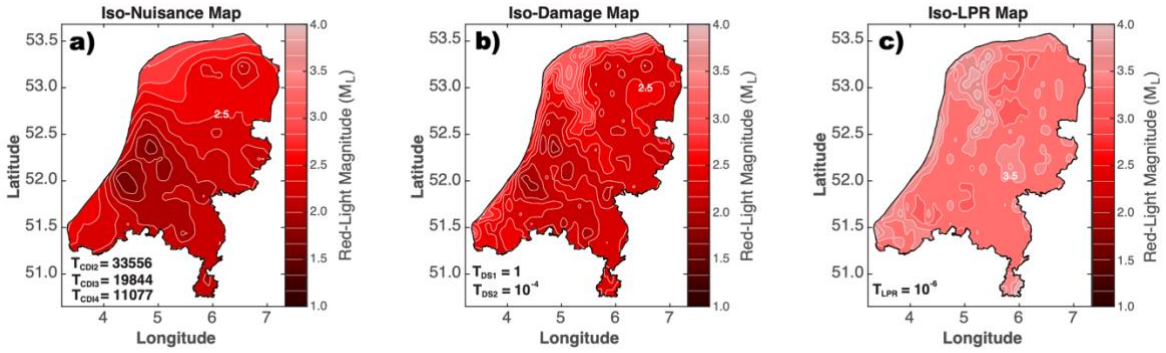

Figure 2. Red-light thresholds for enhanced geothermal prospects in the Netherlands from Schultz et al. [2022b]. a) iso-nuisance map; b) iso-damage map; c) iso-LPR map. All maps have their tolerances for risk displayed as text.

In addition to these primary concerns from earthquake ground shaking, we also note that there is the potential for earthquakes to cause secondary concerns: liquefaction [Barnhart et al., 2018], landslides, and subsidence [Fan et al., 2019]. Currently the induced seismicity community has been focusing on primary concerns but could shift to incorporate these concerns as/if they become relevant. We note that secondary concerns may be particularly important when damage to critical infrastructure (e.g., hydroelectric dams or

pipelines) comes into consideration. Usually, ground-effects (e.g. liquefaction) require very strong and long-duration ground-motions that are relatively rare when it comes to induced seismicity.

3.3 Traffic light systems (TLS)

One of the *de facto* techniques often used to limit the severity of earthquake risks is a traffic light system (TLS), or synonymously a traffic light protocol. TLS are typically stratified into three tiers: at the green-light threshold operators are allowed to proceed unrestricted, at the yellow-light the operator must enact their mitigation procedures to curb the growth of seismicity, and at the red-light the operator is forced to stop under a regulatory intervention (Figure 3). Typically, TLSs are implemented as a risk management tool, in regions that are concerned with encountering induced seismicity (e.g., via pre-screening approaches). The first case of a TLS implementation was for the geothermal project at Berlín in El Salvador [Bommer et al., 2006]. Since then, TLSs have been implemented in a wide variety of regions and operational settings [Bachmann et al., 2011; Kao et al., 2018; Ader et al., 2020]. While TLSs have critiques [Baisch et al., 2019; Roy et al., 2021], they remain an important regulatory tool to preemptively define operational endpoints. In this sense, we argue that all cases of induced seismicity have a red-light threshold: either explicitly predefined through a TLS or implicitly via the premature end of an operation in reaction to public outrage. Any operation without an explicitly defined red-light is essentially hoping that this scenario will never be triggered. Likely, this rationale has influenced the widespread adoption of the TLS.

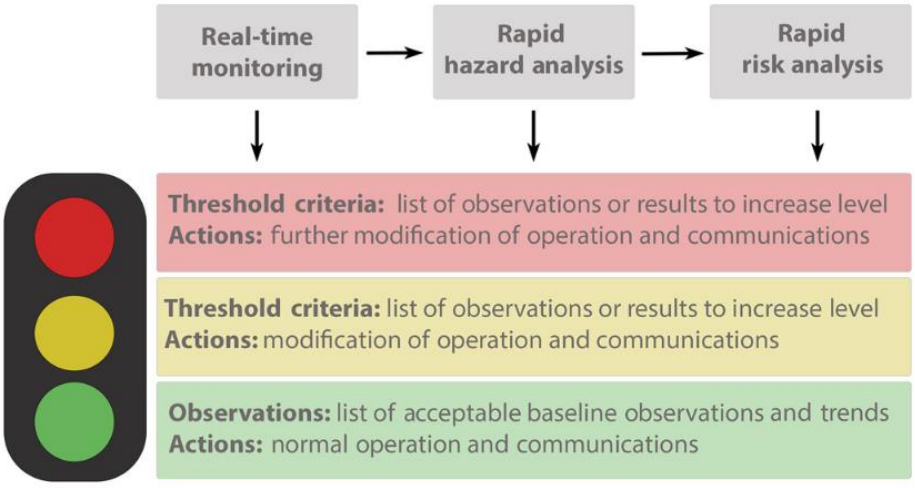

Figure 3. Example of a TLS with green, yellow, and red-light thresholds. Figure from Templeton et al., [2023].

Previously, most TLS thresholds were defined in a somewhat subjective manner, based on expert judgement. However, recent research has focused on defining red-light thresholds in a more quantitative way. For example, by addressing some of the previously recognized deficiencies of TLSs: the potential for trailing seismicity (i.e., earthquakes that continue to occur after the operation ending), thresholds informed

by risk calculations, and the incorporation of real-time information. Currently, induced seismicity caused by short-term operations have been statistically modelled to account for trailing events [Verdon & Bommer, 2020; Schultz et al., 2022a], which define acceptable buffers to account for 'jumps' in magnitude during the yellow-light and trailing events following the red-light. As well, workflows have started to define the red-light threshold based on risk tolerances such as nuisance, damage, and fatality [Schultz et al., 2020b; 2021a; 2021b; 2022b]. Finally, to address the rigidity of the conventional TLS, the adaptive TLS can incorporate real-time information to forecast seismicity rates and update the red-light threshold if/when necessary [Mignan et al., 2017].

3.4 Real-time monitoring

Crucial to the successful management of induced seismicity is the monitoring of relevant data in real-time. This information provides the cornerstone to virtually all the steps within this guideline: either directly through the data collected or indirectly from subsequent analyses and feedback challenging prior assumptions. In the general context of induced seismicity, catalogue building from seismological waveforms and timeseries of injection/extraction information are staples for data collection. The importance of collecting this information comes from providing constraints on reactivated faults, the intensity of ground shaking observed, and understanding/forecasting the seismicity-operation relationship. Recently, there has been a recognition to also collect earthquake engineering data relevant to quantifying hazard/risk. Specific to extraction induced seismicity, monitoring of surface subsidence and reservoir pressure decline has also been established as important – largely due to the relationship between poroelastic stress changes, ground/reservoir subsidence/compaction, and induced events. To quantitatively establish the geomechanical links along the causal chain of petroleum extraction, reservoir depletion induced stress changes, reservoir/surface compaction/subsidence, and ultimately induced earthquakes. For additional discussion on this topic, we also refer the reader to in-depth guidelines on induced seismicity monitoring guidelines, as best practices have already been established for the monitoring techniques mentioned [Majer et al., 2012; NRC, 2013; Wiemer et al., 2017; Kraft et al., 2020; GWP, 2021; Templeton et al., 2021; 2023].

3.5 Quantifying the observed seismic hazards/risks

Due to the complexity of this analysis, we have dedicated an entire section (Section 4) to this topic, where we provide greater details on the workflow and limitations imposed by the nature of induced seismicity.

3.6 Mitigation strategies

In this context, mitigation strategies are the actions that jurisdictions take to decrease the hazards or risks of induced seismicity – either in preparation to operations, in reaction to incoming real-time data, or in reinforcing against risks.

The first two categories are unique to induced seismicity, in that they aim for a reduction of the hazards. Longer term mitigation strategies can encompass geophysical exploration and monitoring, hazard

pre-screening, operational siting, and injection/extraction pumping design. Often, these approaches will be explicitly defined in a regulatory framework, such as a TLS. Reactionary strategies often include injection/extraction reductions (rate/pressure/volume), well flowback, temporary pauses, reorganization of injection/extraction locations or timing, and finally project abandonment. Examples of mitigation strategies (related to either injection or extraction of fluids) include fracture caging [Frash et al., 2021], cyclic stimulation [Zang et al., 2013], injection schemes that promote aseismic slip [Wang et al., 2020], well flow back [Schultz et al., 2023], or redistribution of extraction/injection volumes [Vlek et al., 2019]. Many of these mitigation strategies have been driven by close examination of laboratory and decameter-scale *in situ* fault slip and/or expectations from conceptual/modelling frameworks. Obviously, as far as gas production is concerned, the only hazard mitigation strategies are redistribution/reduction of extraction volumes and project abandonment. We note, however, that in many field applications, these techniques have had mixed results: by sometimes failing to prevent the growth of event magnitudes, and spurring operation-ending consequences [King et al., 2014; Grigoli et al., 2018]. Thus, the topic of hazard-reducing mitigation has been an area of open-ended research that is often stymied by a lack of access to data.

The last category of mitigation strategies (mostly) inherits ideas from tectonic earthquakes, which aim to reduce the risk by structural reinforcement or exposure reduction. Here, techniques can include changes to building design codes, building retrofitting [Zhang et al., 2022], or possibly even relocation (or abandonment) of exposed infrastructure. In this sense, the earthquake risks are reduced by bolstering the fragility of or limiting exposure to infrastructure. Unique to induced seismicity, the attitudes of the exposed population can also be influenced. Typically labelled the 'social license to operate' is a concept that qualifies to the willingness of nearby inhabitants to accept the ongoing operations [van der Voort & Vanclay, 2015]. Approaches here have included communication/outreach programs [Templeton et al., 2021], insurance/liability deferment, and exposure compensation packages [Bal et al., 2019]. In this sense, project loss risks are being reduced by reinforcing the tolerance of the local community.

3.7 Communication and outreach

The issue of communication and outreach is an important consideration for effective management. For example, by improving the tolerance to earthquake risks like nuisance. In fact, the quality of communication and outreach has the potential to significantly impact local perceptions [Verdoes & Boin, 2021]. More generally though, the issue of communication and outreach is broad in scope, with aims to improve acceptability of the project, provide a participatory feedback mechanism, and keep all relevant stakeholders and impacted populace updated/informed. Dissemination of information can be accomplished through both periodic meetings for planning alongside real-time reporting of events. The specifics of these outreach programs will likely vary for each jurisdiction, depending on the existence of authoritative agencies, pre-existing communication channels, and prior relationships amongst stakeholders. For additional discussion on this topic, we also refer the reader to in depth guidelines on induced seismicity outreach and communication programs, as best practices have already been established for the monitoring techniques mentioned [Majer et al., 2012; NRC, 2013; GWP, 2021; Templeton et al., 2021; 2023].

4 Seismic hazard and risk analysis

4.1 Introduction

Seismic hazard analysis or assessment (SHA), forecasts future earthquake-caused ground shaking for a proposed location or region. An SHA is typically used for decision making for societal or industry purposes. As explained in Gerstenberger et al [2020], SHA models are developed so that they encapsulate the earthquake process from earthquake interaction, rupture initiation, and crustal attenuation through to local site effects. The presence of numerous uncertainties in SHA requires a probabilistic description of seismic (natural) hazards which allows all known uncertainties to be included. Despite this, SHA is very often divided into deterministic analysis (DSHA) and probabilistic analysis (PSHA). The primary difference is related to the treatment of the uncertainty on the occurrences of the next earthquakes. A so-called deterministic model handles, at most, only the ground shaking uncertainties, thereby becoming a probabilistic model conditioned to the occurrence of a single earthquake source or a limited set of specific earthquake sources (e.g., the "maximum expected earthquakes"), regardless of the probability of occurrence of these sources. Conversely, a probabilistic analysis takes into account all possible earthquakes including their probability of occurrence in time, space and magnitude. Both methods can produce a probability of expected ground shaking. The methods may be used on their own, or they may be used together to provide complementary information for decision making. In modern times, the probabilistic approach has more or less prevailed, with very few exceptions [Bommer 2022].

Seismic risk analysis (SRA) deals with the undesirable consequences of earthquakes, which include death, injury, physical damage to buildings and infrastructure, interruption of business and social activities, and the direct and indirect costs associated with such outcomes. In a generic sense, risk can be defined as the possibility of such consequences occurring at a given location due to potential future earthquakes. In a more formal probabilistic framework, seismic risk is quantified by both the severity of a given metric of loss and the annual frequency or probability of that level of loss being exceeded (Bommer 2022). More details about how PSHRA is implemented in practice can be found in section 4.7.

PSHRA has been considered as a valuable tool to develop hazard estimates for induced seismicity. The framework has been used by the United States Geological Survey (USGS) to produce one-year hazard maps in areas with induced seismicity [e.g. Petersen et al., 2017], and by Convertito et al. [2012] and Bourne et al. [2014, 2015] to assess the time-dependent seismic hazard due to geothermal operations and fluid extraction, respectively. A number of studies have gone one step further performing seismic hazard and risk assessment of varying complexity for the Groningen gas field [Crowley et al., 2019; van Elk et al., 2019], for an Enhanced Geothermal System in Basel [Mignan et al., 2015], for a HF sequence in the UK [Edwards et al., 2021] and for large-scale wastewater-disposal activities in Oklahoma [Gupta and Baker 2019; Grigoratos et al. 2021] (Figure 4).

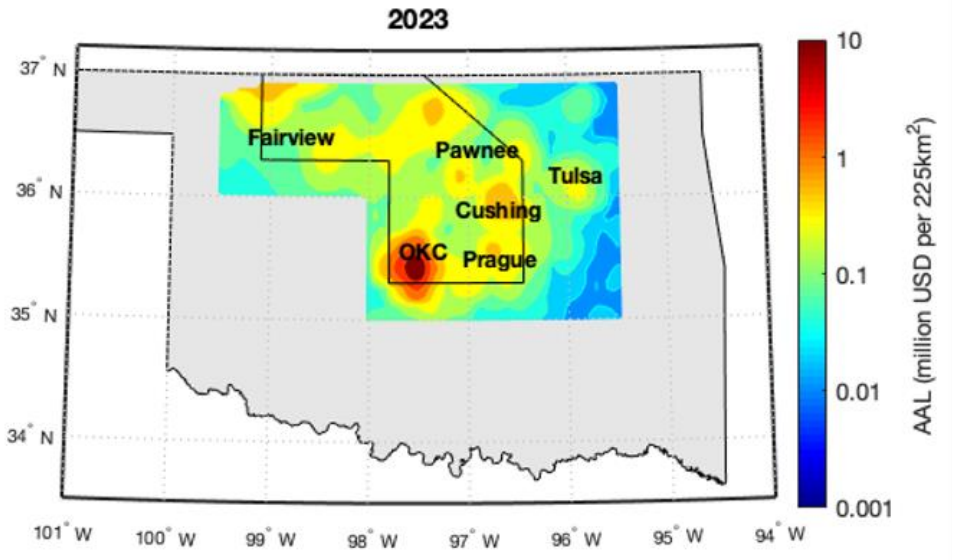

Figure 4. Spatial distribution of the forecasted average annual direct economic losses (AAL) related to wastewater disposal in Oklahoma, for the year 2023. The labels indicate the epicenters of the four largest earthquakes since 2006 and the two biggest cities, i.e. Tulsa and Oklahoma City (OKC). The black polygon indicates the borders of the induced seismicity model. Figure taken from Grigoratos et al. [2021].

4.2. Seismicity rates

4.2.1 Geomechanical modeling

Fluid extraction, injection, compaction, cooling, depletion, or pressurization in subsurface reservoirs can cause significant deformation of the surrounding rock formations, leading to the development of fractures and induced seismicity. In recent years, researchers have developed analytical and numerical geomechanical models to simulate and predict the behavior of reservoirs and faults under different conditions. The phenomenon of seismicity triggered by hydrocarbon production is a complex interplay of various physical and chemical processes, making it challenging to develop a perfect model that considers all contributing factors. In this review, we explored some of the prevalent geomechanical models used to study production-induced seismicity and discuss their limitations and trade-offs. The findings summarized here are later used to inform sections 5.1 and 6.1

Understanding the effect of fluid pressure changes on porous media, like hydrocarbon or geothermal reservoirs, is important to comprehend the seismicity rates. Segall and Fitzgerald [1998] investigated the stress changes caused by different types of disturbances, including earthquakes, injection and withdrawal of fluids, and thermal effects – including how these stress changes affect the behavior of reservoirs. They assume that the medium is isotropic, homogeneous, and elastic, and that Darcy's law governs fluid flow within it. The increased stress due to injection and production processes causes rock instability and results in frictional sliding on pre-existing faults, leading to induced seismicity. The large Biot coefficient, which measures the poroelastic properties of rocks, and regional stress changes within the reservoir promotes normal faulting. The isothermal reduction in pore pressure creates relative horizontal tension within circular disk-shaped reservoirs, highlighting the role of poroelasticity in inducing stress

changes in hydrocarbon and geothermal reservoirs. This tension can promote fracturing and enhance fracture permeability in nearby tight rocks, affecting reservoir productivity.

The properties of rocks, the different orientations of fracture networks, and the stress condition of faults are simply one of the few aspects that need great attention for understanding the relationship between fluid injection and induced seismicity. Hager et al. [2021] employ a process-based approach that uses motion and fluid flow equations to simulate subsurface behavior under various injection scenarios and investigates how changes in fluid pressure and rock properties can lead to fault slip and seismic activity. Successful implementation of this approach has been reported in the Val d'Agri oil field, located in seismically active southern Italy, where the geomechanical and earthquake source physics models were calibrated using comprehensive subsurface information. The models were then validated by comparing their predictions to subsequent observations, and the approach was found to be successful in managing and mitigating triggered seismicity.

To evaluate the seismic risk associated with geothermal and hydrocarbon reservoirs intersected by faults, van den Hoek and Poessé [2021] developed an analytical solution to model the stress changes induced by cooling, depletion, or pressurization along representative faults exists, which can be linked to elastic finite element calculations to estimate the maximum fault displacements and subsequent seismic magnitudes. The model predicts how the stress changes in the reservoir will affect the stability of pre-existing faults and fractures in the rock, potentially causing them to slip and generate earthquakes. This paper concludes that certain fault geometries are more prone to seismic activation than others. The activation risk is generally lower for geothermal operations than for situations where large parts of the reservoir are depleted or pressurized. The authors use this information to assess the seismic risk associated with fluid injection and extraction in the reservoir.

Over the years, the occurrence of production-induced seismicity in natural gas fields has raised concerns due to its potential risks and consequences. Gaining a comprehensive understanding of the fundamental physical processes driving these induced earthquakes is essential for effective management and mitigation approaches. Zbinden et. al. [2017] investigates the physical processes occurring in fault zones intersecting gas reservoirs during production. A geomechanical model is proposed, analyzing stress and pressure evolution within faults. The study identifies three processes: reservoir compaction leading to increased shear stress, pressure drop affecting stress through poroelastic effects, and fluid flow influencing pore pressure and normal stress. The assumption of similar pressure drops in fault and adjacent reservoirs is found to be inadequate. Variations in shear stress, fault strength, and caprock rheology contribute to deviations in induced earthquake magnitudes. Mitigation strategies, such as production shut-in and reinjection in the reservoir compartment, can prevent fault reactivation, while fluid injection in nearby compartments may not be effective. Although the model has limitations, its findings provide valuable insights into the geomechanics of production-induced seismicity.

Jansen et al. [2019] also present an analytical solution for the stress and strain fields induced by fluid injection or production in the vicinity of a displaced fault and consider the poroelastic behavior of the

reservoir and the fault zone, which means the stress changes depending on the compressibility of the rocks and the fluids in the reservoir. The authors also consider the effects of fluid pressure changes on fault friction, which can affect the potential for fault slip or reactivation. This work evaluates the elastic displacements, strains, and stresses resulting from fluid injection or production in a reservoir with displaced faults. The model considers a reservoir with a single fault plane displaced by a certain amount, and the fault plane is assumed to be impermeable. This paper concludes that even small amounts of injection or production can result in some amount of slip or nonelastic deformation due to the development of infinitely large elastic shear stresses in a displaced fault, particularly at the internal and external reservoir/fault corners.

Similarly to the injection process, the depletion of hydrocarbon reservoirs through pumping causes subsurface deformation and is thoroughly studied by Odonne [2019]. The study demonstrated that reservoir deflation leads to the formation of steeply dipping reverse faults that enclose a downward- opening cone, which moves downward in response to the reservoir contraction. The study also shows faults along the cone are straight beneath a thick reservoir cover and tend to curve upwards with decreasing cover. As the pressure within the reservoir decreases due to depletion, the overburden becomes unstable and undergoes deformation. This deformation can result in the formation of reverse faults that propagate upward toward the surface. The model suggests that the nature of the faults that develop depends on the mechanical properties of the overburden and the underlying basement rock. The overburden may have low strength and high compressibility, which can cause it to deform and form faults more easily. The basement rock may also have variable strength and can contribute to fault formation by either resisting or facilitating deformation. The presence of other geological structures, such as pre-existing faults, can also affect the development of reverse faults.

There is a need to understand the mechanical stratigraphy and structural complexities that exist in reality, but are often neglected in available analytical poroelastic models. Haug et al. [2018] present a geomechanical numerical modeling perspective to study the phenomenon of production-induced seismicity in gas fields located in North Germany. To investigate a parameter space including reservoir depth, thickness, mechanical properties, and compartment geometries typically found in North German Rotliegend gas fields, the study utilizes 2D finite element models. Furthermore, the paper discusses the effects of mobile salt layers with varying thickness atop the reservoir on fault stability. The results indicate that salt diapirism and variations in the sandstone-shale succession controlling the distance between the reservoir horizon and viscoelastic evaporite layers play a crucial role in focusing production-induced seismicity in specific locations within the gas fields. Furthermore, the study reveals, that steeply dipping faults (>60°) are more likely to be reactivated due to the dominant contribution of reservoir compaction to fault loading, even if they are considered unfavorable for reactivation in the tectonic stress field. The findings of this paper indicate that production-induced fault reactivation potential is highest at the upper reservoir level and a narrow interval above the reservoir. Fault loading is strongest directly below the viscoelastic salt layer in the overburden, but upward propagation is limited due to the isotropic stress state and shear stress relaxation in the salt.

Analysing the North German basin again, Hergert et al. [2020] investigated the reactivation of faults caused by the decline in pore pressure and reservoir compaction, using hydromechanically coupled finite element models. One of the primary observations is the occurrence of normal faulting slip at the depth of the reservoir, with nucleation near its top in the hanging wall. The paper also reveals that the displacement does not fully extend to the lowermost part of the reservoir in the hanging wall, except under specific conditions of low horizontal stresses prior to production. The timing and size of rupture are found to be influenced by the relative position of production wells in relation to the fault. An important aspect of the study is the role of frictional properties on the fault and the pre-production stress state, which significantly impacts coseismic displacements. Specifically, the tectonic stress field, characterized by the ratio of effective horizontal to vertical stress (k0), plays a crucial role in determining the duration of production and the extent of pore pressure decrease before reaching a critical state of stress. This research offers valuable insights into the interplay between tectonic stresses and depletion-induced stress changes, which collectively drive the occurrence of earthquakes in the region. Notably, the study emphasizes that the earthquakes in Northern Germany are particularly influenced by pore pressure drawdown during production due to the region's low-deformation rates.

There are arguments that the lithosphere's tectonic drive cannot be represented solely through stresses or displacements at boundaries, as in technical structures. Instead, Gudehus et al. [2022] propose the use of quasi-local and -momentary quantities combined with fractional derivatives to better capture the fractal and non-fractal features of rock behaviour. The paper examines rock fabric evolution in the context of dilatant-driven and spontaneous contractant critical phenomena, to understand the behaviour of faults, shear bands, and cracks in the lithosphere in NW Germany. The study emphasizes that seismicity in gas fields is not solely attributed to rapid shearing along faults but involves both slow driven dilatation and fast spontaneous contraction of the pore system. The authors suggest that hydraulic fracturing estimates of the smallest principal stress may be insufficient due to the neglect of fractality in the system. Through triaxial tests and X-ray tomography, the paper reveals the occurrence of fractal patterns of shear bands in sandstone samples, which dominate when the minor quasi-local effective stress exceeds the cohesion. The study also explores the use of neutron beam diffraction to observe changes in lattice plane distances, indicating elastic strains in rock samples. The paper concludes by proposing further investigations involving multi-stage triaxial tests with advanced boundary conditions, seismometry, X-ray tomography, and neutron beam diffraction. The authors believe that such experiments could provide valuable insights into the successions of driven and spontaneous critical phenomena and their underlying mechanisms. The ultimate goal is to improve seismic early warning and calculation models for geotechnical operations involving faults and to better understand rockbursts.

Hettema [2022] presents a practical methodology to assess seismic hazard in low-enthalpy geothermal doublet systems designed for heat exchange in porous and permeable aquifers. The study focuses on the depth range of 1800 to 3300 m, with temperatures in the range of 60 °C to 100 °C, specifically in the context of The Netherlands. The paper aims to determine the probability distribution for

mechanical reactivation along pre-existing weak faults. The geomechanical model is based on the finite element method and includes parameters such as the rock properties (e.g., Young's modulus, Poisson's ratio, density), the fluid properties (e.g., viscosity, density), and the injection and extraction rates. The model includes a representation of the subsurface geology, which is divided into layers of different rock types and properties. These parameters are considered to simulate the deformation of the subsurface and the stress changes that result from fluid injection and extraction. The workflow is demonstrated both for early period operation times and at final thermal breakthrough, and the uncertainty is addressed through probabilistic logic tree analysis quantifying the variation of the four most uncertain input parameters.

A publication by van Eijs et al. [2006] investigates the correlation between hydrocarbon reservoir properties and induced seismicity in the Netherlands. The authors use Bayes' theorem and the Rule of Succession to predict the probability of induced earthquakes in fields with no historical earthquake record. The method uses three key parameters that show a good correlation with the occurrence of earthquakes: pressure drop, fault density of the reservoir, and stiffness ratio between seal- and reservoir rock. The authors have defined four groups of hydrocarbon fields having different probabilities based on the observed correlation between the key parameters and the occurrence of earthquakes. However, the method is inconclusive concerning frequency and magnitude, and the definitions and values in their method need to be updated regularly as more data becomes available or more earthquakes occur. A more detailed critical review of this paper is provided in section 5.1.

The article by Dahm et al. [2017] presents a quantitative approach to distinguish between induced, triggered, and natural earthquakes occurring close to hydrocarbon fields. The authors propose a probabilistic approach that considers the uncertainties of earthquake location and seismicity rate in terms of joint probabilities. The approach involves modeling the Coulomb stress changes induced by hydrocarbon production and using a rate and state-dependent seismicity model to estimate the probability of induced events, while the natural earthquakes are estimated from the tectonic loading. The authors then compare the occurrence probability distributions of earthquakes to distinguish between induced, triggered, and natural earthquakes. The approach is applied to two case studies: the Mw 4.3 Ekofisk 2002 North Sea earthquake close to the Ekofisk oil field and the 2004 Mw 4.4 Rotenburg, Northern Germany earthquake in the vicinity of the Soehlingen gas field. The study found that the Mw 4.3 Ekofisk 2002 North Sea earthquake and the 2004 Mw 4.4 Rotenburg, Northern Germany earthquake were clearly triggered and induced, respectively, while the other earthquakes analyzed were possibly only triggered. The results also showed that the induced seismicity probability increased with the depletion rate of the hydrocarbon reservoir, while the triggered seismicity probability was mainly affected by the stress transfer from nearby faults.

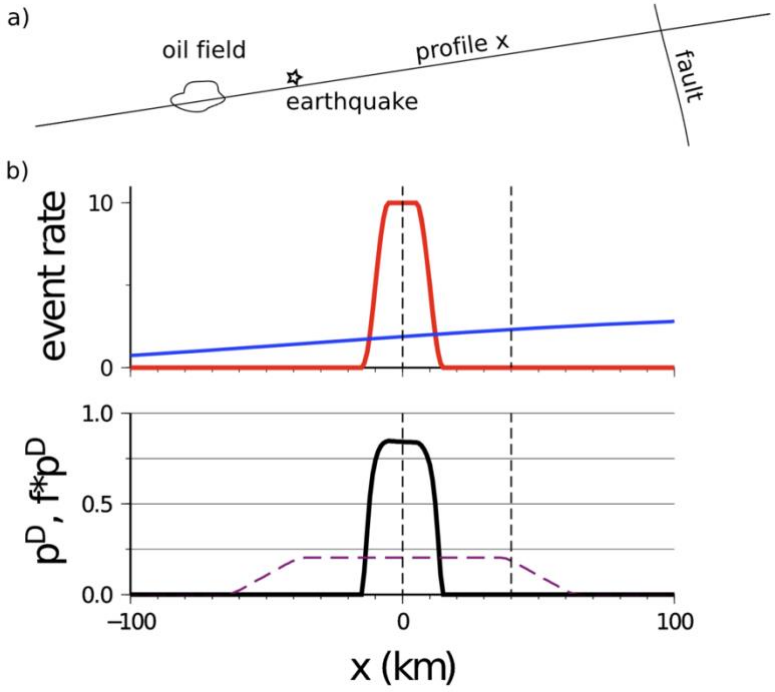

Figure 5. Sketch to illustrate the problem with an earthquake near an oil field and an active tectonic fault. (b) Depletion-induced (red) and tectonic event rates (blue) plotted along the x-profile, along with trigger potential pD and filtered function f∗pD. Figure from Dahm et al. [2017].

Hettema [2020] published an article that provides analytical solutions for fault reactivation mechanics induced by pressure depletion in hydrocarbon reservoirs. The study aims to establish initiation criteria for fault reactivation and determine the critical pressure depletion required for seismicity in gas reservoirs in the Netherlands. The study considers various factors, such as rock properties, fluid properties, reservoir pressure and temperature, and the stress state of the rocks, to determine the critical Coulomb stress required for seismicity to occur as the first necessary mechanical condition for fault reactivation. The study reveals that poro-elastic stressing is more important than differential compaction in determining the critical reservoir pressure depletion for fault reactivation. The results of the study shed light on the reasons for the observed seismicity in the Netherlands being attributed to steeply dipping fault planes. The paper also discusses how the induced shear stress can be caused by fault throw or pressure differences created by sealing faults or boundary faults. Overall, the article provides insights into fault reactivation mechanics and their relationship to reservoir management.

Both previously named publications provide valuable insights into the mechanics of induced seismicity in hydrocarbon reservoirs. While the first paper (Dahm et al. [2017]] emphasizes the importance of understanding the correlation between hydrocarbon reservoir properties and induced seismicity for predicting the occurrence of earthquakes in fields with no historical seismic record, the second paper (Hettema [2020]) highlights the importance of understanding the geomechanical processes that govern fault reactivation induced by pressure depletion. The analytical solutions presented in the second paper can be

used to develop reliable initiation criteria for fault reactivation and to assess the risk of induced seismicity in hydrocarbon reservoirs.

As mentioned in section 2.1.1, the Groningen gas field is one of the largest gas fields in Europe that has experienced induced seismicity as a result of gas extraction. To understand the relationship between gas production and seismic activity, researchers have proposed various models that can be broadly classified into deterministic, empirical, and stochastic models. In their review paper, Kühn et al. [2022] provide an extensive overview of these types of models and discuss their strengths and limitations:

I) Deterministic models: a) Coulomb stress transfer models use physical principles to predict the occurrence and location of seismic events based on the stress changes in the subsurface caused by gas production. b) geomechanical models simulate the deformation of the reservoir and surrounding rock formations due to gas production, and can provide information on the timing and magnitude of seismic events.

II) Empirical models: a) rate-and-state friction models use empirical relationships between the rate of gas production and the rate of seismicity to predict future events. They are based on the concept of rate-and-state friction, which describes the behaviour of faults in response to changes in the stress field. b) statistical models use statistical relationships between gas production and seismicity to predict future events. They consider both the magnitude and frequency of seismic events and can provide probabilistic estimates of future seismicity.

III) Stochastic models: a) epidemic-type aftershock sequence (ETAS) models simulate the random occurrence of seismic events based on the statistical properties of past earthquakes. They consider the cascading triggering of aftershocks by previous events and can provide probabilistic estimates of future seismicity rates. b) Brownian motion models simulate the random movement of particles in response to external forces, and can be used to model the diffusion of stress changes in the subsurface caused by gas production. The authors highlight the need for a multi-disciplinary approach that combines geomechanical, statistical, and probabilistic models to improve the accuracy of predictions and reduce the risks associated with gas production in the Groningen gas field.

One of the physics-based models proposed to understand the relationship between natural gas extraction and induced seismicity at the Groningen reservoir is described in a paper by Dempsey and Suckale [2023]. The paper focuses on forecasting felt seismicity (M>2.5) from February 2017 to 2024. The model considers the injection of gas into the subsurface, which can cause the pore pressure to increase and the rock to expand, leading to stress changes in the surrounding rock and potential seismic activity. The model incorporates a variety of physical processes, including poroelasticity, which describes the deformation of porous materials under the influence of fluid pressure changes; Coulomb failure criteria, which describe the conditions under which a fault will fail and generate an earthquake; and frictional sliding, which can cause fault slip and earthquake activity, to simulate the mechanical behavior of the subsurface as well as the heterogeneity and anisotropy in the subsurface: which can affect the propagation of seismic waves and the likelihood of earthquake occurrence. The researchers used data from the Groningen gas field

to calibrate the model and then tested its predictive power by comparing its forecasts to actual seismic activity. A post-hoc evaluation and forecast update by Dempsey and Suckale [2023] suggested that the model provides accurate forecasts for larger events, but tends to underestimate the likelihood of smaller events.

Another seismological model proposed to understand the relationship between subsurface reservoir volume changes and induced earthquakes is described in a paper by Bourne et al. [2014]. The paper derives a probability distribution for the total seismic moment as a function of time using an evolving earthquake catalog, which is taken to be a Pareto Sum Distribution with confidence bounds estimated using approximations. The paper applies the method to the Groningen gas field and demonstrates that the predicted seismic moment strongly depends on planned gas production. The method utilizes seismic data to estimate the probability of seismic hazard due to changes in the reservoir where fluid extraction occurs. However, it is important to note that the method assumes that the seismic moment is proportional to the total strain in the reservoir.

In another paper, Postma and Jansen [2018] use numerical experiments and an idealized Groningen- like geometry to explore the factors that influence the severity of near-well seismic events following sudden production changes and to determine whether production strategies can avoid triggering them. The authors observe a temporary increase in stress, which induces a slip, following a sudden increase in gas production rate in the Groningen natural gas field. This increase in stress is caused by the time it takes for the pressure disturbance to propagate through the reservoir, inducing a state of relative radial tension and growing shear stress. The authors found this effect is more significant in geological formations with steeper dip angles, higher gas production rates, and lower reservoir pressures. It can also be more pronounced in clusters of production wells. However, compared to the ambient stresses in the subsurface, the increase in stress caused by the production-induced pressure changes is relatively small and insignificant in terms of its contribution to the total stress field. In other words, the increase in stress is not enough to significantly alter the overall stress state in the subsurface. It is unlikely to be the primary factor in causing earthquakes in the Groningen gas field. Other factors, such as the pre-existing state of stress and the properties of the geological faults, are likely to be the primary factors determining whether production-induced pressure changes can trigger earthquakes in the Groningen gas field. The authors suggest that production strategies that avoid rapid changes in production rates can reduce the likelihood of such events.

Candela et al. [2019] developed a model based on the Coulomb rate-and-state friction law, which describes the evolution of fault slip rate as a function of the state variable and the shear stress. The state variable represents the internal condition of the fault, which evolves due to mechanical and chemical processes. The authors also consider the effect of differential compaction, which refers to the fact that the reservoir rock and the overburden rock have different mechanical properties and hence respond differently to changes in stress. This effect can lead to deformation and stress changes that can trigger earthquakes. They find that the spatiotemporal evolution of seismicity in the Groningen field is influenced by both the spatial variability in the induced stressing rate history and the spatial heterogeneities in the rate-and-state

model parameters. The paper also highlights that the Groningen fault system is unsteady and becoming more sensitive to the stressing rate, which can explain the long delay in the seismicity response relative to the onset of reservoir depletion.

Richter et al. [2020] developed a statistical model that describes the relationship between gas extraction and seismicity. The authors begin by analyzing data on the location, magnitude, and timing of seismic events that occurred between 1991 and 2013. They also analyze data on the volume of gas extracted during this period. Based on this data, they develop a statistical model that describes the relationship between gas extraction and seismicity. The authors use a statistical method called "point process modeling" to estimate the rate of seismic events as a function of the volume of gas extracted and the current stress state of the earth's crust. The model also takes into account the fact that seismic events can trigger other seismic events, creating a "cascade" effect. This is modeled using a "Coulomb stress transfer" model, which calculates the stress changes caused by each seismic event and predicts the likelihood of subsequent events. Both the changes of the fluid pressure and of the reservoir compaction are tested as input to approximate the Coulomb stress changes. The authors find that the rate-and-state model with a constant tectonic background seismicity rate can reproduce the observed long delay of the seismicity onset. In contrast, the Coulomb failure models with instantaneous earthquake nucleation need to assume that all faults are initially far from a critical state of stress to explain the delay.

Zöller and Hainzl [2023] combines a statistical analysis of historical seismicity data and geomechanical modeling to predict the likelihood of different levels of seismicity over the remaining operating period of the gas field. The historical seismicity data was used to identify patterns and correlations between seismic events and operational parameters of the gas field, such as the volume of gas produced and the depth of the gas reservoir. The geomechanical modeling was used to simulate the response of the gas reservoir to changes in operational parameters, including scenarios where gas production is reduced or stopped altogether, such as the production rate and the pressure within the reservoir. Despite the overall decreasing earthquake rate resulting from decreasing production volumes, the authors use scenario calculations based on simulated pressure and compaction data to indicate a considerable probability that the maximum expected magnitude in the next 30 years exceeds the maximum observed magnitude from the past 30 years. This finding highlights the importance of continued monitoring and mitigation efforts to manage the risks associated with induced seismicity in the Groningen gas field.

Shapiro [2018] proposes a quantitative measure, called the Seismogenic Index (SI), for forecasting the seismogenic effects of subsurface fluid operations, including both fluid injections and productions. The SI represents the seismogenic reaction of rocks to a unit volume fluid impact and allows for a quantitative comparison of tectonic conditions and fluid operations in terms of their potential to induce earthquakes and produce seismic hazard. The model uses a combination of geomechanical and fluid flow simulations to estimate the pressure changes induced by fluid injections or extractions and their effects on the stability of the surrounding rock formations. The SI is then calculated based on the magnitude of these pressure changes and the properties of the reservoir rocks. The paper also provides estimates of the SI and of the

poroelastic coupling characterizing the Groningen gas field, which is an idealized homogeneous reservoir layer similar to the Groningen field at normal faulting. The presence of production-induced seismicity in the Groningen field indicates a combination of the friction coefficient and of the poroelastic coupling unfavorable for inducing seismicity by injections.

Finally, here we summarize the key takeaways from this section.

- One common approach in geomechanical modeling is to consider permeability changes due to pressure variations. These models account for the dynamic nature of fluid flow and pore pressure changes in the reservoir, which can lead to fault reactivation and seismic events. While these models are effective in capturing the fluid-driven processes, they often overlook other essential factors that contribute to seismicity.
- Another set of models incorporates rate and friction equations to simulate fault slip and shear stress changes during production. These models take into account the mechanical behavior of the rocks and the interactions between fault surfaces. While such models provide valuable insights into the mechanics of faulting, they may neglect the impact of fluid migration and pressure changes, which are crucial drivers of seismicity in some regions.
- Porosity changes and chemical dissolution are yet other important aspects that can influence production-induced seismicity. These models consider the effects of compaction and deformation of reservoir rocks due to fluid depletion, as well as the dissolution of minerals, leading to pore collapse and increased stress in the reservoir. However, they might not fully account for the complexities arising from fluid flow and shear stress variations.
- In practice, no single geomechanical model encompasses all the physical and chemical factors that influence production-induced seismicity. This is understandable since adding more complexity to the model may lead to decreased accuracy and computational challenges. A trade-off between model complexity and accuracy needs to be carefully balanced to ensure meaningful results.
- Furthermore, the heterogeneity of geological settings and the lack of complete data often hinder the development of comprehensive models. Each gas field or reservoir may have unique geological characteristics that require specific considerations, making it challenging to create a universally applicable model.
- Despite the inherent limitations of geomechanical modeling, the presented approaches have significantly contributed to our understanding of production-induced seismicity and the development of safety protocols in gas field operations.

4.2.2 Maximum magnitude

The maximum possible earthquake for the Groningen gas field has been a matter of debate for many years [Muntendam-Bos & De Waal 2013], with estimates among various studies converging around M 4.0 to 4.5 [Zoller & Hainzl 2022; Muntendam-Bos & Grobbe 2022; Beirlant et al 2018], but with values up to 5.4 being mentioned under certain modeling assumptions [Zoller & Hainzl 2022]. It would be

reasonable to assume that the largest possible size for Groningen will also be the upperbound for the smaller Dutch gasfields.

Zoller & Holschneider [2016; 2018], Zoller & Hainzl [2022], and Beirlant et al. [2018] focused on statistical methods to estimate the maximum possible magnitude at Groningen. A few years later, Bourne & Oates [2020] argued that the magnitude-frequency distribution is not a pure power law, but contains a stress-dependent exponential taper, something that lowers the magnitude estimates significantly. However, in 2022, Muntendam-Bos & Grobbe [2022] found no clear evidence that a tappered distribution is a better fit to the limited data.

We also consider the largest magnitude events from prior extraction-related induced cases, for comparison (section 2). The most extreme cases (i.e., Gazli & Coalinga with M_S 7.0 & M_L 6.7, respectively) occurred at tectonic depths and had been argued to be triggered (or even naturally occurring), rather than truly induced. Most of the clear-cut cases of extraction-induced events typically have exhibited events up to M 5.5. Notably, events of magnitude 4 are quite common, even in areas with little tectonic seismicity. For example, the Lacq case in France reported a M_L 4.2 event, the North Sea reported events as large as M_W 4.3, and the German gas fields reported events up to M_W 4.4. The results of the March 2016 workshop on possible maximum magnitudes at Groningen suggested a distribution, partly influenced by the observation of these extraction-induced analogues [Bommer & van Elk, 2017].

4.3 Ground motion modelling

4.3.1 Ground motion prediction models

Once a potential earthquake source is identified, the next step is to estimate how much ground shaking will occur at a given location, based on that source. The probabilistic nature of the ground shaking (Figure 6) is due to the lack of knowledge of all details of the physical process involved and of the seismic wave propagation medium [Gerstenberger et al., 2020]. The primary predictor variables are usually: magnitude, distance to the rupture, and site characterization [Esteva and Rosenblueth, 1964; Boore et al., 1997]. Additional variables may include: style of faulting, depth to top of the rupture, average shear-wave velocity in top 30 m, or depth to a velocity of 1 km/s [Gerstenberger et al., 2020]. Some Ground Motion Prediction Models (GMPMs) may incorporate additional constraints from simulated ground shaking data. Usually the output metrics of a GMPM are spectral accelerations at different periods (e.g., 0.01 to 10s), Peak Ground Velocity (PGV), Peak Ground Acceleration (PGA) or Arias intensity.

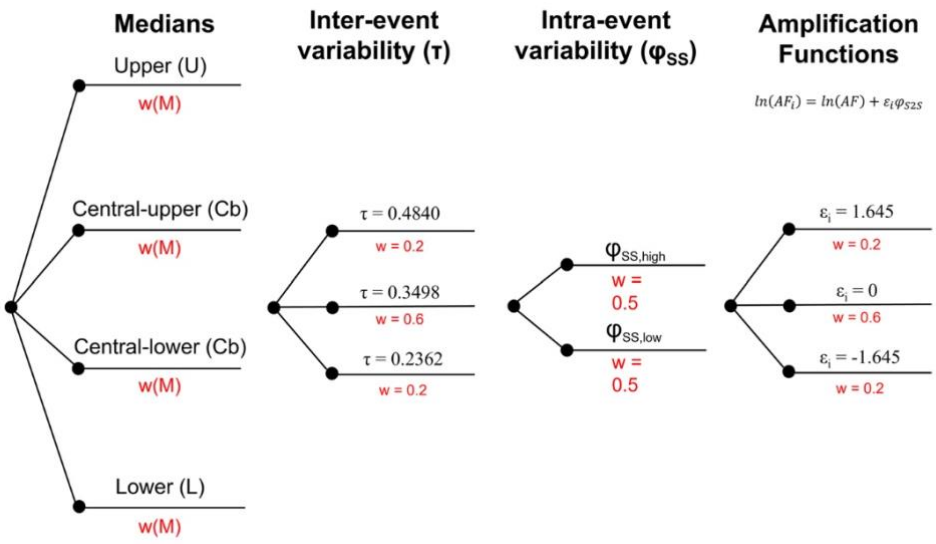

Figure 6. Logic tree for response spectral ordinates for the Groningen GMPM [taken from Bommer et al., 2022a].

GMPMs are inherently limited by the scarcity of data related to large shaking amplitudes and/or near-source recordings. This is particularly challenging for stable continental regions, where low seismicity rates and typically sparse seismic networks exacerbate the lack of data [Gerstenberger et al., 2020]. As far as induced events are concerned, due to their triggering process, they are likely to be of smaller magnitude and at shallower focal depth than typical tectonic earthquakes [Grigoratos et al., 2021]. The focal depths of potentially induced events generally lie within the upper 6 km of the crust, making the seismic wave propagation more dependent on the heterogeneous properties of the uppermost crustal layers [Bommer et al., 2016].

To address these issues, several studies have developed region- or even sequence-specific GMPM for induced seismicity. Here, we do not consider cases of mining-induced seismicity. Novakovic et al. [2018; 2020] and Zalachoris & Rathje [2019] developed GMPMs for Oklahoma (USA); Douglas et al. [2013] for low-magnitude earthquakes from geothermal areas in Europe; Sharma et al. [2013] for the Geysers Geothermal Area (USA), Edwards et al. [2018] for the Basel sequence (Switzerland), Sharma et al. [2022] for the St. Gallen sequence (Switzerland), and Cremen et al. [2020] for the Preston New Road HF sequence (UK). To our knowledge, the only GMMs developed based on data related to fluid-extraction, are based on the Groningen datasets [Bommer et al. 2016; 2017; Paolucci et al. 2020; Ruigrok et al. 2022; Bommer et al. 2022ab].

Notably, when Cremen et al. [2020] tested the model by Douglas et al. [2013] against the Preston New Road data, the fit was not satisfactory despite the broad similarities in magnitude range, focal depth and tectonic setting. Furthermore, Grigoratos et al. [2021] demonstrated that even relations developed from similar datasets can exhibit very different attenuation functions (Figure 7). Therefore, it is very difficult to confidently select a GMPM unless it can be re-calibrated or at least tested against local data.

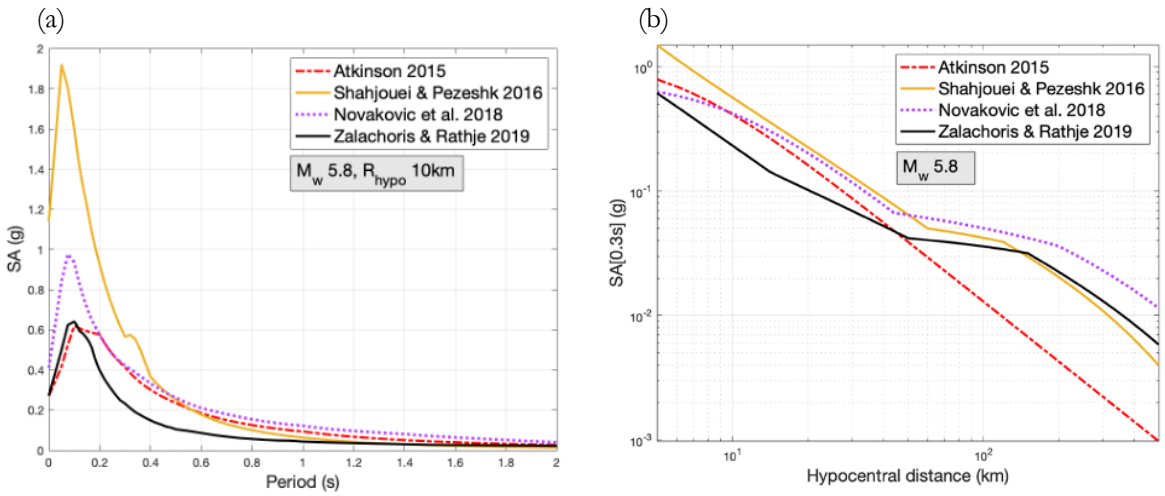

Figure 7. Comparison of GMPMs for Mw 5.8, 5 km focal depth and Vs30 = 760 m/s: (a) 5% damped pseudo-acceleration response spectra at 10 km hypocentral distance (Rhypo) and (b) attenuation of SA (0.3 s) with distance. Taken from Grigoratos et al. [2021].

This is the reason why the studies dealing with the seismicity in Groningen developed their own GMPMs [e.g., Bommer et al. 2016; 2017; Paolucci et al. 2020; Ruigrok et al. 2022; Bommer et al. 2022ab], and even updated them as new data were becoming available. Notably, v7 and v6 of the GMPM for Groningen have significant differences in the resulting SA values, especially at low periods, despite being conceptually similar in their framework [Bommer et al. 2022b]. Ideally, we would like to see greater stability between sequential updates. The v7 model predicts 5% damped horizontal acceleration response spectra at oscillator periods between 0.01 and 1.5 seconds for magnitudes from M_L 2.5 to about 7.3 and rupture distances ranging from the epicentral location of Groningen earthquakes to distances of around 40 to 50 km. The predictions account for nonlinear site amplification effects through a zonation map and associated frequency dependent amplification factors (Figure 8). The reference rock-horizon is at 800 m depth, with a reference shear-wave velocity of about 1400 m/s. The GMM is defined in terms of a logic-tree that captures the epistemic uncertainty in the predictions, particularly at the larger magnitudes currently considered in the hazard and risk calculations. The authors clarified that "the model cannot be applied outside the boundary of the [Groningen] gas field plus a 5 km buffer onshore". That said, the alternatives have critical drawbacks as well; the latest (tectonic) GMMs developed for the SERA (Seismology and Earthquake Engineering Research Infrastructure Alliance for Europe) project did not use any Dutch data as input (Figure 9).

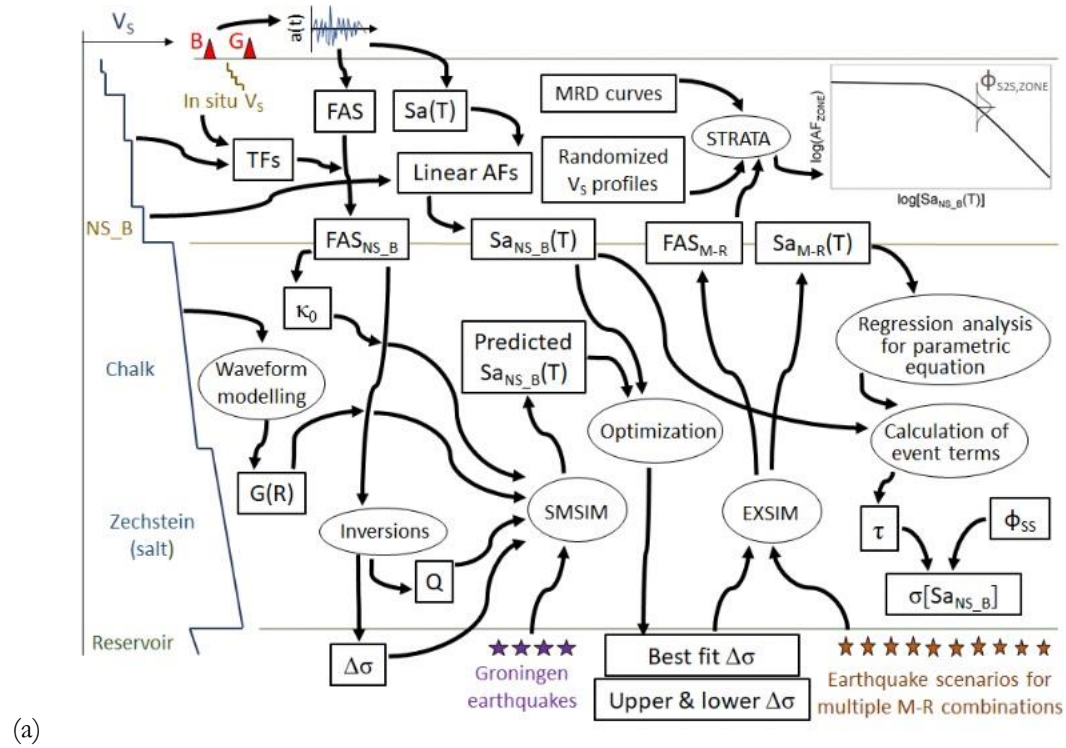

(a)

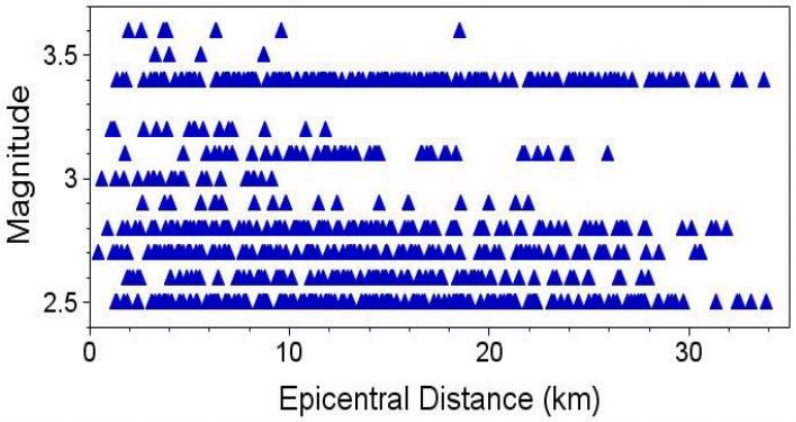

(b)

Figure 8. (a) Schematic illustration of the derivation of the V7 GMM for Groningen; (b) magnitude-distance distribution of the Groningen ground-motion database [both figures from Bommer et al., 2022b].

To deal with uncertainties, it is common practice to combining multiple GMMs via logic trees [Bommer & Scherbaum, 2008; Bommer, 2012]. As explained in Gerstenberger et al. [2020], in practice, this approach begins with the selection of suitable GMMs by first applying a criteria of quality assurance [Cotton et al., 2006; Bommer et al., 2010]. Next, performance tests of the GMMs with respect to a dataset provide quantitative ranking of the models [e.g., Scherbaum et al., 2009]. Sensitivity analyses and expert elicitation [e.g., Delavaud et al., 2012] can provide a final logic tree structure for GMMs. That said, recent studies [e.g., Mak et al., 2014] have highlighted the inconsistency of a pure data-driven approach, in particular with a lack of independency of the data or incomplete (or biased) datasets that may favor one model over another [e.g., Ghasemi and Allen, 2017].

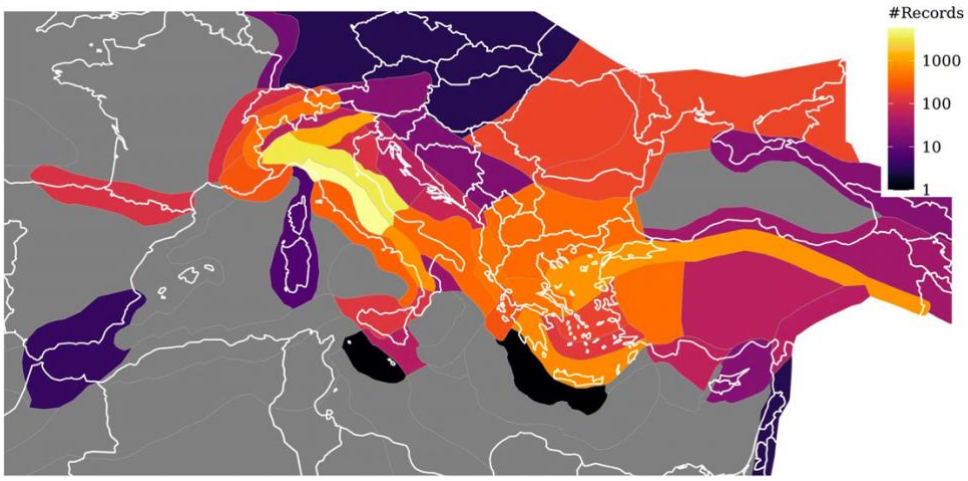

Figure 9. Number of records in each of the 46 attenuation regionalisation polygons used for the calibration of the latest European GMM used in the SERA project [from Kotha et al., 2020].

Beyond the use of multiple GMPMs, the scaled backbone approach [Bommer, 2012; Atkinson and Adams, 2013; Atkinson et al., 2014a; Douglas, 2018] provides an alternative for handling the wide range of uncertainties. In this approach, one GMPM is typically used to generalize the attenuation and magnitude-scaling behavior required for a specific tectonic region type for a range of magnitudes and distances. As explained in Boore et al. [2022], the selected backbone model is first adjusted to match the earthquake source and path characteristics of the target region, and then it is separately adjusted to account for the site-specific geotechnical profile. For a GMPM to be amenable to such host-to-target adjustments, the magnitude scaling of response spectral ordinates should be consistent with the theoretical scaling of Fourier amplitude spectra. In addition, the influence of individual source and path parameters should be clearly distinguished in the model to allow the adjustments to be applied individually, and reliable estimates of the source and path parameters from the host region of the GMPM should be available, as should a reference rock profile for the model. Using data analysis and judgment, upper and lower alternatives about the central GMPM are defined to capture the epistemic uncertainty of a representative suite of published GMPMs. A referenced backbone model allows tuning the size of the alternative branches while preserving statistical independence of the newly predictive models. This approach is gaining ground in recent years and its implementation details are outlined in Boore et al. [2022].

4.3.2 Ground shaking intensity

Ground Shaking Intensity Prediction Models (GSIPMs) have been developed to estimate Intensity Scales (e.g. modified Mercalli intensity (MMI)) expected for a given set of earthquake parameters and site distances. Unlike other intensity measures such as spectral acceleration or peak ground acceleration (PGA), MMI depends solely on observations, such as felt intensities and structural damage [Wood and Neumann, 1931]. Due to their empirical and generic nature, GSIPMs cannot be paired with specific exposure and fragility models, nor do they explicitly account for soil amplification. Therefore, the dataset used in their regression is a key factor for their applicability.

Popular GSIPMs have been developed by Atkinson & Wald [2007], later revised by Atkinson et al. [2014b], focusing on North American data above M 3. Allen et al. [2012] developed a globally applicable GSIPM based on earthquakes with Mw > 5 for active crustal regions. Ahmadzadeh et al. [2020] developed an GSIPM for Iran, Le Goff et al. [2014] one for Portugal, and Dowrick & Rhoades [2005] one for New Zealand. None of the aforementioned GSIPMs is easily applicable to very shallow small-magnitude earthquakes in a low seismicity region like the Netherlands. A better fit would be the GSIPM by Teng et al. [2021], which is based on likely-induced earthquakes from Texas, Oklahoma and Kansas, with magnitudes between M 1.5 and 3.5 and hypocentral distances within 30 km. Alternatively, one could compute PGV or PGA estimates using an applicable GMPM for the Netherlands [e.g., Bommer et al. 2022], and then convert those to MMI using the conversion-relations of Schultz et al. [2021c], originally derived for Central and Eastern US.

4.4 Site-response analysis

4.4.1 Introduction

The variability in the near-surface geology is well known to have a strong influence on the level of amplification of seismic ground motion during an earthquake. The presence of low seismic velocity sediments overlying stiffer bedrock, especially near the surface, modifies earthquake ground motions by affecting amplitudes and frequency content. This phenomenon is referred to as seismic site response or site effects and is critical when assessing seismic hazard levels in a given area. Amplification effects resulting from site effects have been observed and studied after multiple earthquakes, including the 1985 Mexico City earthquake [Bard 1988] and the 2010 Darfield earthquake in New Zealand [Bradley, 2012], as well as in densely populated regions such as Tokyo and Los Angeles [Bonilla et al., 2011; Hartzell et al., 1996]. This issue of near-surface effects on earthquake ground shaking is globally recognized, and several methods have been established to investigate these effects.

This section provides a literature review of state-of-the-art research on site response and soil amplification in Europe and the Netherlands. Firstly, the description of how site response is included in the European seismic hazard reference model is presented. Then, developments on site response and soil amplification in the Netherlands are discussed, including the digital geological model, a nationwide site response zonation map, seismic methodology to estimate site response, amplification of compressional waves, and a brief review of studies on liquefaction potential.

4.4.2 State-of the art on site response in Europe

The determination of site response heavily relies on the knowledge of shear wave velocities and lithological conditions in the shallow subsurface. However, direct measurements of these factors are usually sparse. To estimate site response, many studies employ site-specific response analysis through Ground-Motion Prediction Equations (GMPEs), as demonstrated by Bommer et al. [2017] and Kruiver et al. [2017]. These models use site terms derived from global data sets such as Akkar et al. [2014] and Bindi et al. [2014], which condition the equations on the average shear wave velocities of the top 30 meters of the subsurface (Vs30). Consequently, only average levels of site response can be obtained for a given Vs30 class. However,

studies [Derras et al., 2017; Lee and Trifunac, 2010; Stewart et al., 2014] have highlighted that using only Vs30 as a proxy for site response is insufficient, as it does not account for resonances due to high impedance contrasts or only considers shallow Vs intervals that might correlate with amplification.

In recent years, national and international projects have been undertaken to establish standards and guidelines for individual parameters related to seismic site characterization (e.g., Foti et al., 2018; Crow and Hunter, 2015; SESAME project: http://sesame.geopsy.org; and Consortium of Organizations for Strong Motion Observation Systems, http://www.cosmos-eq.org). However, as there is no European standard for site characterization analysis, the SERA project (Seismology and Earthquake Engineering Research Infrastructure Alliance for Europe; http://www.sera-eu.org) was initiated in 2017. SERA aimed to mitigate the risk posed by natural and human-induced earthquakes and has resulted in a revised European seismic hazard reference model and a framework for seismic risk modeling at a European scale. On the website there is an extensive list of deliverables (http://www.sera-eu.org/en/Dissemination/deliverables/). For site response guidelines, the following deliverables are recommended:

- D7.2 best practices for site characterisation
- D7.4 improvement site indicators
- D26.4 method for estimating site effect in city-based risk assessments.

To ensure a reliable site characterization, SERA has identified a set of mandatory indicators including the fundamental resonance frequency (f0), S-wave velocity profile (Vs(z)), VS_{30}, depth of seismological and engineering bedrock, surface geology, and soil class. Additionally, SERA has developed a quality metrics strategy to evaluate the overall quality of site characterization analysis. With this list of indicators, SERA has adopted an approach that surpasses the traditional use of averaged shear-wave velocity over the top 30 meter (VS_{30}) as proposed by Allen and Wald (2009), which has been found to have shortcomings [Weatherill et al., 2020, 2023]. Another outcome of the site characterization analysis workflow is the repository created by Weatherill (2023), which includes the exposure to site tool used to construct site amplification files for a given exposure model configuration as applied in the European Seismic Risk Model [ESMR20, https://gitlab.seismo.ethz.ch/efehr/esrm20_sitemodel].

The ESMR20 provides additional information on the local site condition across all of Europe, and subsequently determines its influence on the prediction of seismic ground motion. The approach adopted for characterising the ground motion at the surface is specifically defined for application in a probabilistic seismic risk context. It ensures that for every 30 arc-second cell in Europe we are able to, in some way, account for local site effects and we do so in a manner that is consistent with the GMM adopted for shallow seismicity in the ESMR?20.

4.4.3 HVSR for site characterization

Assessing earthquake damage requires detailed records of ground motion, but these records are not always available. Moreover, developing a detailed ground-motion model requires extensive knowledge of geomechanical and sedimentary properties at a specific site, which can be challenging to obtain and vary from site to site. However, various studies have shown that the HVSR (horizontal-to-vertical spectral ratio)

of ambient seismic recordings can indicate the subsurface features and local variations of a given area, as it exhibits a peak across a frequency range where seismic wave amplification occurs [Nakamura, 1989, 2019; Bonnefoy-Claudet et al., 2006; Fäh et al., 2001]. This peak frequency is typically interpreted as the fundamental resonance frequency of the soft sediments at a site, which is linked to the elastic impedance contrast in the subsurface with stiffer material. Therefore, the microtremor HVSR can be used as an indicator for site response assessment [e.g., Molnar et al., 2018; Perron, 2022; Bonnefoy-Claudet et al., 2009; Chieppa et al., 2020, Falcone, 2021]. While HVSR amplitude values can approximate the ratio of S-wave and P-wave amplification spectra [Herak, 2008], they tend to underestimate the actual level of site amplification and cannot be directly used to approximate the levels of S-wave amplifications [Zhu et al., 2020]. Arai and Tokimatsu [2004a] proposed a method to estimate the S-wave velocity profile at specific sites by inverting the HVSR amplitude spectrum and resonance frequencies of microtremors, which is now widely used as a simple approach to seismic three-component surveys [van Noten, 2022; Spica et al., 2017; van Ginkel et al., 2020].

4.4.4 Developments on site-response analysis in the Netherlands

The unconsolidated top sedimentary layer is a major concern throughout the Netherlands due to the increased risk of building damage from earthquake amplification. Currently, only for the Groningen region, significant efforts are made to evaluate site response as part of seismic hazard and risk resulting from gas extraction. Thus, in regions that are not currently monitored or affected by seismic activity, additional observations are needed to gain knowledge about site response. In recent years, the high-resolution 3D geological subsurface models, GeoTOP [Stafleu et al., 2011, 2021] and NL3D [Van der Meulen et al., 2013], have become available digitally from the web portal of TNO – Geological Survey of the Netherlands (GDN; https://www.dinoloket.nl/en/subsurface-models/map). GeoTOP provides a representation of the shallow subsurface in the Netherlands, with voxels measuring 100m by 100m by 0.5m (x, y, z) up to a depth of 50m below ordnance datum. Each voxel includes an estimate of the lithostratigraphic unit it belongs to and the representative lithologic class. GeoTOP was constructed using around 275,000 borehole descriptions from the national Dutch subsurface database operated by GDN, and is continuously updated with new subsurface data.

4.4.4.1 Site response in Groningen

Multiple versions of a large, multidisciplinary project have been developed to construct a Groningen Ground-Motion Model (GMM), which aims to estimate the level of induced seismic hazard [Bommer et al., 2016, 2017b, 2019]. To provide information for the seismic hazard assessment, the GMM includes a detailed analysis of the local and geology-dependent site response, including amplification factors and estimates of shear-wave velocity. Kruiver et al. [2017a] developed a regional shear-wave velocity model from the surface down to 800 meters, forming the basis for a seismic microzonation of the Groningen gas field. Subsequently, Kruiver et al. [2017b] constructed a "Geological model for site response in Groningen," consisting of a microzonation based on the GeoTOP grid cells. Using this model, Rodriguez-Marek et al.

(2017) developed a field-wide zoning of frequency-dependent nonlinear amplification factors. Additionally, a SCPT campaign was undertaken in Groningen to determine the V s30 adjacent to each borehole in the B- and later the G-network. These detailed shear-wave velocities reduce the uncertainties in the GMM (Kruiver et al., 2021; Noorlandt et al., 2018). The GMM is specifically designed for the seismic hazard induced by earthquakes in the Groningen gas field region and cannot be directly extrapolated for seismic hazard assessment and site-response estimations throughout the Netherlands, because of the strong lateral variations in the subsurface geology.

The GMM used the base of the North Sea Group (NSG) as reference rock horizon and amplification is computed from that depth level. However, the base of the NSG is variable throughout the Netherlands. Earthquake transfer function from the seismic borehole data analyzed by van Ginkel et al., [2019, 2022a, 2022b] showed that most of the wave amplification takes place in the top 50 m, especially with very soft Holocene clay and peat overlying stiffer Pleistocene sands. Hence, a shallower reference horizon and corresponding velocity has been determined to compute amplifications factors from. At 200 m there is a homogeneous sand formation across the Netherlands, from which the seismic velocities (500 m/s) are computed based on the borehole seismic data.

Dwelling mounds (~900 exist), which were constructed in ancient times to defend against floods in the Northern Netherlands, are significant in terms of seismic risk because several populated village centres are located on them. To assess the impact of these mounds on ground shaking during earthquakes, Kruiver et al. (2022) presents a dynamic site-response analysis to determine the modification of ground shaking due to the presence of the mound. A scheme has then been developed to incorporate the dwelling mounds into the risk calculations, which included an assessment of whether the soil-structure interaction effects for buildings founded on the mounds required modification of the seismic fragility functions. Additionally, Groningen is bounded by dikes to protect against the Wadden sea; however, no ground motion studies of these structures exist.

Although the majority of site-response and soil parameter characterization for ground-motion studies focus on the Groningen region [e.g. Kruiver et al., 2022; Kruiver, 2017a,b; Ntinalexis et al., 2022; Ruigrok et al., 2022, van Ginkel et al., 2019], this phenomenon is arising throughout the country. Gariel et al. [1995] quantified ground motion variations based on Green's functions and spectral ratios of aftershocks from the 1992 earthquake in Roermond. They observed a variety in peak ground acceleration attenuation over different stations, which could point to a site effect of laterally varying shallow sedimentary deposits. [TNO 2016] conducted several studies on the seismic hazard caused by induced earthquakes, including a site-response map that identifies three types of soils (stiff, weak, and special study). The weak soil and special study soil have assigned amplification factors of 1.5 and 2.0, respectively, while stiff soil is considered to have no amplification. This map covers regions in the north and west of the Netherlands.

4.4.4.2 Seismic site-response map for the Netherlands

Van Ginkel et al. [2022] developed a nation-wide zonation map to predict seismic site response, using lithological sequences as proxies (Figure 10). They analyzed earthquake and ambient seismic vibration

records at 69 stations of the Groningen borehole network to obtain empirical relationships for amplification. They applied earthquake and ambient vibration frequency band-pass filtering in the range of 1-10 Hz based on shallow subsurface resonance frequencies and earthquake amplitude spectra. From the Groningen empirical relationships, they showed that the HVSR approach is a simple way to determine the amplification potential for most subsurface conditions in the Netherlands. In a second stage, they determined the HVSR curves for an additional 46 surface seismometers throughout the Netherlands and calculated the subsequent peak amplitudes. These peak amplitude distributions were related to specific lithological profiles and amplification factors. With this knowledge of the amplification potential of different lithological sequences, they designed a classification scheme, which was a useful tool to translate geological models into five classes and establish a nation-wide site-response zonation map. Most classes have an AF_{NL} assigned to which values can be added to input seismic responses that conform to the reference seismic bedrock conditions.

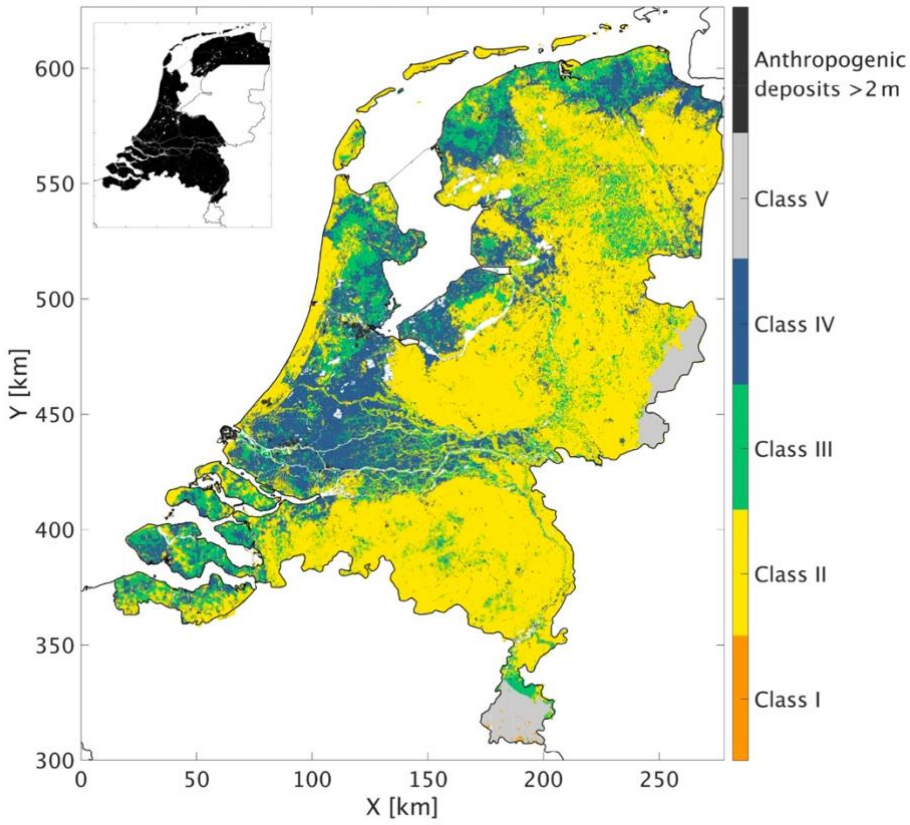

Figure 10. Seismic site-response zonation map for the Netherlands designed for low-magnitude induced earthquakes. Each color represents a class with an amplification factor assigned. ©KNMI, from van Ginkel et al. [2022].

Class I represents sites with a hard rock setting, which are only found in the southern and eastern parts of the Netherlands. These locations are assigned an amplification factor (AF) of 1, indicating no amplification. Class II is associated with sites having Pleistocene sediments without strong impedance

contrasts in the near surface. Small amplification is expected at these sites. Class III includes sites with relatively soft sediments (clays, sandy clays, loess) overlying stiffer sands, resulting in impedance contrasts in the near surface. Class IV is mostly related to very soft and unconsolidated Holocene clay and peat successions overlying stiffer sands, forming a strong impedance contrast. These sites experience the largest amplification, with an AF of 4.5. Class V comprises sites where the bedrock occurs shallower than 100 m, which is uncommon in the Netherlands. Insufficient data exists to assign an amplification factor.

The zonation map is not applicable to regions with strongly deviating lithological sequences, or for earthquakes with very strong low-frequency ($f < 1.0$ Hz) shaking. In this study, site-response is assessed as a linear process, since the earthquake magnitudes are too low to generate non-linear site effects.

4.4.5 Compressional wave amplification

Van Ginkel et al. [2022] presents an interdisciplinary approach that involves detailed geological and geophysical analyses to assess the potential for local amplification of compressional-wave (P-wave) in shallow, unconsolidated sediment settings. The study empirically and analytically demonstrates that vertical ground motion amplification occurs especially at sites with low P-wave velocities. The influence of shallow local geology is also observed, with peat-generated gas impacting the P-wave velocities. The study identifies P-wave amplifications (up to a factor of 2.7) primarily in the eastern part of the Groningen study area, where large industrial facilities are present. The authors conclude that since the amplitude distribution of vertical ground motion amplification differs from that of horizontal ground motion amplification, the former cannot be treated as an average percentage of the latter for low magnitude earthquakes at shallow depth. Unconsolidated sediments with low P-wave velocities can lead to significant P-wave amplification, and this should be taken into account when developing predictive ground motion equations.

4.4.6 Liquefaction potential

Korff et al. [2016] has developed a geological model for liquefaction in the Groningen province, utilizing CPT, GeoTOP, and various other sources. The model includes maps that define the extent of geological units containing sand, a detailed description of the known properties of the sand within these units, and an analysis of the total and relative sand densities. This information allows for the assessment of which geological units are most susceptible to liquefaction based on their relative density, and where and how deep these potentially susceptible areas occur.

Green et al. [2019] and Green and Bommer [2018] applied the liquefaction triggering potential to the specific conditions of the Groningen field and embedded it into a fully probabilistic assessment of liquefaction triggering hazard [Green et al., 2020]. They found that liquefaction is a very minor hazard and effectively negligible in contributing to induced seismic risk for the Groningen-specific setting. Their study concludes that earthquakes as small as moment magnitude 4.5 can trigger liquefaction in extremely susceptible soil deposits, which are typically areas such as mudflats outside dikes, riverbeds, impoundment areas, or tailings ponds where building construction is not viable.

4.5 Exposed assets

When conducting any type of risk analysis, it is important to understand which assets are exposed to the seismic hazard. These assets can be, for example, residential or industrial buildings, special buildings (e.g. schools, hospitals), or critical infrastructure (e.g. bridges, pipelines, energy plants, dams). Each asset has its own fragility against seismic loads and its own replacement cost. In theory, individuals are also exposed assets, although their vulnerability is dependent on the structure they reside at the time of the earthquake. These assets are aggregated at different spatial resolutions depending on the data-availability. Notably, the spatial resolution itself can have an impact on the loss estimates [Dabbeek et al., 2021].

The state-of-the-art for risk exposure models in Europe was developed within the SERA project [Crowley et al., 2020]. Version v0.1 of this model has been integrated within the Global Earthquake Model's global exposure and risk maps [Silva et al., 2020]. All development versions of the European Exposure Model are being made available on a GitLab repository (https://gitlab.seismo.ethz.ch/efehr/esrm20_exposure1). A literature review of previous attempts at creating national, European or global building inventories can be found within Crowley et al. [2020]. The SERA model is based on the European FP7 NERA project [Crowley et al., 2012]. SERA updated the NERA database with more recent census data and mapping schemes created by local experts. It also expanded to include non-residential (commercial and industrial) buildings. The buildings in the exposure model are classified according to their seismic performance using a building taxonomy that is based on an updated version of an international standard (the GEM Building Taxonomy, Brzev et al., 2013, as updated by Silva et al., 2018) that allows buildings to be classified according to a number of structural attributes. The main attributes that have been selected for the consistent definition of building classes across Europe are as follows:

- Main construction material (e.g. reinforced concrete, unreinforced masonry, reinforced/confined masonry, adobe, steel, timber).
- Lateral load resisting system (LLRS; e.g. infilled frame, moment frame, wall, dual frame-wall system, flat slab/plate or waffle slab, post and beam).
- Number of stories.
- Seismic design code level (CDN: pre-code, CDL: low code, CDM: moderate code, CDH: high code).
- Lateral force coefficient used in the seismic design.

Non-residential buildings fall into two broad categories: light industrial buildings (manufacturing, mining, quarrying, and construction sectors) and commercial buildings (offices, wholesale and retail trade, and hotels and restaurants). The distribution of the non-residential buildings across the most likely building classes has also been developed for each country. For the Netherlands, most of the data are updated to the year 2017, and include: 4.8 million residential buildings, 0.4 million non-residential buildings, 2.5 trillion

Euros total replacement cost and 17.8 million population. This exposure model does not include information on critical infrastructure, roads, bridges, or dykes.

4.6 Structural fragility and vulnerability

Any regional risk assessment model assigns to each class of structure in its inventory a specific fragility (or vulnerability) curve that estimates the probabilistic distribution of damages (or direct economic losses) that this structure is expected to experience when subject to ground motions of different intensity. For the damages, modelers use standardized damage-states as labels, with typical cases being "light-damage", "significant damage", "heavy damage", and "collapse". The economic losses are measured in terms of loss ratio, which is defined as the ratio of cost of repair to cost of replacement. Indirect economic losses (such as business interruption or economic disruptions) are more difficult to model and are often neglected, even though they can be very important [Sousa et al., 2022; Markhvida & Baker, 2023]. The IMs are usually related to the fundamental period of the structure [Silva et al., 2019], for example 5% damped pseudospectral accelerations (SA) at 0.3s.

In recent years, GEM has developed an extensive suite of fragility and vulnerability functions [Martins & Silva 2020; Martins et al., 2021; https://github.com/lmartins88/global_fragility_vulnerability] for all the building typologies they used in their global seismic risk model [Silva et al., 2020]. Nearly five hundred functions were developed to cover the majority of combinations of construction material, height, lateral load resisting system and seismic design level. The fragility and vulnerability were derived using nonlinear time-history analyses on equivalent single degree-of-freedom oscillators and a large set of ground motion records representing several tectonic environments [Martins and Silva, 2020].

We should note that most fragility and vulnerability functions were developed for large (tectonic) events, at least larger than magnitude 5, and hence they might be biased towards higher loss estimates, compared to the short duration and high frequency content of induced motions. In general, these functions also ignore damage accumulation effects that might occur when buildings are subjected to a series of earthquakes [Papadopoulos et al., 2020].

Luckily, due to the extensive studies conducted for Groningen, there are several fragility functions available for typical Dutch buildings. A few key studies are outlined below.

Malomo et al. [2021] examined the impact of ground floor openings on the dynamic response of typical Dutch URM cavity wall structures. They developed numerical models that were calibrated against a shake-table test of a full-scale building specimen, tested up to near-collapse. They found that ---the presence of large ground floor openings may significantly increase the seismic vulnerability of typical URM Dutch terraced houses.

Korswagen et al. [2022] conducted an experimental testing campaign oriented towards the initiation and progression of light damage of replicated clay brick masonry walls. Based on these tests, calibrated finite element models were produced to simulate the effect of earthquake ground motion on a variety of initial conditions, wall geometry, material properties, and number, type and intensity of earthquakes. The results are used to produce fragility curves for these types of walls. The curves show that

visible damage, with cracks wider than 0.1 mm, appears, with a 10% exceedance probability, at 13 mm/s of peak ground velocity; but, if the masonry had already undergone some light, yet imperceptible damage, a PGV of 6 mm/s was sufficient to aggravate it into visible cracks.

Grant et al. [2021] produced collapse fragility curves for SA (1.5s) for various configurations of Dutch unreinforced masonry terraced houses. They used detailed 3D numerical models of the structures, running time-history analyses on the finite-element software LS-DYNA.

Kallioras et al. [2019] performed a numerical study aimed at extending the utility of a shake-table test on an unreinforced masonry building prototype for the seismic assessment of terraced houses in the Groningen region of the Netherlands. The structure represented the end-unit of a typical Dutch terraced building with cavity walls and a flexible timber roof. They also derived fragility curves (Figure 11) for the given buildings-type, for PGA, modified Housner intensity, SA at the fundamental period of the building, and Arias intensity. For example, the earthquake of 2012 near Huizinge, produced shaking with maximum recorded PGA equal to 0.084 g. At these intensities, the fragility curves they derived suggest that for the terraced house model the probability for damage exceeding DL1 (i.e., onset of slight structural damage) is between 1 and 45%, respectively. Meanwhile, the authors claim that in the aftermath of that earthquake, "damage surveys in local buildings revealed no significant damage other than hairline cracks on walls and slight damage to plaster". That said, other claims mention cracks and very limited structural damages.

Sarhosis et al. [2019] addressed whether small and sometimes invisible plastic deformations prior to a major earthquake affect the overall final response if masonry buildings, examining available experimental and numerical data reported in the literature. They found that in relatively large acceleration levels, residual deformations become evident especially for the in-plane motion. Much fewer residual deformations were observed in the case of out-of-plane direction, possibly due to the re-centering ability of the slender walls used in the terrace houses in the Groningen gas field.

Crowley et al. [2019] developed fragility curves for various Dutch building types (URM, RC, steel, timber) for slight non-structural, slight structural and moderate structural damage. Fragility functions for non-structural damage are PGV-based and have been developed considering the observed damage from damage reports (rather than from damage claims). The curves for structural damage have been estimated using analytical models and are anchored on more complex IMs. This study does not always provide clear numerical results, with the quality of figures also varying to a certain degree. Edwards et al. [2021] seem to have employed the same fragility functions for detached and terraced masonry houses and light steel frame buildings.

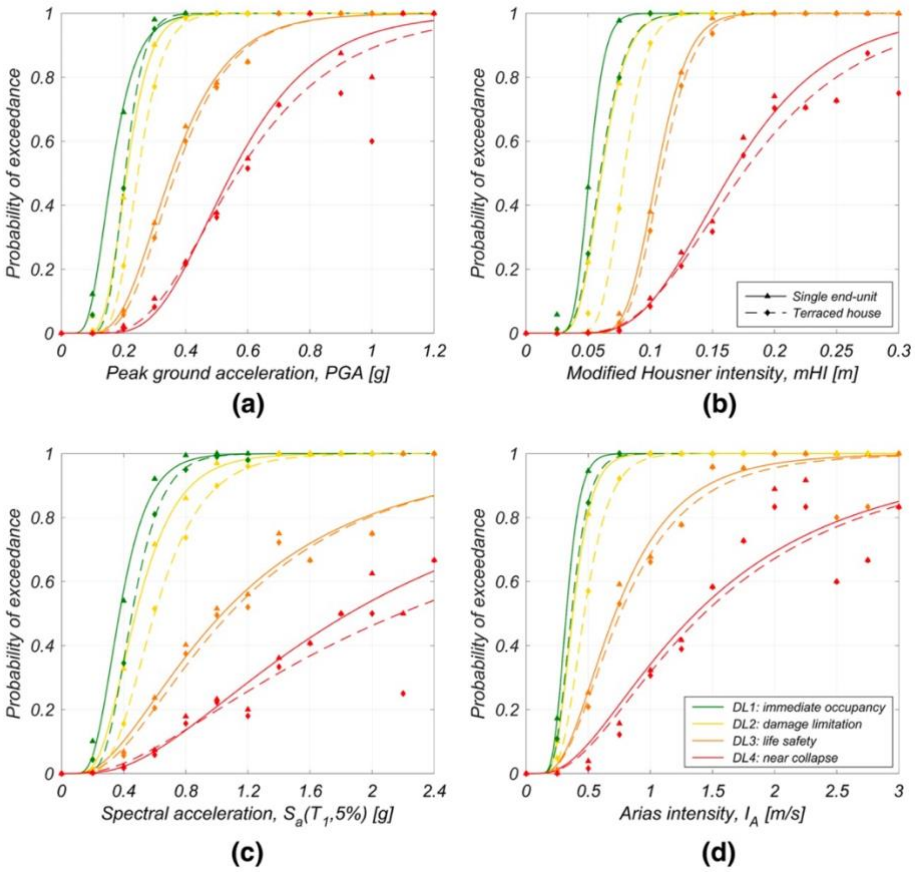

Figure 11. Observed fractions of exceedance and fitted fragility curves as a function of: (a) PGA; (b) modified Housner Intensity; (c) Sa(T1,5%); and (d) Arias Intensity. Comparison between a single end-unit (solid lines) and a terraced house (dashed lines). Figure from Kallioras et al. [2019].

Crowley et al. [2017] describe experimental and analytical activities that were carried out to develop fatality and consequence models for the estimation of 'Inside Local Personal Risk' (ILPR) of buildings within the Groningen field. To estimate the collapse potential of buildings in Groningen, structural numerical models are subjected to increased levels of ground shaking to estimate the probability of collapse, and the associated consequences are estimated from the observed collapse mechanisms, in particular translating the area of debris into a probability of loss of life inside the building. Following a number of crude assumptions, the ratio of the area of debris to floor area gives an estimation of the probability of an occupant being trapped/hit by debris. This study only provides qualitative estimates and not usable consequence functions. More information can be found in Crowley & Pinho [2020].

Finally, a recent study by Tasiopoulou et al., [2019] concluded that for all scenarios under consideration, the Groningen levee/dykes crest settlements remain well below the allowable limits. As far as pipelines are concerned, Kruse & Hölscher (2010) found that the seismic risk to pipelines in the northern part of the country is small (lower than 1 damage per 1000km of pipeline).

4.7 Computational methods

In this section we will describe how regional probabilistic seismic risk assessment studies are performed using a stochastic Monte Carlo based approach [Barbat et al., 1996; Cramer et al., 1996; Crowley and Bommer, 2006]. In case of scenario-based (deterministic) analyses, the stochastic catalog described below is of course a lot simpler and includes only a handful of earthquakes, which in any case are usually processed separately, rendering the book-keeping process described below trivial.

It is customary to simulate many realizations (e.g. 10000) of next year's mainshock seismicity employing a memoryless Poissonian recurrence model under a Monte Carlo approach. The collection of simulated realizations of future seismicity years is often loosely called a stochastic catalog. Each event in the stochastic catalog is described by the geometry of the rupture, its focal mechanism, its magnitude, and by its time of occurrence within the simulated year [Cramer et al., 1996]. Then, for each simulated rupture one generates many random fields of ground motion intensity measures (IMs) that are relevant to the prediction of response [Kohrangi et al., 2016] and, therefore, of the damage that may be experienced by the structures exposed to the earthquake threat [Crowley and Bommer, 2006]. The random fields are then used as input to the fragility model to estimate the damage severity that any given structure may suffer when subject to the level of IM as predicted by the given random field at the structure's location for the given rupture. Next, for each rupture and IM random field, the loss for the entire affected portfolio of structures is estimated by simply summing the losses predicted for each structure (given its damage state and value) in the footprint of the random field. This procedure is repeated for all random fields of each simulated rupture. Finally, the rate of exceeding any portfolio loss is empirically found by keeping track of the number of exceedances occurring over all the simulated realizations. This general approach to estimate earthquake risk to portfolios of structures at a regional level still holds for the case of induced seismicity but, given to the peculiarities of the phenomenon, some modifications may be appropriate, especially in order to ensure that the traditional Poissonian recurrence models are valid (Gupta and Baker 2019; Grigoratos et al. 2021]. This approach also allows for implementation of spatial correlation between ground shaking at multiple sites from the same earthquake [Jayaram and Baker, 2009], due to common source and wave traveling paths and to similar distance to fault asperities. Incorporating this spatial correlations improves the reliability of the risk estimates when dealing with spatially distributed structural portfolios [Park et al., 2007]. It is common practice to assume statistical independence between losses experienced by structures of the same class located at different sites, but perfect correlation when they are located at the same site (functional dependence, however, is assured by the utilization of the same vulnerability curve). An imperfect positive statistical correlation is to be expected between losses of different structures belonging to the same class. This is because of all the unknowns that are not captured by the knowledge of the building code, structural material, lateral load resisting systems and height, which are the only criteria used to parse structures into classes for regional risk assessment studies. In plain words, all the structures of the same class may systematically respond either worse or better than what the vulnerability curve for that class predicts. However, data to quantify such a positive correlation do not exist. A discussion on the effects of correlation

on the rate of exceedance of portfolio losses can be found, for example, in Sousa et al. [2018] and in You et al [2022].

Several open-source software packages of varying complexity exist to perform such analyses, with a commonly used one being the OpenQuake engine (Pagani et al., 2014; Silva et al., 2014), developed by the Global Earthquake Model (GEM; http://www.globalquakemodel.org).

5 Current Dutch Seismic Risk Protocol for small gas fields

In the Netherlands, seismicity in the (previously quiescent) northeast region is dominated by induced earthquakes caused by gas extraction (sections 2.1.1 & 2.1.2). The risks and hazards posed by these earthquakes have created a need for a systematic assessment of all onshore gas-fields, as required by Dutch law [Muntendam-Bos et al., 2015]. At a high-level, this risk assessment guideline is currently separated into three steps (Figure 12):

1) a prescreening of the likelihood of seismicity and of the maximum magnitude (using simple empirical relations and field-data)

2) a prescreening of the hazards/impacts using a qualitative risk-matrix approach

3) a detailed quantitative risk analysis resulting from a special research study

The steps progress sequentially, where escalation to the next step only occurs if the current step assesses a significant amount of concern. The highest step required for a field, defines its Category, with the exceptional case where a Step 3 (detailed) analysis reclassifies a Category III field (from Step 2) down to Category II. Monitoring requirements also escalate alongside the assigned category level.

- Category I requires only KNMI's established nation-wide monitoring network
- Category II requires supplemental monitoring down to completeness of M_L 1.5 in the vicinity of the gas field (including accelerometers), and a generic (loosely defined) risk management plan (proposed measures if certain magnitudes are exceeded).
- Category III requires a detailed site-specific research study on the seismic risk, further monitoring down to completeness of M_L 0.5 (including accelerometers), vibration-monitoring for residencies, and a detailed risk management plan (proposed mitigation actions if certain risk-thresholds are exceeded). To date, Groningen is the only gas field assigned to Category III.

The calculations for all the needed steps and the potential risk management plans are prepared by the operator who is submitting a request for a permit (based on a specified extraction plan) to the regulator, i.e. the Ministry of Economic Affairs and Climate Policy. Next, the regulator receives advice from local stakeholders, SodM (for safety matters), TNO (for technical matters), and the Technical Commission for ground motion (Tcbb). Finally, the Ministry of Economic Affairs and Climate Policy asks the advice of the Mining Council (Mijnraad), who incorporates all previous advice the Ministry has received. We should highlight that the regulators might not always be able to fully verify all the parameters adopted by the operator. A certain level of trust is required, especially when it comes to the calculation of the maximum possible magnitudes. If the operator wants to make modifications to the extraction plan, either a formal update to an existing permit or a new permit must be issued.

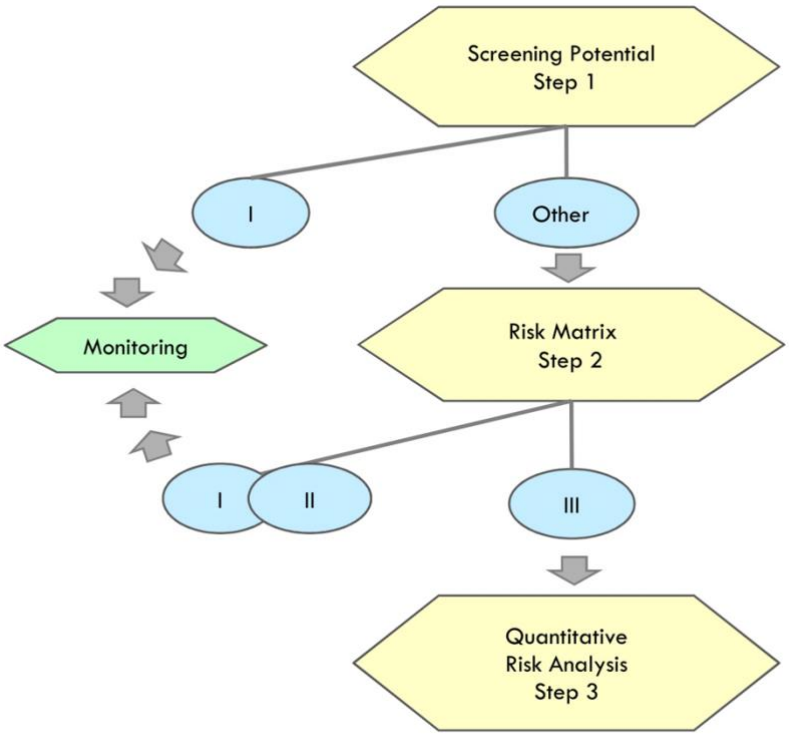

Figure 12. The three steps of the seismic risk analysis for small gas fields in the Netherlands [from Muntendam-Bos et al., 2015; SodM, 2016]. The three categories (I, II, III) are defined above in the text.

5.1 Step 1: Screening potential

The first step in the Dutch assessment of risks related to induced seismicity from production at small gas fields is to assess the likelihood of events occurring at a given gas field and the maximum potential magnitude [Muntendam-Bos et al., 2015; SodM, 2016].

The assessment of the likelihood of and induced event occurring in the Netherlands has been labelled the Deterministic Hazard Analysis for Induced Seismicity (DHAIS) [TNO, 2021]. The nature of assessing (or pre-screening for) the susceptibility of future events is necessarily uncertain, which precludes the use of most traditional hazard assessment tools. The Dutch DHAIS has followed a Bayesian approach using the 'Rule of Succession', in which measurable proxy parameters are used to estimate the likelihood of an induced event occurring [van Eijs et al., 2006]. The original input parameters into this method were pressure drop, fault density, and reservoir-seal stiffness ratio – these parameters were included both because of their theoretical expectation of importance and observed statistical discriminatory power. This method used Boolean data (yes/no of earthquakes occurring) to solve a binary classification problem, in which critical values of key parameters were calibrated based on the input data. This model then binned the likelihood of earthquakes into 4 classes, dependent on their values of fault density and stiffness contrast (between the seal and the reservoir rock) with respect to critical values. This approach also excludes cases which are not expected to have significant pressure drops. This simplistic approach inputs temporally biased data (e.g., in some gas fields induced seismicity may not have yet occurred but will later after sufficient pressure drop). Thus, there is a need to periodically update the critical parameters in the approach. The DHAIS has undergone periodic updates and revisions, as new information has become available [TNO,

2012; 2021]. For example, the pressure drop parameter was updated to a pressure drop ratio (divided by the initial pressure observation) in 2012. The 2021 update modified the critical values of the key parameters based on an assessment that partially accounted for the spatiotemporal variations in detection thresholds and was calibrated on recent seismicity data [TNO, 2021], without any methodological changes. No uncertainties have been considered during the classification analysis. The most complete description of the DHAIS is found in a recent report from TNO [2021]. We note that issues with the reproducibility of the 2006 and 2012 results have been documented by Tutuarima (2020). Most critically, almost no work has quantified the performance or predictive power of the DHAIS. This makes it impossible to assess the validity of the model and the underlying assumptions. Our later recommendations (section 6.1) will centre on this critique.

The maximum possible magnitude is assessed for each field via two methods: the first considers tectonic limits based on the dimensions of the fault and the second considers a relationship between the radiated seismic moment and reservoir volume change from extraction-induced compaction [SodM, 2016]. The first method uses a simple scaling relationship between seismic moment (M_o) and fault geometry [Stein & Wysession, 2009].

$$M_0 = GAu = \frac{3\pi}{8}\Delta\sigma(w^2 L)$$

Here, the stress drop $\Delta\sigma$ (assumed 5 MPa), fault height w, and length L contribute to the released moment. For determining magnitude estimates, the largest fault surface that is in contact with the reservoir is used to estimate the largest possible magnitude. In the second approach, an energy balance is considered [Kostrov, 1974].

$$M_o \approx \frac{4G}{3}\alpha|\Delta V(t)|$$

Where G is the shear modulus, α is the seismic partition coefficient, and $|\Delta V(t)|$ is the (absolute) volume change of the reservoir driven by extraction-related compaction. This volume change can be estimated with a number of modelling approaches. The seismic partition coefficient plays a significant role in changing the. Step 1 considers a value of 1/100 for α, which is likely a conservative estimate considering the value observed (5/10,000) for Groningen [Bourne et al., 2014]. Both methods convert the seismic moment release into magnitude, via a scaling relationship [Hanks & Kanamori, 1979].

Based on these assessed probabilities and maximum magnitudes, screening criteria for Step 1 have been defined [SodM, 2016]. If the gas field is determined to have a low maximum magnitude ($<M_L$ 2.5) and low probability of encountering induced seismicity (Figure 12), then no further action is required. At this step, the current regional monitoring from KNMI will suffice. If either of the magnitude/probability screening criteria are exceeded, then evaluation escalates to Step 2. Additionally, if monitoring determines that a field has (already) encountered induced seismicity, then it is automatically assigned to Step 2.

Hydrocarbon reservoirs with seismic activity	
$DP/P_{ini} \geq 20\%$	B ≥ 0.84 and E ≥1.07: Probability of an event
	B < 0.84 and/or E <1.07: Negligible probability
$DP/P_{ini} < 20\%$	Negligible probability

Figure 13. DHAIS-based screening of induced seismicity. Cases with low changes in pressure ratio (dP/P_{ini}) or those with low fault density (B) and relative stiffness (E) parameters are considered to have a negligible probability of inducing earthquakes. Figure from TNO [2021].

5.2 Step 2: Risk Matrix

Various so-called *subsurface factor*s determine whether an induced earthquake could cause strong ground motion, and other so-called *surface factors* determine the severity of the potential motions (Figure 14). The scores of the individual factors are added and normalized to determine an overall score for both the subsurface and surface factors. In the end, a qualitative risk matrix is constructed, to identify the field's risk category; the combined points for the subsurface and surface factors are indicated with dots in the risk matrix graph (Figure 15). The risk classification (in three categories) is derived from the location of the dot in the matrix graph. There is no general interpretation of the risks per risk category [SodM 2016].

As we will later articulate in section 6.2, this risk matrix approach is overly simplistic, neglects a lot of readily available data and is not quantitative enough. As a result, it does not adequately model the *impacts* listed in Figure 14. Recent national and European projects have provided plenty of databases and models that can be employed to avoid a lot of the adopted qualitative proxies. Explicitly accounting for the entire population and built environment, and for the fragility of each structural typology is both desirable and feasible nowadays. Determining a probabilistic magnitude range for the earthquake sources would also be a step forward.

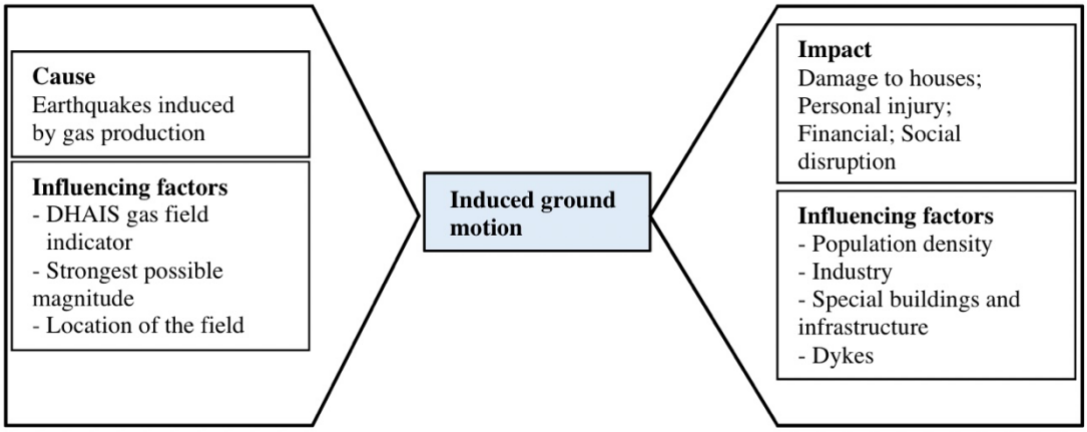

Figure 14. Schematic representation of the causes and effects of induced earthquakes and the various influencing factors [from SodM 2016].

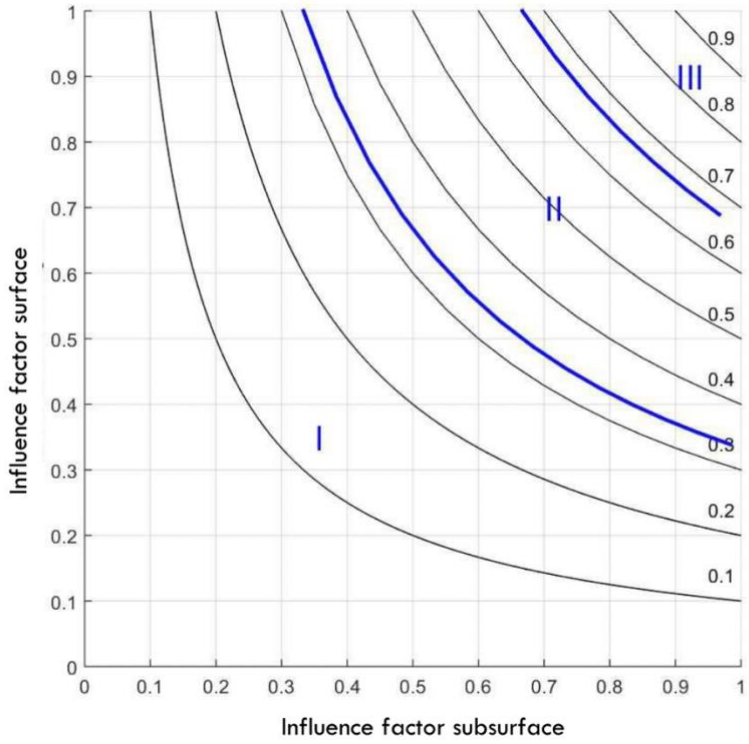

Figure 15. Normalised risk matrix visualisation into risk categories. The black lines depict the normalised risks. The categories are simply defined as 1/3 and 2/3 of the normalised risk [from SodM 2016].

5.2.1 Subsurface factors

The *subsurface factors* are proxies for the seismicity rate, the maximum expected magnitude, and the site-response. They are:

- The probability of induced earthquakes: it is determined based on the DHAIS analysis (see section 5.1).
- The strongest possible earthquake that should realistically be taken into account: The two values are calculated in Step 1.
- The location of the field: in the north of the Netherlands (including the Noord-Holland region), there is a thick layer of Zechstein salt which often forms a sealing layer over the gas fields there. Salt becomes fluid at a depth of about 3km and will flow to relax the stresses in the salt. This results in additional stresses just above and below the thick layer of salt (Orlic & Wassing 2012). Since the gas production activities started, there have been no induced earthquakes in any fields south of the Amsterdam-Arnhem line, south of which the Zechstein salt deposits are absent.
- The local site-response, based on the distribution of shallow soil types (a map has been provided) and the associated seismic wave amplification.

The number of points (Table 1) associated with the classification of the four factors are summed and normalised to the maximum number of points that can be obtained for all subsurface factors (equal to 14).

Table 1. Classification of the subsurface factors and the corresponding point system [from SoDM 2016].

	DHAIS	M	Location of the field	Seismic wave amplification
5		All methods >4.5		
4	Seismically active field >5 earthquakes per year of M≥1.5	1 method >4,5 and/or All methods 4.1-4.5		
3	Seismically active field <5 quakes per year of M≥1.5	1 method 4.1-4.5 and/or All methods 3.6-4.0		>60% weak soils ($V_{s,30}$ = <200m/s) and/or >30% soils that are particularly susceptible to amplification, such as peat layers thicker than 3m and soft peat layers of 1-3m thickness above a firm substrate.
2	P=42% Or Seismically active field M<1.5	1 method 3.6-4.0 and/or All methods 3.1-3.5	Above the Amsterdam-Arnhem line	30-60% weak soils ($V_{s,30}$ = <200m/s) and/or 15-30% soils that are particularly susceptible to amplification, such as peat layers thicker than 3m and soft peat layers of 1-3m thickness above a firm substrate.
1	P=19%	1 method 3.1-3.5 and/or All methods 2.6-3.0		10-30% weak soils ($V_{s,30}$ = <200m/s) and/or 5-15% soils that are particularly susceptible to amplification, such as peat layers thicker than 3m and soft peat layers of 1-3m thickness above a firm substrate.
0		1 method 2.6-3.0 and/or All methods ≤2.5	Below the Amsterdam-Arnhem line	<10% weak soils ($V_{s,30}$ = <200m/s) and/or <5% soils that are particularly susceptible to amplification, such as peat layers thicker than 3m and soft peat layers of 1-3m thickness above a firm substrate.

Here, our review is focused on the Amsterdam-Arnhem line and the local site-response function, given that the DHAIS has been already addressed in section 5.1 (and 6.1). As a general note, this point-system has an implicit weighting scheme attached to it (Table 1). We believe the implicit weights assigned to "the probability of induced earthquakes" and to the "maximum magnitude" should be higher in relative terms. In any case, in section 6.2, we propose a new more probabilistic way of estimating the size of the expected induced earthquake in each field, that replaces these two aforementioned factors.

Given the overall low levels of seismicity and spatially varying levels of station-density for the monitoring network, it is hard to conclude whether the salt deposits are the true cause for the lack of detected earthquakes. Although a physical explanation for this phenomenon has been provided (Orlic & Wassing, 2012), we encourage revisiting this assumption once the monitoring network becomes more regularly spaced.

The following points are of main concern, as far as the site-response is approximated:

- the term "seismic wave amplification" is a bit confusing here; it is the site response that needs to be classified.
- using the term 'amplification factor' is misleading in this context. Based on the percentages, a weighting factor is determined for the risk matrix calculations. The numbers assigned to each seismic wave amplification category are not computed amplification factors.
- it is unclear how the percentages of the soil types and the thickness of the peat are determined to be susceptible soil.
- it is unclear where the numbers for Vs30 are based on.

Ideally, earthquake signals are needed to accurately estimate the earthquake amplification factor in shallow sediments. However, in the absence of earthquake records, alternative methods have been developed to estimate the amplification factor at locations with a soft sedimentary top layer. The SERA

project [Weatherill, 2023] has defined a list of mandatory indicators, including fundamental resonance frequency (f0), S-wave velocity profile (Vs(z)), Vs30, depth of seismological and engineering bedrock, surface geology, and soil class, for a reliable site characterization.

Extensive site-response assessments, as part of the ground-motion models for the Groningen field, have shown the need for a high level of detail due to the heterogeneity and very soft composition of the shallow subsurface. Groningen has a rich database, and analysis of passive seismic records using the HVSR methodology provides the first indication of sites with the potential for earthquake wave amplification. The availability of a high-resolution subsurface model, GeoTOP, allows for the linking of seismic wave amplification to the lithology of the top 50 m, forming the basis for the seismic site-response zonation map for the Netherlands [van Ginkel et al., 2022a; section 4.4.4.2]. The AF factors assigned to each class can be used as input for seismic hazard and risk analysis for induced earthquakes. However, the heterogeneous character of the shallow Dutch subsurface results in uncertainties, even though the shallow subsurface is well-documented compared to other countries.

A summarized comparison of the input for the workflow for the creation of the ESRM20 and the site-response zonation map for the Netherlands is shown in Table 2. The induced seismicity potential related to gas production in the Netherlands generates overall low-magnitude and shallow earthquakes. The European projects like SERA mainly assume tectonic strong motion (M>4) earthquakes. The workflow from SERA and the list of site characterization indicators is a great example to follow. However, for seismic hazard and risk analysis for small gas field in the Netherlands, the approached tailored to shallow and low-magnitude events and the site-response map by van Ginkel et al. [2022a] would be of preference to use for building response analysis. Here, not only the Vs30 is used as proxy, but also the f0, empirical earthquake AFs, impedance contrast and lithological sequence. The site-response assessment for the Netherlands clearly indicates the need for adopting alternate site classification schemes than Vs30 only, as discussed in literature and in SERA.

Therefore, the site-response map presents a zonation for interpretation at the province, municipality, and district levels, and if there are no other models available the map can be used for assessment of individual building responses to an earthquake, since the generalized amplification models (e.g. SERA) are of lower resolution.

Table 2. overview of the input parameters for the SERA workflow and from the site-response zonation map of van Ginkel et al. [2022a].

Input parameter	SERA/ESRM20	van Ginkel et al., 2022
Grid cell scale	30 arc-second (~1 km)	100 m / 250m
Geological data	Pan-European Stratigraphic map. For NL, only subdivision in Holocene and Pleistocene	3D digital geological models: GeoTOP (cell size =100*100*0.5m), NL3D (cell size = 250*250*1 m). In GeoTOP, the Holocene is subdivided into 25 formations
lithologies	Simplified lithologies and codes for the European lithological map (NL mainly classified as SAGR: sand and gravels, few clay)	Six lithology classes: peat, clay, clayey sand & sandy clay, fine sand, medium sand, coarse sand and gravel.

Vs30	Vs30 linked to each simplified lithology. Input from Noorlandt et al. [2018]	No direct use of Vs30, for NL considered not descriptive enough to use as proxy.
Amplification factors	Computed based on all parameters	Empirically determined from local earthquakes.
Reference velocity	800 m/s	500 m/s (in NL ~ 200 m depth). At 200 m depth and directly below, the subsurface conditions are laterally relatively homogeneous; deeper this is not the case
HVSR resonance frequency f0	Not used	Measured at 115 sites
Additional comments	Site to-site ground motion residuals (δS2SS), based on strong motion data from Southern Europe (France, Italy, Switzerland, Turkey, Romania, Greece)	Amplification classes based on f0, the strong contrast between the Holocene clays/peat and Pleistocene sands.

5.2.3 Surface factors

The *surface factors* are proxies for the number of exposed assets, their type and their significance. They are:

- population density: the number of inhabitants per km^2
- industrial plants: presence of one or more industrial facilities
- special buildings and infrastructure: presence of schools, hospitals, care institutions, energy plants and public buildings
- dikes: presence of primary and/or secondary dikes

To determine the consequences of the influencing factors listed above, the number of points (Table 3) resulting from the classification of the five factors are summed and normalised to the maximum number of points that can be obtained for all surface factors (equal to 16).

Table 3. Classification of the surface factors [from SodM 2016].

	Population density (number of inhabitants per km^2)	Industrial installations	Special buildings and vital infrastructure	Dikes
4	>2500	Multiple directly above the field	Multiple hospitals and/or energy supply facility directly above the field	Primary dikes above the field
3	1000-2500 and/or 500-1000 with neighbourhoods consisting of apartment blocks within 5km of the edge of the field	1 above the field and/or several within 5km of the edge of the field	1 hospital and/or energy supply facility directly above the field or more than 1 within 5km of the edge of the field. More than 1 school, care institutions and/or public buildings directly above the field	Primary dikes within 5km of the edge of the field and/or secondary dikes above the field
2	500-1000 and/or 250-500 with neighbourhoods consisting of apartment blocks within 5km of the edge of the field	1 within 5km of the edge of the field	1 school, care institution or public building above the field or more than 1 within 5km of the edge of the field	Secondary dikes within 5km of the edge of the field
1	250-500 and/or <250 with neighbourhoods consisting of apartment blocks within 5km of the edge of the field		1 school, care institution or public building within 5km of the edge of the field	
0	<250	None within 5km of the edge of the field	None above or within 5km of the edge of the field	No dikes within 5km of the edge of the field

A 5km buffer zone is applied from the edge of the field, "because earthquakes at boundary faults may still cause significant ground vibrations within this distance". We consider this 5km value to be quite small, given that maximum magnitudes above 4 have been estimated for several small fields. Distances at least up to 25km would seem quite reasonable to include, given the shallow nature of these potential rupture zones, the fragility of the buildings and the potential for soft soil-conditions. Attenuation functions from ground-motions at the Groningen gas-field or from other shallow induced earthquakes could be used to inform this parameter.

The adopted point-system has an implicit weighting scheme attached to it (Table 3). We believe the relative weights assigned to "population density" should be higher, given that 75% of the implicit weights are assigned to special structures. Most of the issues in Groningen originated from the population cohort and not from the other three factors. The fragility of the houses should also be a critical factor.

Overall, although the *surface factors* seem straightforward, they are qualitative proxies of easily quantifiable vulnerabilities. There are spatially gridded datasets of the entire population and built environment that are available for the country, paired with corresponding fragility functions for each building typology (section 4.5 & 4.6). Ground-motion models from Groningen or other induced seismicity sequences in stable continental regions (section 4.3) can also be directly adopted or adapted to compute the input needed for the fragility functions. Based on the expected structural damages, one can empirically estimate probabilities for the loss of life. The computational framework for such an analysis is described in section 4.7. The only missing piece are the scenario magnitudes which are introduced in section 6.2.

5.3 Step 3: Quantitative Risk Analysis

The methodology for the detailed quantitative seismic risk analysis (in terms of individual and societal risks) has been only applied to the Groningen gas field. According to the current protocol, the seismic risk of any other fields that fall under Category III will have to be quantified in a similar way. The current report does not address this Step, since it is supposed to be done on an ad-hoc basis by a special research study.

6 Recommendations

In this chapter, we propose changes to the existing protocol, based on the critical review conducted in section 5. The overall design of the protocol (3 steps, 3 risk-categories, Figure 12), as well as the monitoring requirements, remain the same. We recommend refinement of Step 1 (section 6.1), and replacement of Step 2 (section 6.2). Step 3 was not under review in this report. Furthermore, we recommend a more specific and data-driven risk management plan under Category II (section 6.3). The improvements proposed for Step 1 are methodological, rather than conceptual, while the new version of Step 2 is much more quantitative and in line with the latest regulatory framework. That said, practical considerations were made to render Step 2 easily enforceable by practitioners without specialized scientific or computational background.

Notably, our recommendations assume that any generated seismicity is only linked to gas-extraction and that there are no injection-wells (aiming at stabilizing the reservoir-pressure) in the producing field. Gas-producing fields where fluid injection does occur are outside the scope of our assignment and need to be governed by a different set of guidelines, especially when it comes to their seismic and aseismic potential, their favorable stress field, the estimation of the maximum magnitude, and the spatial extent of the seismicity. In that sense, the presence of fluid injection would demand substantial changes to section 6.1 and perhaps minimal changes to section 6.2.

6.1 Refinement of Step 1

For Step 1 (screening potential), we recommend a refinement of the current approach. We come to this recommendation based on our review of the literature and the current protocol. Currently, Step 1 is conceptually in line with the intended goals, although some of the implementation details could be improved. Here, we will outline our Step 1 refinement proposal alongside our justifications for this recommendation.

The intention of Step 1 is to provide a simplified pre-screening of possible hazards/risks assessment, at an early stage when data availability will (likely) be limited. Because of this limitation, simplifications (like using a risk matrix) are necessary. While not explicitly stated, Step 1 implicitly takes a risk-matrix-like approach: the DHAIS provides an estimate of the likelihood of earthquake occurrence and the maximum magnitude estimates provide a proxy for the severity of hazard/risk. A combination of these two variables is used to decide if the hazards/risks potential are worrisome enough to require a more serious hazard/risk quantification (i.e., Step 2). Of these two risk matrix components (likelihood and severity), our refinement recommendations focus on better constraining the likelihood.

The refinement recommendation is directed toward estimating the likelihood of hazard/risk (i.e., the DHAIS). The DHAIS acronym is a misnomer: it isn't deterministic, and it doesn't compute hazard. The current DHAIS uses a Naïve Bayes approach to solve a binary classification problem [van Eijs et al., 2006]: there are gas fields that (yes/no) caused earthquakes and each of these gas fields have some underlying factors (e.g., dP/P_{ini} B, & E) that can influence the susceptibility to induced earthquakes. In this type of problem, we would like to use these (yes/no) training examples to fit some likelihood function (L-fxn) that

estimates susceptibility using the underlying factors as inputs. Susceptibility has been defined as a term to denote this type of likelihood, which is precursory to hazard estimates. In Step 1, the DHAIS is one example of how the L-fxn can be determined. Since the DHAIS was first developed, the literature around machine learning for solving binary classification problems has grown substantially (Figure 16). This provides an opportunity for DHAIS improvement using insights derived from these new tools, concepts, and study results. For example, there are other case studies that have also solved binary classification problems to estimate the susceptibility of induced seismicity [e.g. Pawley et al., 2018; Amini et al., 2021; Wang et al., 2022]. In fact, expert panels have recommended this susceptibility analysis as an important regulatory tool [SHFRP, 2019]. Based on this, we suggest that the DHAIS could be refined in three ways: by better quantifying model performance, testing alternative models for fitting L-fxns, and reconsidering the input assumptions (with uncertainties). We discuss each of these inter-related refinement points in detail below.

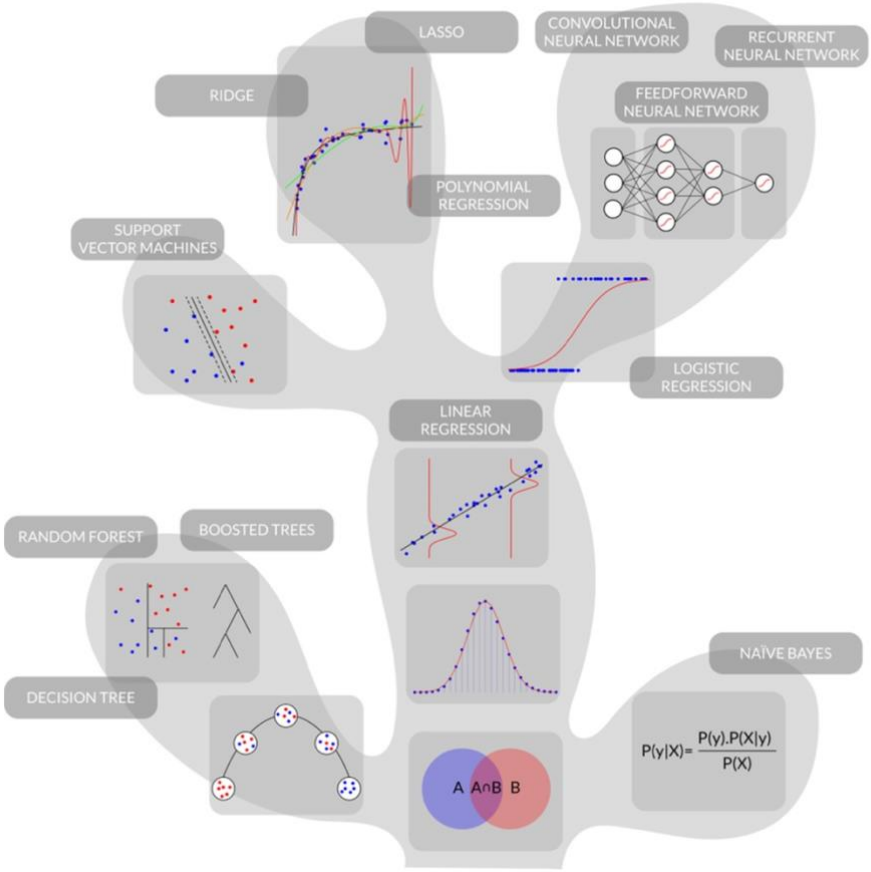

Figure 16. Hierarchy of machine learning techniques. Simpler techniques are lower, more complex models are higher. Naïve Bayes (used in the DHAIS) is a fundamental machine learning technique. Figure by A. Mignan [2022].

The first (likelihood) refinement to be made is in better quantifying model performance. In regression problems, metrics like goodness-of-fit (e.g., R^2) are used to quantify the performance of the model. Similarly, in binary classification problems, performance metrics like accuracy, recall, precision, ROC, AUC,

F1-score are used for a variety of comparison purposes [James et al., 2013]. In general, these metrics consider the minimization (and balancing) of false-negatives and false-positives cases. We emphasize that for Step 1, there is an imbalance between these two error types: a false-positive can only escalate a gas field from Step 1 to Step 2, while a false-negative means real seismicity eluded pre-screening. Performance metrics should be skewed to account for this imbalance. Likely, approaches like k-fold cross validation or AIC/BIC scores will be needed in this case, as there is limited data [James et al., 2013]. Within the literature on DHAIS, almost no effort has been placed on quantifying model performance. These sorts of metrics are crucial for understanding if a model is providing useful information and for judging if an alternative model provides better resolving power.

The second (likelihood) refinement to be made is in considering alternative models for fitting L-fxns. Since the DHAIS was first implemented [van Eijs et al., 2006], there has been significant algorithm development in solving binary classification problems. Likely, there will be alternative models that outperform the DHAIS – even given the same input and training data. Studies should explore alternative models, using performance metrics to both assess validity and quantify improvements.

The last refinement to be made to the DHAIS is to better question the assumptions around the inputs. For the classification data (yes/no for earthquakes at a gas field), this data will depend on the magnitude-of-completeness (Mc) which is spatially heterogenous in the northern Netherlands. When comparing the station-density and irregular configuration of the Dutch network (outside of Groningen) with other global networks, there is a case to be made that the current consensus estimates for the M_c (Fig. 3-1 in TNO 2021) are very optimistic and may be revised lower in the future, affecting the classification results by up to 58% (Tutuarima 2020). For similar reasons, the epicentral uncertainty behind the earthquake solutions might be much larger than currently foreseen (3km), something that should be also taken into account in an explicit way. Furthermore, the classification data is biased temporally, in the sense that events above the M_c will only be recorded after sufficient reservoir changes have occurred. Estimation of susceptibility should explicitly consider these spatiotemporal biasing effects – either within the model construction or in the data handling. Additionally, the input underlying factors (e.g., dP/P_{ini} B, & E) should also consider the uncertainty of these parameters, given that this uncertainty may have very significant effects on the results [Tutuarima, 2020]. Last, the machine learning concept of data exploration should be considered for input features – where gains of L-fxn predictive power are assessed for all available inputs (and combinations). The original DHAIS suggested three parameters were sufficient: however, other inputs such as extraction rates, rock heterogeneities, reservoir geometry/dimensions, in situ stress field, and stress ratios [Oumejjoud, 2023]. These old assumptions around inputs could be corroborated or refuted using new machine learning concepts and performance metrics.

Here, we have provided refinement suggestions for Step 1, largely focusing on applying new machine learning concepts and more input variables on the DHAIS. Machine learning competitions (e.g., Kaggle) could be used as a platform to encourage this exploration.

6.2 Replacement of Step 2

We propose a replacement of DHAIS as a reference point for the likelihood and size of the expected seismicity in a field. We do not believe it captures well the nonlinear relationship between magnitude size and likelihood of occurrence. It also does not increase the modelled risks as the observed magnitudes (above M_c) in a field increase, but yet not exceed the modelled M_{max} values. We also recommend a replacement of the risk-matrix approach by a much more quantitative seismic risk framework.

6.2.1 Seismic source

Given that in most cases the operator submits a permit-request with little to no seismicity data available at the site, a detailed seismic source model cannot be derived. To be pragmatic, we aim to capture in a probabilistic way the next critical earthquake that might be triggered due to gas-extraction in a given field.

To that end, we first define a range of possible magnitudes; M_1 is the lower bound, M_2 is the upper bound. Ideally, these magnitudes should have the same magnitude scale as the one used by the GMM and in the derivation of the fragility curves. For the lower bound, M_1 is defined as the largest observed magnitude thus far. To be on the conservative side, if no magnitudes above M_c have been recorded around the field, then M_1 is set equal to Mc. When associating events to fields, one should take into account the epicentral uncertainties (across time) plus a buffer distance (e.g. 10 km) that implies that the stress-state within that zone is similar. For the upper bound, M_2 is defined as the largest of the two estimates for the maximum possible event from Step 1 (section 5.1). In that way, we bound the magnitude of the next critical earthquake somewhere between the largest recorded event and the largest possible event. Obviously, under this framework, underestimating the true M_c across time can lead to underestimation of the modelled scenario magnitude. The upper truncation bound M_2 could even be informed by a distribution of M_{max} values, like the workflow used for Groningen [NAM, 2022], although this would add complexity to the calculations.

Notably, if the measurement uncertainty behind the computed magnitude solutions is non-negligible (e.g. above 0.1 magnitude units), then it must be taken into account by conservatively adjusting M_c and M_1 (towards larger values). Next, assuming a binning of 0.1 for the range of magnitudes, one can calculate for any field the risk metrics of choice (section 6.2.6) for every binned magnitude value. Each rupture is assumed to be centered in the middle of the field, at the depth of the reservoir with a focal mechanism compatible with the local stress field and mapped faults. Notably, depending on the risk metric targeted by the analysis, there is a minimum magnitude (M_{min}), below which there is no engineering interest [Bommer & Crowley 2017]. In other words, the rupture is too short (in duration) or limited in frequency-content to cause any damages to structures. Therefore, in practice, M_1 cannot be lower than M_{min}, when performing the risk calculations. Note that for each field, there might be more than one value for M_{min}, depending on the risk metric analyzed. For MMI calculations, for example, this M_{min} value is very low and likely below Mc. The issue of M_{min} is further discussed in section 6.2.5.

Now, we should clarify that these discrete magnitudes within the range do not exhibit the same likelihood of occurrence. The likelihood that the scenario earthquake will have a given size decreases with

magnitude. This is captured by a normalized Gutenberg-Richter magnitude-frequency distribution (GR-MFD), doubly truncated between a magnitude interval defined by M_1 and M_2. The probabilistic treatment is applied to the risk outputs after the fact and not at the seismic source level. This post-processing probabilistic scheme is described in section 6.2.8.

6.2.2 Ground motions

Section 4.3 has some important information about the available GMMs for the country. Here, we build upon that discussion. Bommer et al. [2022b], who developed the latest GMM for Groningen, clarified that "the model cannot be applied outside the boundary of the (Groningen) gas field plus a 5 km buffer onshore". That said, this statement did not take into account the available alternatives for the rest of the country, which are derived using either tectonic or geothermal-related datasets from other European countries (mostly from France, Switzerland and Germany) of different magnitude scale, focal depth, triggering mechanism and mirror a wide range of dissimilar subsurface geology. The level of scrutiny we apply to any available model has to be proportional to the valid available alternatives.

When it comes to shallow gas-extraction earthquakes, we believe that the Groningen GMM [Bommer et al., 2022ab] remains a great starting point for a nation-wide model for the Netherlands. The model is calibrated on the right magnitude scale, magnitude range, nucleation process, focal depth, tectonic conditions, and has been developed using state-of-the-art methods following extensive peer-review protocols. We agree that the subsurface geology does differ in the rest of the country, affecting path-effects (especially near-field), and that the amplification factors in the rest of the country might differ. However, the latter point is addressed in section 4.4 and 6.2.3, while the path-effects of other GMMs developed in totally different tectonic environments, under different triggering conditions and focal depths, will likely be even more inappropriate. Furthermore, the Groningen GMM can be applied following a backbone approach (see section 4.3) with the median being scaled by expert judgement to account for path-effects. In reality, the biggest obstacle in using a derivative of this GMM in the rest of the country is its very high computational complexity and the fact that it is not available in an open-source software engine (e.g. OpenQuake). Thankfully, the strong-motion database (and all its metadata) behind the derivation of this GMM is publicly available and peer-reviewed [Ntinalexis et al. 2022)] Therefore, we would encourage using this database to re-calibrate an existing European stable-continental GMM (with a typical function form that is much less complex than in v7) following the procedure adopted by Zalachoris & Rathje [2017]. Further research into the scaling needed to capture the near-field path-effects in the rest of the country would be beneficial.

6.2.3 Site-response analysis

Using a uniform approach for site-response assessment (as is currently done) is not advisable as it may not account for the diverse conditions found in different locations. Groningen is a good example. The site response empirically determined in Groningen exhibits significant spatial variation due to the heterogeneous characteristics of the shallow subsurface. This heterogeneity is prevalent in various regions

across the Netherlands, particularly in areas with unconsolidated Holocene infill. Therefore, using only Vs30 values is not a sufficient proxy (chapter 4.4). As a result, the following steps are recommended to be included in the protocol regarding site-response estimation and its amplification factors:

- **No new available data:**

When no new data (seismic measurements, updated geological model) are available, we recommend using the default amplification factors (on 100m grid cell scale) from the site-response zonation map from van Ginkel et al [2022a] (https://dataplatform.knmi.nl/dataset/seismic-site-response-zonation-map-1-0). See section 4.4.4.2 and 5.2.1 for a detailed description of this map and for a discussion on why it is the current state-of-the-art for the country.

- **New available data:**

When additional field measurements, such as the fundamental resonance frequency (with HVSR from seismic measurements, either from the existing KNMI seismic network, or new measurements), or seismic cone penetration tests (SCPT) for Vs30, lithostratigraphy and impedance contrast presence, are available, they can be incorporated in the framework of Ginkel et al [2022a] to obtain a more site-specific calibration for the amplification class.

The flowchart of Figure 17 is designed to define a sediment profile class based on the subsurface composition. Due to the presence of the digital geological model GeoTOP, one can define in quite high resolution the shallow soil composition. We recommend estimating not only the presence of the 'weak soils', but also the impedance contrast between the Holocene top sediments and the Pleistocene sands. Additionally, the uncertainties in the actual GeoTOP lithostratigraphic profile can be minimized by on-site SCPT recordings and borehole logging. Based on the sediment profile class (II-IV), one can assign an amplification factor, including the range of uncertainties, that are empirically derived in van Ginkel [2022a] (Table 4).

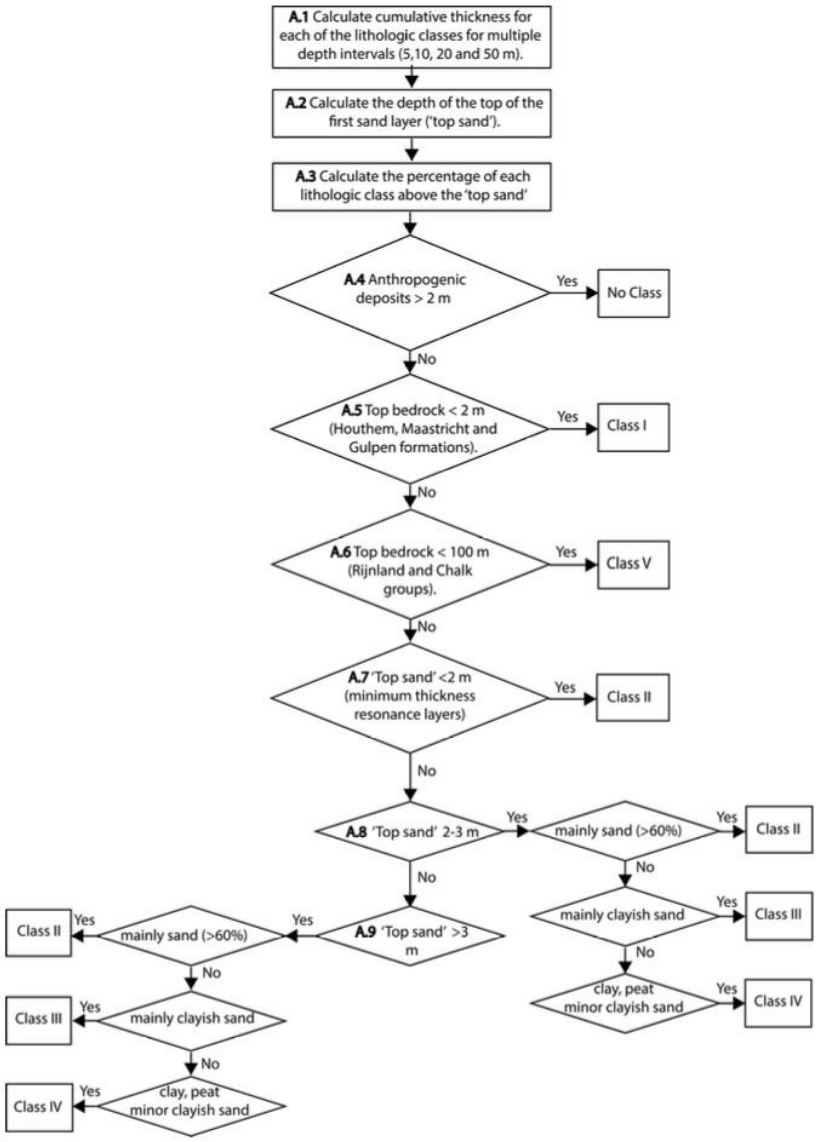

Figure 17. Workflow to assign the appropriate sediment class into an amplification class of the seismic site response zonation map by van Ginkel et al. [2022a].

Table 4. Amplification factors (AF) and uncertainties for the sediment profile classes by van Ginkel et al. [2022a].

Class	AF	Sigma
I	1.00	-
II	1.94	0.30
III	2.4	0.28
IV	3.03	0.34
V	NA	NA

We should note that the amplification factors of van Ginkel et al. [2022a] are based on reference shear-wave velocities of 500 m/s, based on a reference horizon at 200m depth. At a depth of 200 meters, the Dutch subsurface primarily consists of laterally extensive Pleistocene and Pliocene sediments, accounting for approximately 95% of the composition. As a result, the estimated amplification factors can be applied over a significant portion of the country. It is critical to note that the output of the GMM (section 6.2.2)

must either directly match or be convertible to the reference velocity of van Ginkel et al. [2022a] (500m/s). Obviously, no amplification factors are to be applied to the ground shaking intensity output (e.g. MMI scale).

6.2.4 Exposure database, nuisance and fragility/vulnerability functions

The state-of-the-art for risk exposure models in Europe was developed within the SERA project [Crowley et al., 2020]. See section 4.5 for details. The SERA taxonomy is quite broad and (apart from population) includes both residential, industrial and commercial buildings. That said, it does not take into account the peculiarities of some of the Dutch houses, for which targeted fragility models from Groningen do exist. Therefore, all unreinforced masonry (URM) residential buildings could be considered Groningen-like and be assigned these special fragility models.

The available nuisance functions are listed in section 4.3.2. A good fit would be the GSIPM by Teng et al. [2021], which is based on likely-induced earthquakes from Texas, Oklahoma and Kansas, with magnitudes between M 1.5 and 3.5 and hypocentral distances within 30 km. Alternatively, one could compute PGV or PGA estimates using an applicable GMPM for the Netherlands [e.g., Bommer et al. 2022b], and then convert those to MMI using the conversion-relations of Schultz et al. [2021c], originally derived for Central and Eastern US.

In terms of fragility functions, the ones by Kallioras et al. [2019] should be used for the URM residential buildings, the ones from Crowley et al. [2019] should be used for RC, steel and timber residential buildings and the ones from Martins & Silva [2020] for anything else. The consequence functions (damage-state to loss-of-life probabilities) of Crowley et al. [2017] should be used for the LPR calculations. The computational framework for such fragility and vulnerability analyses is described in section 4.7.

Finally, a recent study by Tasiopoulou et al., [2019] concluded that for all seismic scenarios under consideration, the Groningen levee/dykes crest settlements remain well below the allowable limits. Verification is needed to make sure that this observation can be extrapolated to dykes outside Groningen. As far as pipelines are concerned, Kruse & Hölscher (2010) found that the seismic risk to pipelines in the northern part of the country is small (lower than 1 damage per 1000km of pipeline). Further research is required to ensure that other types of critical infrastructure in the country (e.g. hospitals, power plants) can sustain moderate earthquakes, up to say magnitude 6, a level that is very unlikely to be exceeded under normal circumstances in any of the small gas fields.

6.2.5 Minimum magnitude for engineering purposes

One issue that arises is that the fragility curves of Martins & Silva [2020] have been derived with tectonic earthquakes in mind, and are thus representative of damages caused by ground motions originating from moderate to large magnitude events, say above magnitude 4.5. The focal depth of these tectonic events is also much larger than the depths of the gas-fields. The Groningen-specific fragility curves on the other

hand, are calibrated mostly on shallow induced earthquakes say above 2.5. Furthermore, a Dutch URM house in reality should be paired with a lower M_{min} value than a steel-frame office building.

The complexity around M_{min} does not end there, however. The risk metric under analysis (section 6.2.6) also affects the selected M_{min} value. Structural damages require a larger M_{min} than nonstructural damages, with the latter requiring a larger M_{min} than nuisance calculations (via MMI). Therefore, ideally one would use M_{min} values specific to both the taxonomy and the risk-metric, to overcome this issue, increasing the complexity of the calculations.

If one assumes that the Dutch residential URM buildings will dominate the risk results and wants to avoid taxonomy-specific M_{min}, then one could choose from the following indicative (M_L) values: M_{min} value of 2.5 for structural damages (and LPR), of 1.8 for non-structural damages and of 1.5 for nuisance. The thresholds for the damages are influenced by observations from Groningen, while the nuisance threshold is based on US data (https://earthquake.usgs.gov/data/dyfi/).

6.2.6 Risk metrics and decision variables

We propose the following risk-metrics as decision variables for whether an application will be escalated to level 3 or eventually be accepted or denied:

- aggregate nuisance level: total number of people that felt the event (equivalent MMI scales above III)
- aggregate structural damages: total number of structures with moderate structural damages.
- aggregate non-structural damages: total number of structures with severe non-structural damages.
- mean local personal risk: the annual probability of fatality for a person, who is continuously present without protection at a location.

Indirect economic losses (such as business interruption or economic disruptions) are more difficult to model and are neglected here. That said, they can be relatively high and site-dependent [Sousa et al., 2022; Markhvida & Baker, 2023].

The damage-states adopted by the global risk map of GEM [Silva et al. 2020] or the ones from HAZUS [FEMA 2013] could be used as reference points. If the consequence function assumes different fatality ratios for daytime and nighttime, the mean of the two should be used.

We recommend using the open-source OpenQuake engine [Pagani et al., 2014; Silva et al., 2014] for the hazard and risk calculations, which are described in greater detail in section 4.7.

Given an estimate for each of these four risk metrics, the next step is to decide if these risks are worrisome enough to escalate to Step 3. We propose using the modelled scenario risks from the Huizinge event as a benchmark for risk tolerance. The Huizinge event caused extensive unrest in the public and the eventual termination of gas extraction at Groningen, so escalation criteria should ensure the avoidance of similar levels of risk. These modelled risk metrics will have to be computed using the same model-components (GMM, exposure data, site-amplification factors, fragility/vulnerability functions) as for the

small gas fields. Furthermore, the protocol needs to escalate a case to Step 3 sufficiently before encountering Huizinge levels of risk. For that reason, we propose scaling the Huizinge risk tolerance by a reduction factor that is yet to be determined based on a sensitivity analysis. Values between 30 and 60% for this scaling factor could be reasonable. If any of the four computed risk metrics exceeds this scaled Huizinge risk tolerance, then the examined case should be escalated to Step 3. Sanity checks for when escalation occurs must respect the potential for trailing seismicity [Schultz et al., 2022a], although fluid-extraction related trailing events have not been well quantified yet. We also note that a bias toward preferring false-positives over false-negatives would be warranted here as well. We should clarify that escalation to Step 3 does not automatically result in the rejection of the proposed gas-extraction plan, it just leads to a more holistic analysis that more rigorously captures the nuances of the source model, potential mitigation strategies, and potential recalibration of the GMM.

Although we propose the aforementioned list, we should note that under current legislation, the regulator can only use mean LPR as a decision variable for the eventual rejection of an operator's plan (threshold of 10^{-5}). We would encourage modifications that would expand the discretionary power of the regulator, given that in Groningen nuisance levels and non-structural damages were a key driver behind the eventual termination of the project. We do not believe the public was aware or able to quantify its LPR, when protesting against the elevated seismicity levels. If the majority of the people start feeling seismicity for the first time in their lifetime on a regular basis or experience non-structural damages (that often they cannot distinguish from structural damages), then there will be social unrest and protests against gas-extraction. Finally, the threshold of 10^{-5} for mean LPR is higher than other countries, with the value of 10^{-6} being more common.

6.2.7 Precomputed risk tables

Mandating that every operator performs the proposed seismic risk calculations, which admittedly have significant computational complexity are require familiarity with specialised software engines, seems undesirable. To address this issue, we propose that the regulator hires experienced practitioners or consultants to precompute tables of risk outputs covering every scenario rupture envisioned by the proposed protocol (Figure 18). This task is simpler that it looks at first glance. The location of all small onshore gas-fields is known, while the magnitude range of the scenario earthquakes is finite. Given that the exposure model covers the entire country, and that the fragility and vulnerability model remains static, automatic the whole process is straightforward. The only task the operator has is to extract the right values from the risk tables (based on M_1, M_2 and the location of the field), and then post-process the risk metrics according to section 6.2.8. The risk tables could be available on spread-sheets, and both the data-mining and the weighting scheme could be done with simple predetermined input functions. The risk tables might require rare updates if new fields are found (or existing ones are extended), if new incompatible strong-motion data become available, or if the population or built environment changes significantly.

nuisance level # reached by

	M_1	$M_1 + 0.1$	$M_1 + 0.2$	…	M_2
gas field 1	100 people	120 people	150 people	…	1000 people
gas field 2	50 people	70 people	110 people	…	1200 people
gas field 3	20 people	25 people	30 people	…	450 people
…	…	…	…	…	…
gas field 190	30 people	45 people	60 people	…	700 people

Damage State X reached in

	M_1	$M_1 + 0.1$	$M_1 + 0.2$	…	M_2
gas field 1	55 buildings	70 buildings	90 buildings	…	900 buildings
gas field 2	50 buildings	70 buildings	110 buildings	…	1200 buildings
gas field 3	30 buildings	35 buildings	50 buildings	…	600 buildings
…	…	…	…	…	…
gas field 190	5 buildings	10 buildings	15 buildings	…	250 buildings

mean LPR ($x10^{-5}$)

	M_1	$M_1 + 0.1$	$M_1 + 0.2$	…	M_2
gas field 1	0.10	0.11	0.12	…	0.90
gas field 2	0.20	0.22	0.24	…	1.50
gas field 3	0.05	0.07	0.09	…	0.55
…	…	…	…	…	…
gas field 190	0.10	0.13	0.16	…	0.95

Figure 18. Examples of hypothetical risk tables for different risk metrics. The damage-state could be either for structural or non-structural components.

6.2.8 Post-processing of precomputed risk tables

Given a precomputed risk table (Figure 18; section 6.2.7), we define a post-processing workflow that estimates the probabilistic nature of the relevant risk-metrics.

We begin by considering a (normalized) Gutenberg-Richter magnitude-frequency distribution (GR-MFD), doubly truncated between a magnitude interval of M_1 and M_2. Here, M_1 is the lower bound, M_2 is the upper bound (see section 6.2.1), and *b* is the GR *b*-value providing the proportionality between big and small events. This relationship can be used to define the probability density function and the cumulative distribution function. In this sense, we bound the likelihood of the next largest event's magnitude – somewhere between the current largest observed event and the estimate of the largest possible event. The *b*-value can be informed by prior relevant cases (like Groningen), relevant tectonic events, or an amalgamation of both; we favor the first option. We emphasize that M_1 (and thus the pdf itself) changes as induced seismicity progresses in a gas field, since larger events will be presumably sequentially observed, increasing the overall weighted mean magnitude, even if M_2 remains unchanged.

We use this pdf as a proxy seismic source of the resulting risk. Thus, each (precomputed) risk output can be weighted according to the pdf of its source-magnitude. In the end, a probabilistic distribution is obtained for the given risk metric. We recommend using either the mean or a percentile above 0.50 as the

expected value for this risk metric. We should note that the risk-values are highly sensitive to this statistical metric of choice, e.g. choosing the mean or the median drastically changes the anticipated severity of risk. Mean values for the risk are standard practice in PSHRA [McGuire et al. 2005], but they can be biased by low-probability high-consequence events. Certainly, for the local personal risk, the mean value needs to be adopted to be compliant with the current regulation, although aggregate personal risk is also a useful and consequential metric for society. The exact statistical metric of choice should be informed by a sensitivity study, after the risk tables have been constructed – to ensure that the Step 2 escalation process does not fail to escalate potentially problematic cases (with the Groningen experience in mind). As indicative values of choice we propose either the 66th percentile, the 84th percentile, or the mean. As a crude rule of thumb, mean (structural) risk values are usually close to the 84th percentile.

For demonstration purposes, we provide a simplified example to explain the post-processing workflow. Here, we use data and methods from a prior study that considered induced seismicity risks in the Netherlands [Schultz et al., 2022b]. From this study, we reproduce equivalent risk tables for nuisance, structural residential damages and LPR (Figure 18, first row). Each risk estimate (y axis) corresponds to a different scenario earthquake (x axis). The severity of risk increases monotonically as the scenario magnitude increases, as expected. Next, we use the GR-MFD probability density function weights to perform a weighted mean over the risk table obtained for the magnitude range between M_1 and M_2 (Figure 18, second row). We arbitrarily consider an M_{max} of M_L 4.5 as our upper truncation bound M_2. The lower truncation bound M_1 changes, simulating new largest events being recorded at this hypothetical gas field. Here, we see that the future risk also increases monotonically as the lower truncation bound changes (second row). We also compare against the impacts estimated from the Huizinge event (black horizontal lines). Note that this example has not scaled the Huzinge risk tolerances, contrary to our recommendation. For nuisance, damage, and LPR, all these risk metrics suggest that escalation to Step 3 should occur once an M_L 2.5-3.0 event has been observed. We reiterate that this is a simple example constructed just to demonstrate the conceptual workflow. It does not use the hazard and risk model-components that we proposed, and thus the results may not be indicative.

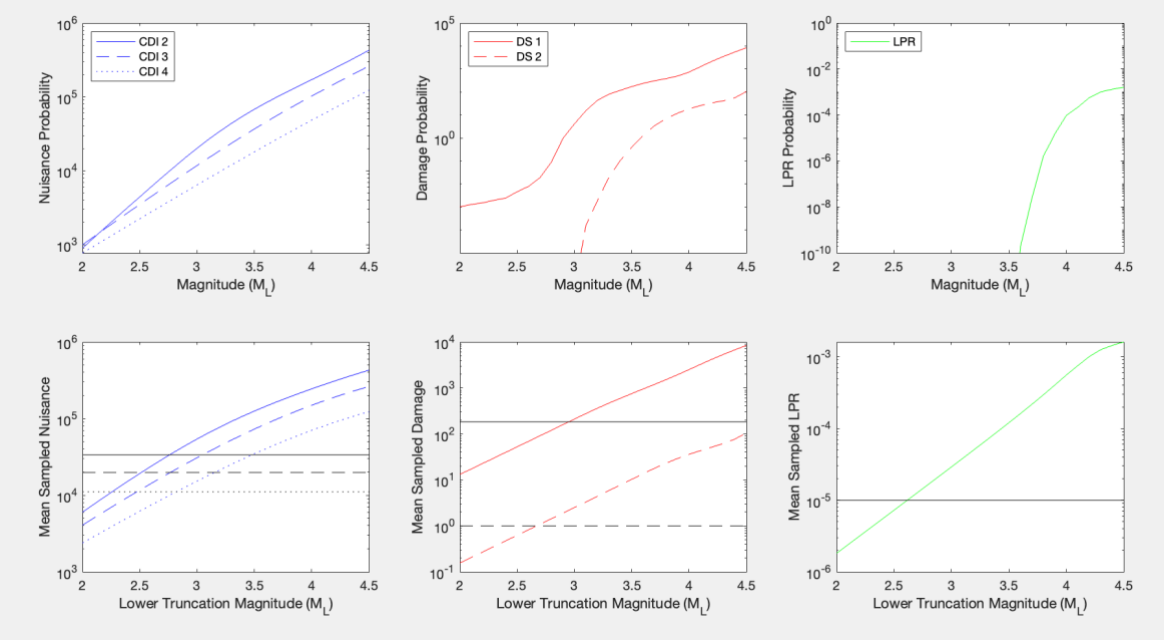

Figure 18. A stochastic application of the newly proposed Step 2 for a hypothetical gas field based on Schultz et al. [2022b]. Risk tables are computed for scenario magnitudes (top row). Risk metrics are estimated for various lower truncation magnitudes (bottom row; M_1) following the concept of a probabilistic scenario earthquake and compared against the Huizinge modelled risk estimates (black lines; benchmark). The upper truncation magnitude M_2 is always set to 4.5. DS are the (structural) damage-states, CDIs are nuisance states.

Here, we have outlined a post-processing approach that takes risk tables from scenario earthquakes to estimate probabilistic aggregate risk metrics. The latter are then compared against the (scaled) impacts of the Huizinge event to decide when to escalate to Step 3. Overall, this proposal is elegant, in the sense that we have decoupled it from source modelling of induced seismicity. This is necessary, since Step 2 can occur even before induced seismicity has been observed. This also allows for a clean transition into Step 3, since escalation will likely occur after earthquakes above M_c have been recorded – allowing for source modelling to begin after this data is collected. Since this approach is source-model agnostic, it may also be indiscriminately applied to other types of induced seismicity (e.g. linked to geothermal energy or carbon storage). Note that we have not explicitly placed a trailing seismicity model within the approach, since the existing trailing seismicity models are only calibrated on short-term cases of induced seismicity triggered by fluid-injection [Schultz et al., 2022a]. This allows for expert judgement to be incorporated – if information directly relevant to gas extraction cases becomes available in the future. This could be accomplished by changing the scaling factor for the Huzinge risk tolerances.

6.3 Specifications on the risk management plan

Under the current guidelines, Category II requires a binding, yet loosely defined, "risk management plan" that the operator must submit as part of the permit application process. This plan outlines a list of measures to be taken by the operator if certain magnitudes are exceeded within the field; it is essentially a magnitude-based TLS (section 3.3). The latest risk management plan of NAM, which operates 175 onshore gas fields in the country, is a good example [NAM 2021; their Table 3]. We will not discuss here the actions

related to communication and outreach, rather we will only focus on production- and permit- related matters. We propose a three-tier TLS, based on two magnitude-thresholds M_Y and M_R that will be defined later on:

- Green light: the maximum observed magnitude is below M_Y. Operations within the field continue as planned and the permit is still valid.
- Yellow light: the maximum observed magnitude is above M_Y but below M_R. Operations within the field continue as planned for another 24 hours, but within that time the operator must submit a report to the regulator with a list of targeted mitigation measures to limit the probability of a larger event. The permit is still valid, as long as the mitigation measures are faithfully implemented.
- Red light: the maximum observed magnitude is above M_R. Subsurface operations within the field must stop within 12 hours. Within 24 hours the operator must submit a report to the regulator with all the available relevant information and data. As long as the final magnitude of the event (as officiated by KNMI) remains above M_R, the permit is no longer valid and the operator must reapply for a Category III permit to the regulator. If the permit is accepted, the operator can restart production.

We define M_Y and M_R following a data-driven approach in line with the framework presented in section 6.2. For M_R, we first derive for each of the four risk metrics, which M_1 value results in escalation to Step 3 (according to section 6.2.6). We can solve for M_1, because M_2, the b-value, the risk thresholds, the source characteristics and all the model components are known. M_R is defined as the smallest from these four M_1 values. M_Y is equal to M_R minus 0.5 magnitude units. Obviously, for this plan to be operational, the M_c must be smaller than M_Y. Finally, if the measurement uncertainty behind the computed magnitude solutions is non-negligible (e.g. above 0.1 magnitude units), then it must be taken into account by conservatively adjusting M_c, M_Y and M_R (towards lower values).

The existing (minimum) monitoring requirements of the protocol also stand:

- Category I requires only KNMI's established nation-wide monitoring network
- Category II requires supplemental monitoring with an M_c of minimum 1.5 (M_L) in the vicinity of the gas field (including accelerometers).
- Category III requires supplemental monitoring with an M_c of minimum 1.5 (M_L) in the vicinity of the gas field (including accelerometers), and vibration-monitoring for residencies.

Acknowledgements

This work was commissioned and funded by the Dutch State Supervision of Mines (SodM). The authors thank Jorien L.N. van der Wal and Annemarie Muntendam-Bos for providing timely clarifications, relevant literature and constructive comments that led to crucial improvements in the contents of this report. We also acknowledge Federica Lanza for helpful discussions during the course of the project. Finally, we acknowledge Shawn Maxwell, Gunter Siddiqi and an anonymous reviewer for reviewing our work and providing their feedback.

References

Ader, T., Chendorain, M., Free, M., Saarno, T., Heikkinen, P., Malin, P. E., Leary, P., Kwiatek, G., Dresen, G., Bluemle, F., & Vuorinen, T. (2020). Design and implementation of a traffic light system for deep geothermal well stimulation in Finland. Journal of Seismology, 24(5), 991–1014. https://doi.org/10.1007/s10950-019-09853-y

Adushkin, V. V. (2016). Tectonic earthquakes of anthropogenic origin. *Izvestiya, Physics of the Solid Earth*, *52*(2), 173–194. https://doi.org/10.1134/S1069351316020014

Adushkin, V. V., Rodionov, V., Turuntaev, S., & Yudin, A. E. (2000). *Seismicity in the Oil Field*.

Akkar, S., Sandıkkaya, M. A., & Ay, B. Ö. (2014). Compatible ground-motion prediction equations for damping scaling factors and vertical-to-horizontal spectral amplitude ratios for the broader Europe region. Bulletin of Earthquake Engineering, 12(1), 517–547. https://doi.org/10.1007/s10518-013-9537-1

Albano, M., Polcari, M., Bignami, C., Moro, M., Saroli, M., & Stramondo, S. (2017). Did Anthropogenic Activities Trigger the 3 April 2017 Mw 6.5 Botswana Earthquake? *Remote Sensing*, *9*(10), 1028. https://doi.org/10.3390/rs9101028

Al-Enezi, A., Petrat, L., & Abdel-Fattah, R. (2008). *Induced Seismicity and Surface Deformation within Kuwait's Oil Fields*.

Allen, T. I., & Wald, D. J. (2009). On the Use of High-Resolution Topographic Data as a Proxy for Seismic Site Conditions (VS30). Bulletin of the Seismological Society of America, 99(2A), 935–943. https://doi.org/10.1785/0120080255

Allen, T. I., Wald, D. J., & Worden, C. B. (2012). Intensity attenuation for active crustal regions. Journal of seismology, 16, 409-433.

Amos, C. B., Audet, P., Hammond, W. C., Bürgmann, R., Johanson, I. A., & Blewitt, G. (2014). Uplift and seismicity driven by groundwater depletion in central California. *Nature*, *509*(7501), 483–486. https://doi.org/10.1038/nature13275

Aochi, H., & Burnol, A. (2018). Mechanism of the ML4.0 25 April 2016 earthquake in southwest of France in the vicinity of the Lacq gas field. *Journal of Seismology*, *22*(5), 1139–1155. https://doi.org/10.1007/s10950-018-9758-5

Arai, H. (2004). S-Wave Velocity Profiling by Inversion of Microtremor H/V Spectrum. Bulletin of the Seismological Society of America, 94(1), 53–63. https://doi.org/10.1785/0120030028

Atkinson, G. M., & Wald, D. J. (2007). "Did You Feel It?" intensity data: A surprisingly good measure of earthquake ground motion. Seismological Research Letters, 78(3), 362-368.

Atkinson, G. M., & Adams, J. (2013). Ground motion prediction equations for application to the 2015 Canadian national seismic hazard maps. Canadian Journal of Civil Engineering, 40(10), 988-998.

Atkinson, G. M., J. J. Bommer, and N. A. Abrahamson (2014a). Alternative approaches to modeling epistemic uncertainty in ground motions in probabilistic seismic-hazard analysis, Seismol. Res. Lett. 85, 1141–1144.

Atkinson, G. M., Worden, C. B., & Wald, D. J. (2014b). Intensity prediction equations for North America. Bulletin of the Seismological Society of America, 104(6), 3084-3093.

Ahmadzadeh, S., G. J. Doloei, and H. Zafarani (2020). New intensity prediction equation for Iran, J. Seismol. 24, no. 1, 23–35. Allen, T. I., D. J. Wald, and C. B. Worden (2012). Intensity attenuation for active crustal regions, J. Seismol. 16, no. 3, 409–433.

Amini, A., Mehrabifard, A., & Eberhardy, E. (2021). Development of an induced seismicity susceptibility framework and map for NEBC using an integrated machine learning and mechanistic validation approach. Geoscience BC Rept. 2021-11.

Assumpção, M., Yamabe, T. H., Barbosa, J. R., Hamza, V., Lopes, A. E. V., Balancin, L., & Bianchi, M. B. (2010). Seismic activity triggered by water wells in the Paraná Basin, Brazil. *Water Resources Research*, *46*(7). https://doi.org/10.1029/2009WR008048

Bachmann, C. E., Wiemer, S., Woessner, J., & Hainzl, S. (2011). Statistical analysis of the induced Basel 2006 earthquake sequence: Introducing a probability-based monitoring approach for Enhanced Geothermal Systems: Probability-based monitoring approach for EGS. Geophysical Journal International, 186(2), 793–807. https://doi.org/10.1111/j.1365-246X.2011.05068.x

Bal, I. E., Smyrou, E., & Bulder, E. (2019). Liability and damage claim issues in induced earthquakes. Conference on Earthquake risk and engineering towards a resilient world. London.

Baisch, S., Koch, C., & Muntendam-Bos, A. (2019). Traffic Light Systems: To What Extent Can Induced Seismicity Be Controlled? Seismological Research Letters, 90(3), 1145–1154. https://doi.org/10.1785/0220180337

Baranova, V., Mustaqeem, A., & Bell, S. (1999). *A model for induced seismicity caused by hydrocarbon production in the Western Canada Sedimentary Basin*. *36*, 18.

Bardainne, T., Dubos-Sallée, N., Sénéchal, G., Gaillot, P., & Perroud, H. (2008). Analysis of the induced seismicity of the Lacq gas field (Southwestern France) and model of deformation. *Geophysical Journal International*, *172*(3), 1151–1162. https://doi.org/10.1111/j.1365-246X.2007.03705.x

Bella, F., Biagi, P. F., Caputo, M., Cozzi, E., Della Monica, G., Ermini, A., Plastino, W., & Sgrigna, V. (1998). Aquifer-induced Seismicity in the Central Apennines (Italy). In S. Talebi (Ed.), *Seismicity Caused by Mines, Fluid Injections, Reservoirs, and Oil Extraction* (pp. 179–194). Birkhäuser Basel. https://doi.org/10.1007/978-3-0348-8804-2_11

Barbat AH, Eeri M, Moya FY and Canas JA (1996). Damage Scenarios Simulation for Seismic Risk. Earthquake Spectra 12(3): 371–394.

Bard, P.-Y., Campillo, M., Chávez-Garcia, F. J., & Sánchez-Sesma, F. (1988). The Mexico Earthquake of September 19, 1985—A Theoretical Investigation of Large- and Small-scale Amplification Effects in the Mexico City Valley. Earthquake Spectra, 4(3), 609–633. https://doi.org/10.1193/1.1585493

Barnhart, W. D., Yeck, W. L., & McNamara, D. E. (2018). Induced earthquake and liquefaction hazards in Oklahoma, USA: Constraints from InSAR. Remote sensing of environment, 218, 1-12.

Beirlant, J., Kijko, A., Reynkens, T., & Einmahl, J. H. J. (2018). Estimating the maximum possible earthquake magnitude using extreme value methodology: The Groningen case. Natural Hazards. https://doi.org/10.1007/s11069-017-3162-2

Bindi, D., Massa, M., Luzi, L., Ameri, G., Pacor, F., Puglia, R., & Augliera, P. (2014). Pan-European ground-motion prediction equations for the average horizontal component of PGA, PGV, and 5 %-damped PSA at spectral periods up to 3.0 s using the RESORCE dataset. Bulletin of Earthquake Engineering, 12(1), 391–430. https://doi.org/10.1007/s10518-013-9525-5

Bilich, A., Clark, S., Creighton, B., & Frohlich, C. (1998). Felt Reports from the Alice, Texas, Earthquake of 24 March 1997. *Seismological Research Letters*, *69*(2), 117–122. https://doi.org/10.1785/gssrl.69.2.117

Bommer, J. J., Oates, S., Cepeda, J. M., Lindholm, C., Bird, J., Torres, R., Marroquín, G., & Rivas, J. (2006). Control of hazard due to seismicity induced by a hot fractured rock geothermal project. Engineering Geology, 83(4), 287–306. https://doi.org/10.1016/j.enggeo.2005.11.002

Bommer, J. J., & Scherbaum, F. (2008). The Use and Misuse of Logic Trees in Probabilistic Seismic Hazard Analysis. Earthquake Spectra, 24(4), 997–1009. https://doi.org/10.1193/1.2977755

Bommer, J. J., Douglas, J., Scherbaum, F., Cotton, F., Bungum, H., & Fäh, D. (2010). On the Selection of Ground-Motion Prediction Equations for Seismic Hazard Analysis. Seismological Research Letters, 81(5), 783–793. https://doi.org/10.1785/gssrl.81.5.783

Bommer, J. J. (2012). Challenges of building logic trees for probabilistic seismic hazard analysis, Earthq. Spectra 28, 1723–1735.

Bommer, J. J., Crowley, H., & Pinho, R. (2015). A risk-mitigation approach to the management of induced seismicity. Journal of Seismology, 19(2), 623–646. https://doi.org/10.1007/s10950-015-9478-z

Bommer, J. J., Dost, B., Edwards, B., Stafford, P. J., van Elk, J., Doornhof, D., & Ntinalexis, M. (2016). Developing an Application-Specific Ground-Motion Model for Induced Seismicity. Bulletin of the Seismological Society of America, 106(1), 158–173. https://doi.org/10.1785/0120150184

Bommer, J. J., Stafford, P. J., Edwards, B., Dost, B., van Dedem, E., Rodriguez-Marek, A., Kruiver, P., van Elk, J., Doornhof, D., & Ntinalexis, M. (2017). Framework for a Ground-Motion Model for Induced Seismic Hazard and Risk Analysis in the Groningen Gas Field, The Netherlands. Earthquake Spectra, 33(2), 481–498. https://doi.org/10.1193/082916EQS138M

Bommer, J. J., & Crowley, H. (2017). The Purpose and Definition of the Minimum Magnitude Limit in PSHA Calculations. Seismological Research Letters, 88(4), 1097–1106. https://doi.org/10.1785/0220170015

Bommer, J. J., & van Elk, J. (2017). Comment on "The Maximum Possible and the Maximum Expected Earthquake Magnitude for Production-Induced Earthquakes at the Gas Field in Groningen, The Netherlands" by Gert Zöller and Matthias Holschneider. Bulletin of the Seismological Society of America, 107(3), 1564–1567. https://doi.org/10.1785/0120170040

Bommer, J. J. (2022). Earthquake hazard and risk analysis for natural and induced seismicity: Towards objective assessments in the face of uncertainty. Bulletin of Earthquake Engineering, 20(6), 2825–3069. https://doi.org/10.1007/s10518-022-01357-4

Bommer, J. J., Stafford, P. J., Ruigrok, E., Rodriguez-Marek, A., Ntinalexis, M., Kruiver, P. P., Edwards, B., Dost, B., & van Elk, J. (2022a). Ground-motion prediction models for induced earthquakes in the Groningen gas field, the Netherlands. Journal of Seismology, 26(6), 1157–1184. https://doi.org/10.1007/s10950-022-10120-w

Bommer JJ, Edwards B, Kruiver PP, Rodriguez-Marek A, Stafford PJ, Ntinalexis M, Ruigrok E, Dost B (2022b). V7 ground-motion model for induced seismicity in the Groningen gas field, Revision 1, 20 February 2022, 282 pp, available for download at https://nam-onderzoeksrapporten.data-app.nl/reports/download/groningen/en/06766b7a-1999-4f48-977c-33a5d94cdd82

Bonilla, L. F., Tsuda, K., Pulido, N., Régnier, J., & Laurendeau, A. (2011). Nonlinear site response evidence of K-NET and KiK-net records from the 2011 off the Pacific coast of Tohoku Earthquake. Earth, Planets and Space, 63(7), 785–789. https://doi.org/10.5047/eps.2011.06.012

Bonnefoy-Claudet, S., Baize, S., Bonilla, L. F., Berge-Thierry, C., Pasten, C., Campos, J., Volant, P., & Verdugo, R. (2009). Site effect evaluation in the basin of Santiago de Chile using ambient noise measurements. Geophysical Journal International, 176(3), 925–937. https://doi.org/10.1111/j.1365-246X.2008.04020.x

Bonnefoy-Claudet, S., Cotton, F., & Bard, P.-Y. (2006). The nature of noise wavefield and its applications for site effects studies: A literature review. Earth-Science Reviews, 79(3), 205–227. https://doi.org/10.1016/j.earscirev.2006.07.004

Boore, D. M., Joyner, W. B., & Fumal, T. E. (1997). Equations for estimating horizontal response spectra and peak acceleration from western North American earthquakes: A summary of recent work. Seismological research letters, 68(1), 128-153.

Boore, D. M., R. R. Youngs, A. R. Kottke, J. J. Bommer, R. Darragh, W. J. Silva, P. J. Stafford, L. Al Atik, A. Rodriguez-Marek, and J. Kaklamanos (2022). Construction of a Ground-Motion Logic Tree through Host-to Target Region Adjustments Applied to an Adaptable Ground-Motion Prediction Model, Bull. Seismol. Soc. Am., doi: 10.1785/0120220056

Borges, F., Landrø, M., & Duffaut, K. (2020). Time-lapse seismic analysis of overburden water injection at the Ekofisk field, southern North Sea. *GEOPHYSICS*, *85*(1), B9–B21. https://doi.org/10.1190/geo2019-0140.1

Bossu, R., & Grasso, J.-R. (1996). Stress analysis in the intraplate area of Gazli, Uzbekistan, from different sets of earthquake focal mechanisms. *Journal of Geophysical Research: Solid Earth*, *101*(B8), 17645–17660. https://doi.org/10.1029/96JB01182

Bou-Rabee, F. (1994). EARTHQUAKE RECURRENCE IN KUWAIT INDUCED BY OIL AND GAS EXTRACTION. *Journal of Petroleum Geology*, *17*(4), 473–480. https://doi.org/10.1111/j.1747-5457.1994.tb00152.x

Bou-Rabee, F. (2000). Seismotectonics and earthquake activity of Kuwait. *Journal of Seismology*, *4*(2), 133–141. https://doi.org/10.1023/A:1009838401027

Bou-Rabee, F., & Abdel-Fattah, R. M. (2004). *Seismological observations in the State of Kuwait*.

Bou-Rabee, F., & Nur, A. (2002). *The 1993 M4.7 Kuwait earthquake: Induced by the burning of the oil fields*.

Bourne, S. J., Oates, S. J., van Elk, J., & Doornhof, D. (2014). A seismological model for earthquakes induced by fluid extraction from a subsurface reservoir. Journal of Geophysical Research: Solid Earth, 119(12), 8991-9015

Bourne SJ, Oates SJ, Bommer JJ, Dost B, van Elk J and Doornhof D (2015) A Monte Carlo method for probabilistic hazard assessment of induced seismicity due to conventional natural gas production. Bulletin of the Seismological Society of America 105(3): 1721–1738.

Bourne, S. J., & Oates, S. J. (2020). Stress-Dependent Magnitudes of Induced Earthquakes in the Groningen Gas Field. Journal of Geophysical Research: Solid Earth, 125(11). https://doi.org/10.1029/2020JB020013

Bradley, B. A. (2012). Strong ground motion characteristics observed in the 4 September 2010 Darfield, New Zealand earthquake. Soil Dynamics and Earthquake Engineering, 42, 32–46. https://doi.org/10.1016/j.soildyn.2012.06.004

Braun, T., Cesca, S., Kühn, D., Martirosian-Janssen, A., & Dahm, T. (2018). Anthropogenic seismicity in Italy and its relation to tectonics: State of the art and perspectives. *Anthropocene*, *21*, 80–94. https://doi.org/10.1016/j.ancene.2018.02.001

Braun, T., Danesi, S., & Morelli, A. (2020). Application of monitoring guidelines to induced seismicity in Italy. *Journal of Seismology*, *24*(5), 1015–1028. https://doi.org/10.1007/s10950-019-09901-7

Brzev, S., Scawthorn, C., Charleson, A. W., Allen, L., Greene, M., Jaiswal, K., & Silva, V. (2013). GEM building taxonomy (Version 2.0) (No. 2013-02). GEM Foundation.

Caciagli, M., Camassi, R., Danesi, S., Pondrelli, S., & Salimbeni, S. (2015). Can We Consider the 1951 Caviaga (Northern Italy) Earthquakes as Noninduced Events? *Seismological Research Letters*, *86*(5), 1335–1344. https://doi.org/10.1785/0220150001

Caloi, P. (1956). *Terremoti della Val Padana del 15–16 maggio*.

CAPP. (2012). CAPP Hydraulic Fracturing Operating Practice: Anomalous induced seismicity: assessment, monitoring, mitigation and response.

Candela, T., Osinga, S., Ampuero, J. P., Wassing, B., Pluymaekers, M., Fokker, P. A., ... & Muntendam- Bos, A. G. (2019). Depletion-induced seismicity at the Groningen gas field: Coulomb rate-and-state models including differential compaction effect. Journal of Geophysical Research: Solid Earth, 124(7), 7081-7104.

Chang, T. M., Ammon, C. J., & Herrmann, R. B. (1998). Faulting parameters of the October 24, 1997 southern Alabama earthquake. *Seismological Research Letters*.

Chen, R., Zhu, J., Li, S., Zhang, S., Chen, X., Li, Q., Wang, P., Zhang, J., Dai, L., & Jia, Y. (2023). Characteristics and mechanisms of human-induced earthquakes in China from the QuakeQuake database. Geological Journal, gj.4713. https://doi.org/10.1002/gj.4713

Cheung, R., Wetherell, D., & Whitaker, S. (2018). Induced earthquakes and housing markets: Evidence from Oklahoma. Regional Science and Urban Economics, 69, 153-166.

Chieppa, D., Hobiger, M., Bergamo, P., & Fäh, D. (2020). Ambient Vibration Analysis on Large Scale Arrays When Lateral Variations Occur in the Subsurface: A Study Case in Switzerland. Pure and Applied Geophysics, 177(9), 4247–4269. https://doi.org/10.1007/s00024-020-02516-x

Cesca, S., Dahm, T., Juretzek, C., & Kühn, D. (2011). Rupture process of the 2001 May 7 Mw 4.3 Ekofisk induced earthquake: The Ekofisk induced earthquake. *Geophysical Journal International*, *187*(1), 407–413. https://doi.org/10.1111/j.1365-246X.2011.05151.x

Convertito V, Maercklin N, Sharma N and Zollo A (2012) From induced seismicity to direct time- dependent seismic hazard. Bulletin of the Seismological Society of America 102(6): 2563–2573.

Cotton, F., Scherbaum, F., Bommer, J. J., & Bungum, H. (2006). Criteria for selecting and adjusting ground-motion models for specific target regions: Application to central Europe and rock sites. Journal of Seismology, 10, 137-156.

Cramer CH, Petersen MD and Reichle MS (1996). A Monte Carlo approach in estimating uncertainty for a seismic hazard assessment of Los Angeles, Ventura, and Orange Counties, California. Bulletin of the Seismological Society of America 86(6): 1681–1691.

Cremen, G., Werner, M. J., & Baptie, B. (2020). A New Procedure for Evaluating Ground-Motion Models, with Application to Hydraulic-Fracture-Induced Seismicity in the United Kingdom. Bulletin of the Seismological Society of America, 110(5), 2380–2397. https://doi.org/10.1785/0120190238

Crow, H., & Hunter, J. (2015). Shear Wave Velocity Measurement Guidelines for Canadian Seismic Site Characterization in Soil and RockOF 7078.

Crowley H and Bommer JJ (2006). Modelling seismic hazard in earthquake loss models with spatially distributed exposure. Bulletin of Earthquake Engineering 4(3): 249–273.

Crowley, H., Özcebe, S., Spence, R., Foulser-Piggott, R., Erdik, M., & Alten, K. (2012, September). Development of a European building inventory database. In Proceedings of the 15th world conference on earthquake engineering (pp. 24-28).

Crowley, H., Polidoro, B., Pinho, R., & van Elk, J. (2017). Framework for developing fragility and consequence models for local personal risk. Earthquake Spectra, 33(4), 1325–1345.

Crowley, H., Pinho, R., van Elk, J., & Uilenreef, J. (2019). Probabilistic damage assessment of buildings due to induced seismicity. Bulletin of Earthquake Engineering, 17(8), 4495–4516. https://doi.org/10.1007/s10518-018-0462-1

Crowley, H., & Pinho, R. (2020). Report on the Fragility and Consequence Models for the Groningen Field (Version 7). NAM Report, p. 83.

Crowley, H., Despotaki, V., Rodrigues, D., Silva, V., Toma-Danila, D., Riga, E., Karatzetzou, A., Fotopoulou, S., Zugic, Z., Sousa, L., Ozcebe, S., & Gamba, P. (2020). Exposure model for European seismic risk assessment. Earthquake Spectra, 875529302091942. https://doi.org/10.1177/8755293020919429

Crowley H., V. Despotaki, D. Rodrigues, V. Silva, C. Costa, D. Toma-Danila, E. Riga, A. Karatzetzou, S. Fotopoulou, L. Sousa, S. Ozcebe, P. Gamba, J. Dabbeek, X. Romão, N. Pereira, J. M. Castro, J. Daniell, E. Veliu, H. Bilgin, C. Adam, M. Deyanova, N. Ademović, J. Atalic, B. Bessason, V. Shendova, A. Tiganescu, Z. Zugic, S. Akkar, U. Hancilar (2021). European Exposure Model Data Repository [Data set]. Zenodo. http://doi.org/10.5281/zenodo.4062044

Cypser, D. A., & Davis, S. D. (1998). Induced seismicity and the potential for liability under US law. Tectonophysics, 289(1-3), 239-255.

Dabbeek, J., Crowley, H., Silva, V., Weatherill, G., Paul, N., & Nievas, C. I. (2021). Impact of exposure spatial resolution on seismic loss estimates in regional portfolios. Bulletin of Earthquake Engineering, 19(14), 5819–5841. https://doi.org/10.1007/s10518-021-01194-x

Davis, S. D., & Frohlich, C. (1993). Did (Or Will) Fluid Injection Cause Earthquakes? - Criteria for a Rational Assessment. Seismological Research Letters, 64(3–4), 207–224. https://doi.org/10.1785/gssrl.64.3-4.207

Dahm, T., Kruger, F., Stammler, K., Klinge, K., Kind, R., Wylegalla, K., & Grasso, J.-R. (2007). The 2004 Mw 4.4 Rotenburg, Northern Germany, Earthquake and Its Possible Relationship with Gas Recovery. *Bulletin of the Seismological Society of America*, *97*(3), 691–704. https://doi.org/10.1785/0120050149

Dahm, T., Kratzsch, T., & Zang, A. (2017). Discrimination between induced, triggered, and natural earthquakes close to hydrocarbon reservoirs: A probabilistic approach based on the modeling of depletion-induced stress changes and seismological source parameters. Journal of Geophysical Research: Solid Earth, 122(11), 9243-9263. doi:10.1002/2017JB014348

Davis, Pennington, & Carlson. (1989). *A compendium of earthquake acitvity in Texas*.

Davis, S. D., Nyffenegger, P., & Frohlich, C. (1995). The 9 April 1993 earthquake in south-central Texas: Was it induced by fluid withdrawal? *Bulletin of the Seismological Society of America*.

de Jager, J., & Visser, C. (2017). Geology of the Groningen field – an overview. *Netherlands Journal of Geosciences*, *96*(5), s3–s15. https://doi.org/10.1017/njg.2017.22

Delavaud, E., Cotton, F., Akkar, S., Scherbaum, F., Danciu, L., Beauval, C., ... & Theodoulidis, N. (2012). Toward a ground-motion logic tree for probabilistic seismic hazard assessment in Europe. Journal of Seismology, 16, 451-473.

Dempsey, D., & Suckale, J. (2017). Physics-based forecasting of induced seismicity at Groningen gas field, the Netherlands. Geophysical Research Letters, 44(15), 7773-7782.

Dempsey, D. E., & Suckale, J. (2023). Physics-Based Forecasting of Induced Seismicity at Groningen Gas Field, The Netherlands: Post Hoc Evaluation and Forecast Update. Seismological Society of America.

Deng, F., Dixon, T. H., & Xie, S. (2020). Surface Deformation and Induced Seismicity Due to Fluid Injection and Oil and Gas Extraction in Western Texas. *Journal of Geophysical Research: Solid Earth*, *125*(5). https://doi.org/10.1029/2019JB018962

Derras, B., Bard, P.-Y., & Cotton, F. (2020). VS30, slope, H800 and f0.

Doblas, M., Youbi, N., De Las Doblas, J., & Galindo, A. J. (2014). The 2012/2014 swarmquakes of Jaen, Spain: A working hypothesis involving hydroseismicity associated with the hydrologic cycle and anthropogenic activity. *Natural Hazards*, *74*(2), 1223–1261. https://doi.org/10.1007/s11069-014-1242-0

Doser, D. I., Baker, M. R., Luo, M., Marroquin, P., Ballesteros, L., Kingwell, J., Diaz, H. L., & Kaip, G. (1992). The not so simple relationship between seismicity and oil production in the Permian Basin, west Texas. *Pure and Applied Geophysics PAGEOPH*, *139*(3–4), 481–506. https://doi.org/10.1007/BF00879948

Doser, D. I., Baker, M. R., & Mason, D. B. (1991). Seismicity in the War-Wink gas field, Delaware Basin, West Texas, and its relationship to petroleum production. *Bulletin of the Seismological Society of America*, *81*(3), 971–986.

Dost, B., Goutbeek, F., van Eck, T., & Kraaijpoel, D. (2012). Monitoring induced seismicity in the North of the Netherlands: Status report 2010. *Scientific Report; WR 2012-03*.

Dost, B., & Haak, H. W. (2007). *Natural and induced seismicity*.

Dost, B., & Kraaijpoel, D. (2013). *The August 16, 2012 earthquake near Huizinge (Groningen)*.

Dost, B., van Stiphout, A., Kühn, D., Kortekaas, M., Ruigrok, E., & Heimann, S. (2020). Probabilistic Moment Tensor Inversion for Hydrocarbon-Induced Seismicity in the Groningen Gas Field, the Netherlands, Part 2: Application. *Bulletin of the Seismological Society of America*, *110*(5), 2112–2123. https://doi.org/10.1785/0120200076

Douglas, J., B. Edwards, V. Convertito, N. Sharma, A. Tramelli, D. Kraaijpoel, B. M. Cabrera, N. Maercklin, and C. Troise (2013). Predicting ground motion from induced earthquakes in geothermal areas, Bull. Seismol. Soc. Am. 103, no. 3, 1875–1897.

Douglas, J. (2018). Calibrating the backbone approach for the development of earthquake ground motion models. Best Practice in Physics-based Fault Rupture Models for Seismic Hazard Assessment of Nuclear Installations: Issues and Challenges Towards Full Seismic Risk Analysis.

Dowrick, D., and D. Rhoades (2005). Revised models for attenuation of modified Mercalli intensity in New Zealand earthquakes, Bull. New Zeal. Soc. Earthq. Eng. 38, no. 4, 185–214.

Eagar, K. C., Pavlis, G. L., & Hamburger, M. W. (2006). Evidence of Possible Induced Seismicity in the Wabash Valley Seismic Zone from Improved Microearthquake Locations. *Bulletin of the Seismological Society of America*, *96*(5), 1718–1728. https://doi.org/10.1785/0120050190

Eaton, D. W., & Schultz, R. (2018). Increased likelihood of induced seismicity in highly overpressured shale formations. Geophysical Journal International, 214(1), 751–757. https://doi.org/10.1093/gji/ggy167

Edwards, B., Staudenmaier, N., Cauzzi, C., & Wiemer, S. (2018). A Hybrid Empirical Green's Function Technique for Predicting Ground Motion from Induced Seismicity: Application to the Basel Enhanced Geothermal System. Geosciences, 8(5), 180. https://doi.org/10.3390/geosciences8050180

Edwards, B., Crowley, H., Pinho, R., & Bommer, J. J. (2021). Seismic Hazard and Risk Due to Induced Earthquakes at a Shale Gas Site. Bulletin of the Seismological Society of America. https://doi.org/10.1785/0120200234

Esteva, L., & Rosenblueth, E. (1964). Espectros de temblores a distancias moderadas y grandes. Boletin Sociedad Mexicana de Ingenieria Sesmica, 2(1), 1-18.

Evans, D. G., & Steeples, D. W. (1987). Microearthquakes near the Sleepy Hollow oil field, southwestern Nebraska. *Bulletin of the Seismological Society of America*, *77*(1), 132–140. https://doi.org/10.1785/BSSA0770010132

Fäh, D., Kind, F., & Giardini, D. (2001). A theoretical investigation of average H/V ratios. Geophysical Journal International, 145(2), 535–549. https://doi.org/10.1046/j.0956-540x.2001.01406.x

Falcone, G., Acunzo, G., Mendicelli, A., Mori, F., Naso, G., Peronace, E., Porchia, A., Romagnoli, G., Tarquini, E., & Moscatelli, M. (2021). Seismic amplification maps of Italy based on site-specific microzonation dataset and one-dimensional numerical approach. Engineering Geology, 289, 106170. https://doi.org/10.1016/j.enggeo.2021.106170

Fan, X., Scaringi, G., Korup, O., West, A. J., Westen, C. J., Tanyas, H., Hovius, N., Hales, T. C., Jibson, R. W., Allstadt, K. E., Zhang, L., Evans, S. G., Xu, C., Li, G., Pei, X., Xu, Q., & Huang, R. (2019). Earthquake-Induced Chains of Geologic Hazards: Patterns, Mechanisms, and Impacts. Reviews of Geophysics, 57(2), 421–503. https://doi.org/10.1029/2018RG000626

Federal Emergency Management Agency (FEMA) (2013). Multi-Hazard Loss Estimation Methodology, Earthquake Model, Hazus-MH 2.1, Technical Manual.

FKPE. (2022). *Sitzungen der AGIS des FKPE*. https://www.fkpe.org/arbeitsgruppen/induzierte-seismizitaet

Foulger, G. R., Wilson, M. P., Gluyas, J. G., Julian, B. R., & Davies, R. J. (2018). Global review of human-induced earthquakes. Earth-Science Reviews, 178, 438–514. https://doi.org/10.1016/j.earscirev.2017.07.008

Foti, S., Hollender, F., Garofalo, F., Albarello, D., Asten, M., Bard, P.-Y., Comina, C., Cornou, C., Cox, B., Di Giulio, G., Forbriger, T., Hayashi, K., Lunedei, E., Martin, A., Mercerat, D., Ohrnberger, M., Poggi, V., Renalier, F., Sicilia, D., & Socco, V. (2018). Guidelines for the good practice of surface wave analysis: A product of the InterPACIFIC project. Bulletin of Earthquake Engineering, 16(6), 2367–2420. https://doi.org/10.1007/s10518-017-0206-7

Frash, L. P., Fu, P., Morris, J., Gutierrez, M., Neupane, G., Hampton, J., Welch, N. J., Carey, J. W., & Kneafsey, T. (2021). Fracture Caging to Limit Induced Seismicity. Geophysical Research Letters, 48(1). https://doi.org/10.1029/2020GL090648

Frohlich, C., & Brunt, M. (2013). Two-year survey of earthquakes and injection/production wells in the Eagle Ford Shale, Texas, prior to the Mw 4.8 20 October 2011 earthquake. *Earth and Planetary Science Letters*, *379*, 56–63. https://doi.org/10.1016/j.epsl.2013.07.025

Frohlich, C., DeShon, H., Stump, B., Hayward, C., Hornbach, M., & Walter, J. I. (2016). A Historical Review of Induced Earthquakes in Texas. *Seismological Research Letters*, *87*(4), 1022–1038. https://doi.org/10.1785/0220160016

Frohlich, C., Glidewell, J., & Brunt, M. (2012). Location and Felt Reports for the 25 April 2010 mbLg 3.9 Earthquake near Alice, Texas: Was it Induced by Petroleum Production? *Bulletin of the Seismological Society of America*, *102*(2), 457–466. https://doi.org/10.1785/0120110179

Frohlich, C., Potter, E., Hayward, C., & Stump, B. (2010). Dallas-Fort Worth earthquakes coincident with activity associated with natural gas production. *The Leading Edge*, *29*(3), 270–275. https://doi.org/10.1190/1.3353720

Fryer, B., Siddiqi, G., & Laloui, L. (2019). Compaction-induced permeability loss's effect on induced seismicity during reservoir depletion. Pure and Applied Geophysics, 176, 4277-4296.

Galloway, E., Hauck, T., Corlett, H., Pană, D., & Schultz, R. (2018). Faults and associated karst collapse suggest conduits for fluid flow that influence hydraulic fracturing-induced seismicity. Proceedings of the National Academy of Sciences, 115(43). https://doi.org/10.1073/pnas.1807549115

Garcia, A., Faenza, L., Morelli, A., & Antoncecchi, I. (2021). *Can hydrocarbon extraction from the crust enhance or inhibit seismicity in tectonically active regions? A statistical study in Italy*. 18.

Gariel, J.-C., C., H., Jongmans, D., & Camelbeeck, T. (1994). Strong motion computation of the april 13, 1992 Roermond earthquake from linear methods using locally recorded aftershocks. Geologie En Mijnbouw, 73, 315–321.

Ghasemi, H., & Allen, T. I. (2017). Testing the sensitivity of seismic hazard in Australia to new empirical magnitude conversion equations. Proceedings of the AEES, Canberra, ACT, Australia, 24-26.

Gestermann, N., & Plenefisch, T. (2016). *Seismic network detection capability within the natural gas fields in Northern Germany*. EPSC2016-16130.

Gestermann, N., Plenefisch, T., & Bischoff, M. (2015). *Seismicity and stress field in the vicinity of natural gas fields in Northern Germany*. 7370.

Gerstenberger, M. C., Marzocchi, W., Allen, T., Pagani, M., Adams, J., Danciu, L., Field, E. H., Fujiwara, H., Luco, N., Ma, K. -F., Meletti, C., & Petersen, M. D. (2020). Probabilistic Seismic Hazard Analysis at Regional and National Scales: State of the Art and Future Challenges. Reviews of Geophysics, 58(2). https://doi.org/10.1029/2019RG000653

Glennie, K. W. (Ed.). (1998). *Petroleum geology of the North Sea: Basic concepts and recent advances* (4th ed). Blackwell Science.

Goebel, T. H. W., & Shirzaei, M. (2021). More Than 40 yr of Potentially Induced Seismicity Close to the San Andreas Fault in San Ardo, Central California. *Seismological Research Letters*, *92*(1), 187–198. https://doi.org/10.1785/0220200276

Gomberg, J., & Wolf, L. (1999). Possible cause for an improbable earthquake: The 1997 Mw 4.9 southern Alabama earthquake and hydrocarbon recovery. *Geology*, *27*(4), 367. https://doi.org/10.1130/0091-7613(1999)027<0367:PCFAIE>2.3.CO;2

González, P. J., Tiampo, K. F., Palano, M., Cannavó, F., & Fernández, J. (2012). The 2011 Lorca earthquake slip distribution controlled by groundwater crustal unloading. *Nature Geoscience*, *5*(11), 821–825. https://doi.org/10.1038/ngeo1610

Grant, D. N., Dennis, J., Sturt, R., Milan, G., McLennan, D., Negrette, P., da Costa, R., & Palmieri, M. (2021). Explicit modelling of collapse for Dutch unreinforced masonry building typology fragility functions. Bulletin of Earthquake Engineering, 19(15), 6497–6519. https://doi.org/10.1007/s10518-020-00923-y

Grasso, J. R., & Wittlinger, G. (1990). Ten years of seismic monitoring over a gas field.

Grasso, J.-R. (1992). Mechanics of seismic instabilities induced by the recovery of hydrocarbons. *Pure and Applied Geophysics PAGEOPH*, *139*(3–4), 507–534. https://doi.org/10.1007/BF00879949

Grasso, J.-R., & Sornette, D. (1998). Testing self-organized criticality by induced seismicity. *Journal of Geophysical Research: Solid Earth*, *103*(B12), 29965–29987. https://doi.org/10.1029/97JB01344

Grasso, J.-R., Amorese, D., & Karimov, A. (2021). Did Wastewater Disposal Drive the Longest Seismic Swarm Triggered by Fluid Manipulations? Lacq, France, 1969–2016. Bulletin of the Seismological Society of America, 111(5), 2733–2752. https://doi.org/10.1785/0120200359

Green, R. (2020). Liquefaction Hazard in the Groningen Region of the Netherlands due to Induced Seismicity. https://ascelibrary.org/doi/epdf/10.1061/%28ASCE%29GT.1943-5606.0002286

Green, R. A., Bommer, J. J., Rodriguez-Marek, A., Maurer, B. W., Stafford, P. J., Edwards, B., Kruiver, P. P., de Lange, G., & van Elk, J. (2019). Addressing limitations in existing 'simplified' liquefaction triggering evaluation procedures: Application to induced seismicity in the Groningen gas field. Bulletin of Earthquake Engineering, 17(8), 4539–4557. https://doi.org/10.1007/s10518-018-0489-3

Green, R., & Bommer, J. (n.d.). Smallest Earthquake Magnitude that Can Trigger Liquefaction.

Grigoli, F., Cesca, S., Rinaldi, A. P., Manconi, A., López-Comino, J. A., Clinton, J. F., Westaway, R., Cauzzi, C., Dahm, T., & Wiemer, S. (2018). The November 2017 M w 5.5 Pohang earthquake: A possible case of induced seismicity in South Korea. Science, 360(6392), 1003–1006. https://doi.org/10.1126/science.aat2010

Grigoratos, I., Bazzurro, P., Rathje, E., & Savvaidis, A. (2021). Time-dependent seismic hazard and risk due to wastewater injection in Oklahoma. Earthquake Spectra, 37(3), 2084–2106. https://doi.org/10.1177/8755293020988020

Grigoratos, I., Rathje, E., Bazzurro, P., & Savvaidis, A. (2022). Distinguishing the causal factors of induced seismicity in the Delaware basin: Hydraulic fracturing or wastewater disposal? Seismological Research Letters, 110(5), 2483–2497.

Grünthal, G. (2014). Induced seismicity related to geothermal projects versus natural tectonic earthquakes and other types of induced seismic events in Central Europe. Geothermics, 52, 22–35. https://doi.org/10.1016/j.geothermics.2013.09.009

Gudehus, G., Lempp, C., Scheffzük, C., Műller, B. I., & Schilling, F. R. (2023). Depletion-induced seismicity in NW-Germany: Lessons from comprehensive investigations. *Acta Geotechnica*, *18*(2), 951–969. https://doi.org/10.1007/s11440-022-01513-9

Gussinklo, H. J., Haak, H. W., Quadvlieg, R. C. H., Schutjens, P. M. F. M., & Vogelaar, L. (2001). Subsidence, tremors and society. *Netherlands Journal of Geosciences - Geologie En Mijnbouw*, *80*(1), 121–136. https://doi.org/10.1017/S001677460002223X

Gupta A and Baker JW (2019) A framework for time-varying induced seismicity risk assessment, with application in Oklahoma. Bulletin of Earthquake Engineering 17(8): 4475–4493.

GWP (2021). Wastewater collection, treatment, and reuse in rural areas of Central and Eastern Europe Report of the Sustainable Sanitation Task Force. Global Water Partnership Central and Eastern Europe. https://www.gwp.org/globalassets/global/gwp-cee_files/taskforces/sustainable-sanitation-task-force-report-2022.pdf

Hager, B. H., Dieterich, J., Frohlich, C., Juanes, R., Mantica, S., Shaw, J. H., ... & Plesch, A. (2021). A process-based approach to understanding and managing triggered seismicity. Nature, 595(7869), 684- 689.

Hanks, T. C., & Kanamori, H. (1979). A moment magnitude scale. Journal of Geophysical Research: Solid Earth, 84(B5), 2348-2350.

Hartzell, S., Leeds, A., Frankel, A., & Michael, J. (1996). Site response for urban Los Angeles using aftershocks of the Northridge earthquake. Bulletin of the Seismological Society of America, 86(1B), S168–S192. https://doi.org/10.1785/BSSA08601BS168

Haug, C., Nüchter, J.-A., & Henk, A. (2018). Assessment of geological factors potentially affecting production-induced seismicity in North German gas fields. Geomechanics for Energy and the Environment, 16, 15–31. https://doi.org/10.1016/j.gete.2018.04.002

Hauksson, E., Göbel, T., Ampuero, J.-P., & Cochran, E. (2015). A century of oil-field operations and earthquakes in the greater Los Angeles Basin, southern California. *The Leading Edge*, *34*(6), 650–656. https://doi.org/10.1190/tle34060650.1

Hergert, T., Haug, C., Henk, A., & Nüchter, J.-A. (2022). Modelling production-induced dynamic rupture of intra-graben faults and related earthquakes in the North German Basin. *Geomechanics for Energy and the Environment*, *32*, 100339. https://doi.org/10.1016/j.gete.2022.100339

Hennings, P. H., Lund Snee, J., Osmond, J. L., DeShon, H. R., Dommisse, R., Horne, E., Lemons, C., & Zoback, M. D. (2019). Injection-Induced Seismicity and Fault-Slip Potential in the Fort Worth Basin, Texas. Bulletin of the Seismological Society of America, 109(5), 1615–1634. https://doi.org/10.1785/0120190017

Hennings, P., Dvory, N., Horne, E., Li, P., Savvaidis, A., & Zoback, M. (2021). Stability of the fault systems that host-induced earthquakes in the Delaware Basin of West Texas and Southeast New Mexico. The Seismic Record, 1(2), 96-106.

Herak, M. (2008). ModelHVSR—A Matlab® tool to model horizontal-to-vertical spectral ratio of ambient noise. Computers & Geosciences, 34(11), 1514–1526. https://doi.org/10.1016/j.cageo.2007.07.009

Hergert, T., Haug, C., Henk, A., & Nüchter, J.-A. (2022). Modelling production-induced dynamic rupture of intra-graben faults and related earthquakes in the North German Basin. Geomechanics for Energy and the Environment, 32, 100339. https://doi.org/10.1016/j.gete.2022.100339

Hettema, M. (2020). Analysis of mechanics of fault reactivation in depleting reservoirs. International Journal of Rock Mechanics and Mining Sciences, 129, 104290.

Hettema, M. (2022). Practical workflow for assessment of seismic hazard in low enthalpy geothermal systems. Geomechanics and Geophysics for Geo-Energy and Geo-Resources, 8(6), 203.

Hicks, E. C., Bungum, H., & Lindholm, C. D. (2000). Stress inversion of earthquake focal mechanism solutions from onshore and offshore Norway. *Norsk Geologisk Tidsskrift*, *80*(4), 235–250. https://doi.org/10.1080/00291960051030545

Hincks, T., Aspinall, W., Cooke, R., & Gernon, T. (2018). Oklahoma's induced seismicity strongly linked to wastewater injection depth. Science, 359(6381), 1251–1255. https://doi.org/10.1126/science.aap7911

Hicks, S. P., Verdon, J., Baptie, B., Luckett, R., Mildon, Z. K., & Gernon, T. (2019). A Shallow Earthquake Swarm Close to Hydrocarbon Activities: Discriminating between Natural and Induced Causes for the 2018–2019 Surrey, United Kingdom, Earthquake Sequence. *Seismological Research Letters*, *90*(6), 2095–2110. https://doi.org/10.1785/0220190125

Hicks, S. P., Goes, S., Whittaker, A. C., & Stafford, P. J. (2021). Multivariate Statistical Appraisal of Regional Susceptibility to Induced Seismicity: Application to the Permian Basin, SW United States. *Journal of Geophysical Research: Solid Earth*, *126*(12). https://doi.org/10.1029/2021JB022768

Horner, R. B., Barclay, J. E., & Macrae, J. M. (1994). earthquakes and hydrocarbon production in the fort st. john area of northeastern british columbia.

Horner, R. B., Barclay, J. E., & MacRae, J. M. (1994). *Earthquakes and Hydrocarbon Production Near Fort St. John, B.C.*

Hough, S. E., & Bilham, R. (2018a). Poroelastic stress changes associated with primary oil production in the Los Angeles Basin, California. *The Leading Edge*, *37*(2), 108–116. https://doi.org/10.1190/tle37020108.1

Hough, S. E., & Bilham, R. (2018b). Revisiting Earthquakes in the Los Angeles, California, Basin During the Early Instrumental Period: Evidence for an Association With Oil Production. *Journal of Geophysical Research: Solid Earth*, *123*(12), 10,684-10,705. https://doi.org/10.1029/2017JB014616

Hough, S. E., & Page, M. (2016). Potentially Induced Earthquakes during the Early Twentieth Century in the Los Angeles Basin. *Bulletin of the Seismological Society of America*, *106*(6), 2419–2435. https://doi.org/10.1785/0120160157

Hough, S. E., Tsai, V. C., Walker, R., & Aminzadeh, F. (2017). Was the Mw 7.5 1952 Kern County, California, earthquake induced (or triggered)? *Journal of Seismology*, *21*(6), 1613–1621. https://doi.org/10.1007/s10950-017-9685-x

IEAGHG (2022). Current State of Knowledge Regarding the Risk of Induced Seismicity at CO2 Storage Projects.

Jamalreyhani, M., Pousse-Beltran, L., Büyükakpınar, P., Cesca, S., Nissen, E., Ghods, A., López-Comino, J. Á., Rezapour, M., & Najafi, M. (2021). *The 2019-2020 Khalili (Iran) earthquake sequence—Anthropogenic seismicity in the Zagros Simply Folded Belt?* https://doi.org/10.1002/essoar.10506454.1

Jansen, J. D., Singhal, P., & Vossepoel, F. C. (2019). Insights from closed-form expressions for injection- and production-induced stresses in displaced faults. Journal of Geophysical Research: Solid Earth, 124(7), 7193-7212.

Jayaram, N., & Baker, J. W. (2009). Correlation model for spatially distributed ground-motion intensities. Earthquake Engineering & Structural Dynamics, 38(15), 1687–1708. https://doi.org/10.1002/eqe.922

James, Gareth, Daniela Witten, Trevor Hastie, and Robert Tibshirani. An introduction to statistical learning. Vol. 112. New York: springer, 2013.

Jerkins, A. E., Shiddiqi, H. A., Kværna, T., Gibbons, S. J., Schweitzer, J., Ottemöller, L., & Bungum, H. (2020). The 30 June 2017 North Sea Earthquake: Location, Characteristics, and Context. *Bulletin of the Seismological Society of America*, *110*(2), 937–952. https://doi.org/10.1785/0120190181

Jiang, G., Liu, L., Barbour, A. J., Lu, R., & Yang, H. (2021). Physics-Based Evaluation of the Maximum Magnitude of Potential Earthquakes Induced by the Hutubi (China) Underground Gas Storage. *Journal of Geophysical Research: Solid Earth*, *126*(4). https://doi.org/10.1029/2020JB021379

Kallioras, S., Graziotti, F., & Penna, A. (2019). Numerical assessment of the dynamic response of a URM terraced house exposed to induced seismicity. Bulletin of Earthquake Engineering, 17(3), 1521–1552. https://doi.org/10.1007/s10518-018-0495-5

Kao, H., Visser, R., Smith, B., & Venables, S. (2018). Performance assessment of the induced seismicity traffic light protocol for northeastern British Columbia and western Alberta. The Leading Edge, 37(2), 117–126. https://doi.org/10.1190/tle37020117.1

Keller, G. R., Rogers, A. M., & Orr, C. D. (1987). Seismic Activity in the Permian Basin Area of West Texas and Southeastern New Mexico, 1975–79. *Seismological Research Letters*, *58*(2), 63–70. https://doi.org/10.1785/gssrl.58.2.63

King, V. M., Block, L. V., Yeck, W. L., Wood, C. K., & Derouin, S. A. (2014). Geological structure of the Paradox Valley Region, Colorado, and relationship to seismicity induced by deep well injection. Journal of Geophysical Research: Solid Earth, 119(6), 4955–4978. https://doi.org/10.1002/2013JB010651

Klose, C. D. (2007). Geomechanical modeling of the nucleation process of Australia's 1989 M5.6 Newcastle earthquake. *Earth and Planetary Science Letters*, *256*(3–4), 547–553. https://doi.org/10.1016/j.epsl.2007.02.009

Klose, C. D. (2013). Mechanical and statistical evidence of the causality of human-made mass shifts on the Earth's upper crust and the occurrence of earthquakes. *Journal of Seismology*, *17*(1), 109–135. https://doi.org/10.1007/s10950-012-9321-8

Kohrangi M, Vamvatsikos D and Bazzurro P (2016). Implications of intensity measure selection for seismic loss assessment of 3-D buildings. Earthquake Spectra 32(4): 2167–2189.

Konovalov, A. V., Patrikeev, V. N., Safonov, D. A., Nagornykh, T. V., Semenova, E. P., & Stepnov, A. A. (2015). M w 5.6 Piltun earthquake of June 12, 2005, and the contemporary seismicity in the area of oil-and-gas fields in the northeastern shelf of Sakhalin Island. *Russian Journal of Pacific Geology*, *9*(1), 47–56. https://doi.org/10.1134/S1819714015010030

Korff, M., de Lange, G., Meijers, P., Wiersma, A., & Kloosterman, F. (n.d.). Liquefaction sensitivity of the shallow subsurface of Groningen.

Korswagen, P. A., Longo, M., & Rots, J. G. (2022). Fragility curves for light damage of clay masonry walls subjected to seismic vibrations. Bulletin of Earthquake Engineering, 20(11), 6193–6227. https://doi.org/10.1007/s10518-022-01404-0

Koster, H. R., & van Ommeren, J. N. (2015). Natural gas extraction, earthquakes and house prices (No. 15-038/VIII). Tinbergen Institute Discussion Paper.

Kostrov, V.V. (1974), Seismic moment and energy of earthquakes and seismic flow of rocks, Izv. Acad. Sci. USSR Phys. Solid Earth, Eng. Transl., 1, 23-44.

Kotha, S. R., Weatherill, G., Bindi, D., & Cotton, F. (2020). A regionally-adaptable ground-motion model for shallow crustal earthquakes in Europe. Bulletin of Earthquake Engineering, 18(9), 4091-4125.

Kouznetsov, O., Sidorov, V., Katz, S., & Chilingarian, G. (1994). Interrelationships among seismic and short-term tectonic activity, oil and gas production, and gas migration to the surface. *Journal of Petroleum Science and Engineering*, *13*(1), 57–63. https://doi.org/10.1016/0920-4105(94)00058-C

Kovach, R. L. (1974). Source mechanisms for Wilmington Oil Field, California, subsidence earthquakes. *Bulletin of the Seismological Society of America*, *64*(3–1), 699–711. https://doi.org/10.1785/BSSA0643-10699

Kraft, T., Roth, P., & Wiemer, S. (2020). Good Practice Guide for Managing Induced Seismicity in Deep Geothermal Energy Projects in Switzerland: Version 2 (p. 69 p.) [Application/pdf]. ETH Zurich. https://doi.org/10.3929/ETHZ-B-000453228

Kruiver, P. P., de Lange, G., Kloosterman, F., Korff, M., van Elk, J., & Doornhof, D. (2021). Rigorous test of the performance of shear-wave velocity correlations derived from CPT soundings: A case study for Groningen, the Netherlands. Soil Dynamics and Earthquake Engineering, 140, 106471. https://doi.org/10.1016/j.soildyn.2020.106471

Kruiver, P. P., Pefkos, M., Meijles, E., Aalbersberg, G., Campman, X., van der Veen, W., Martin, A., Ooms-Asshoff, K., Bommer, J. J., Rodriguez-Marek, A., Pinho, R., Crowley, H., Cavalieri, F., Correia, A. A., & van Elk, J. (2022). Incorporating dwelling mounds into induced seismic risk analysis for the Groningen gas field in the Netherlands. Bulletin of Earthquake Engineering, 20(1), 255–285. https://doi.org/10.1007/s10518-021-01225-7

Kruiver, P. P., Pefkos, M., Rodriguez-Marek, A., Campman, X., Ooms-Asshoff, K., Chmiel, M., Lavoué, A., Stafford, P. J., & van Elk, J. (2022). Capturing spatial variability in the regional Ground Motion Model of Groningen, the Netherlands. Netherlands Journal of Geosciences, 101, e16. https://doi.org/10.1017/njg.2022.13

Kruiver, P. P., van Dedem, E., Romijn, R., de Lange, G., Korff, M., Stafleu, J., Gunnink, J. L., Rodriguez-Marek, A., Bommer, J. J., van Elk, J., & Doornhof, D. (2017). An integrated shear-wave velocity model for the Groningen gas field, The Netherlands. Bulletin of Earthquake Engineering, 15(9), 3555–3580. https://doi.org/10.1007/s10518-017-0105-y

Kruiver, P. P., Wiersma, A., Kloosterman, F. H., Lange, G. de, Korff, M., Stafleu, J., Busschers, F. S., Harting, R., Gunnink, J. L., Green, R. A., Elk, J. van, & Doornhof, D. (2017). Characterisation of the Groningen subsurface for seismic hazard and risk modelling. Netherlands Journal of Geosciences, 96(5), s215–s233. https://doi.org/10.1017/njg.2017.11

Kruse, H. M. G., & Hölscher, P. (2010). Schade aan buisleiding door aardbeving. *Deltares*.

Kühn, D., Hainzl, S., Dahm, T., Richter, G., & Rodriguez, I. V. (2022). A review of source models to further the understanding of the seismicity of the Groningen field. Netherlands Journal of Geosciences, 101, e11.

Kundu, B., Vissa, N. K., Gahalaut, K., Gahalaut, V. K., Panda, D., & Malik, K. (2019). Influence of anthropogenic groundwater pumping on the 2017 November 12 M7.3 Iran–Iraq border earthquake. *Geophysical Journal International*, *218*(2), 833–839. https://doi.org/10.1093/gji/ggz195

Kundu, B., Vissa, N. K., & Gahalaut, V. K. (2015). Influence of anthropogenic groundwater unloading in Indo-Gangetic plains on the 25 April 2015 Mw 7.8 Gorkha, Nepal earthquake. *Geophysical Research Letters*, *42*(24), 10,607-10,613. https://doi.org/10.1002/2015GL066616

Lacan, P., & Ortuño, M. (2012). Active Tectonics of the Pyrenees: A review. *Journal of Iberian Geology*, *38*(1), 9–30. https://doi.org/10.5209/rev_JIGE.2012.v38.n1.39203

Lavecchia, G., de Nardis, R., Ferrarini, F., Cirillo, D., Bello, S., & Brozzetti, F. (2021). Regional Seismotectonic Zonation of Hydrocarbon Fields in Active Thrust Belts: A Case Study from Italy. In F. L. Bonali, F. Pasquaré

Mariotto, & N. Tsereteli (Eds.), *Building Knowledge for Geohazard Assessment and Management in the Caucasus and other Orogenic Regions* (pp. 89–128). Springer Netherlands. https://doi.org/10.1007/978-94-024-2046-3_7

Le Goff, B., J. F. Borges, and M. Bezzeghoud (2014). Intensity-distance attenuation laws for the Portugal mainland using intensity data points, Geophys. J. Int. 199, no. 2, 1278–1285.

Lei, X., Wang, Z., & Su, J. (2019). The December 2018 ML 5.7 and January 2019 ML 5.3 Earthquakes in South Sichuan Basin Induced by Shale Gas Hydraulic Fracturing. Seismological Research Letters, 90(3), 1099–1110. https://doi.org/10.1785/0220190029

Lee, V. W., & Trifunac, M. D. (2010). Should average shear-wave velocity in the top 30m of soil be used to describe seismic amplification? Soil Dynamics and Earthquake Engineering, 30(11), 1250–1258. https://doi.org/10.1016/j.soildyn.2010.05.007

Leydecker, G. (2011). *Erdbebenkatalog für Deutschland mit Randgebieten für die Jahre 800 bis 2008*. herausgegeben von der Bundesanstalt für Geowissenschaften und Rohstoffe und dem Landesamt für Bergbau, Energie und Geologie.

Livingston, L. (n.d.). *Managing coastal subsidence*.

Lund Snee, J.-E., & Zoback, M. D. (2016). State of stress in Texas: Implications for induced seismicity:. *Geophysical Research Letters*, *43*(19), 10,208-10,214. https://doi.org/10.1002/2016GL070974

Majer, E., Nelson, J., Robertson-Tait, A., Savy, J., & Wong, I. (2012). Protocol for Addressing Induced Seismicity Associated with Enhanced Geothermal Systems (DOE/EE--0662, 1219482; p. DOE/EE--0662, 1219482). https://doi.org/10.2172/1219482

Mak, S., Cotton, F., & Schorlemmer, D. (2017). Measuring the performance of ground-motion models: The importance of being independent. Seismological Research Letters, 88(5), 1212-1217.

Malomo, D., Morandini, C., Crowley, H., Pinho, R., & Penna, A. (2021). Impact of ground floor openings percentage on the dynamic response of typical Dutch URM cavity wall structures. Bulletin of Earthquake Engineering, 19(1), 403–428. https://doi.org/10.1007/s10518-020-00976-z

Markhvida, M., & Baker, J. W. (2023). Modeling future economic costs and interdependent industry recovery after earthquakes. Earthquake Spectra, 39(2), 914-937.

Martins, L., & Silva, V. (2020). Development of a fragility and vulnerability model for global seismic risk analyses. Bulletin of Earthquake Engineering. https://doi.org/10.1007/s10518-020-00885-1

Martins, L., Silva, V., Crowley, H., & Cavalieri, F. (2021). Vulnerability modellers toolkit, an open-source platform for vulnerability analysis. Bulletin of Earthquake Engineering, 19, 5691-5709.

Marzocchi, W., Iervolino, I., Giorgio, M., & Falcone, G. (2015). When Is the Probability of a Large Earthquake Too Small? Seismological Research Letters, 86(6), 1674–1678. https://doi.org/10.1785/0220150129

Maury, V. M. R., Grassob, J.-R., & Wittlinger, G. (1992). Monitoring of subsidence and induced seismicity in the Lacq Gas Field (France): The consequences on gas production and field operation. *Engineering Geology*, *32*(3), 123–135. https://doi.org/10.1016/0013-7952(92)90041-V

McGarr, A. (1991). On a possible connection between three major earthquakes in California and oil production. *Bulletin of the Seismological Society of America*.

McGarr, A., Simpson, D., & Seeber, L. (2002). 40 Case histories of induced and triggered seismicity. In International Geophysics (Vol. 81, pp. 647–661). Elsevier. https://doi.org/10.1016/S0074-6142(02)80243-1

McGuire, R. K., Cornell, C. A., & Toro, G. R. (2005). The Case for Using Mean Seismic Hazard. Earthquake Spectra, 21(3), 879–886. https://doi.org/10.1193/1.1985447

Meijdam, C. (2015). Eindadvies Handelsperspectief voor Groningen.

Mereu, R. F., Brunet, J., Morrissey, K., Price, B., & Yapp, A. (1986). A study of the microearthquakes of the Gobles oil field area of southwestern Ontario. Bulletin of the Seismological Society of America, 76(5), 1215-1223.

Mereu, R. F., Asmis, H. W., Dunn, B., Brunet, J., Eaton, D., Dineva, S., & Yapp, A. (2002). The Seismicity of the Western Lake Ontario Area: Results from the Southern Ontario Seismic Network (SOSN), 1992-2001. *Seismological Research Letters*, *73*(4), 534–551. https://doi.org/10.1785/gssrl.73.4.534

Meulen, M. J. van der, Doornenbal, J. C., Gunnink, J. L., Stafleu, J., Schokker, J., Vernes, R. W., Geer, F. C. van, Gessel, S. F. van, Heteren, S. van, Leeuwen, R. J. W. van, Bakker, M. a. J., Bogaard, P. J. F., Busschers, F. S., Griffioen, J., Gruijters, S. H. L. L., Kiden, P., Schroot, B. M., Simmelink, H. J., Berkel, W. O. van, … Daalen, T. M. van. (2013). 3D geology in a 2D country: Perspectives for geological surveying in the Netherlands. Netherlands Journal of Geosciences, 92(4), 217–241. https://doi.org/10.1017/S0016774600000184

Mignan, A., Landtwing, D., Kästli, P., Mena, B., & Wiemer, S. (2015). Induced seismicity risk analysis of the 2006 Basel, Switzerland, Enhanced Geothermal System project: Influence of uncertainties on risk mitigation. Geothermics, 53, 133–146. https://doi.org/10.1016/j.geothermics.2014.05.007

Mignan, A., Broccardo, M., Wiemer, S., & Giardini, D. (2017). Induced seismicity closed-form traffic light system for actuarial decision-making during deep fluid injections. Scientific Reports, 7(1), 13607. https://doi.org/10.1038/s41598-017-13585-9

Milne, W. G. (1970). The Snipe Lake, Alberta earthquake of March 8, 1970. *Canadian Journal of Earth Sciences*, *7*(6), 1564–1567. https://doi.org/10.1139/e70-148

Milne, W. G., & Berry, M. J. (1976). Induced seismicity in Canada. *Engineering Geology*, *10*(2–4), 219–226. https://doi.org/10.1016/0013-7952(76)90022-3

Mirzoev, K. M., Nikolaev, A. V., Lukk, A. A., & Yunga, S. L. (2009). Induced seismicity and the possibilities of controlled relaxation of tectonic stresses in the Earth's crust. *Izvestiya, Physics of the Solid Earth*, *45*(10), 885–904. https://doi.org/10.1134/S1069351309100061

Molnar, S., Cassidy, J. F., Castellaro, S., Cornou, C., Crow, H., Hunter, J. A., Matsushima, S., Sánchez-Sesma, F. J., & Yong, A. (2018). Application of Microtremor Horizontal-to-Vertical Spectral Ratio (MHVSR) Analysis for Site Characterization: State of the Art. Surveys in Geophysics, 39(4), 613–631. https://doi.org/10.1007/s10712-018-9464-4

Mucciarelli, M. (2015). *Seismic Hazard from Natural and Induced Seismicity: A comparison for Italy*. https://doi.org/10.4430/bgta0158

Mukhopadhyay, M., Elawadi, E., Mukhopadhyay, B., & Mogren, S. (2018). Induced and Ambient Crustal Seismicity under the Ghawar Oil-Gas Fields, Saudi Arabia. *Journal of the Geological Society of India*, *91*(4), 449–456. https://doi.org/10.1007/s12594-018-0878-x

Muntendam-Bos, A. G., Roest, J. P. A., & de Waal, J. A. (2015). A guideline for assessing seismic risk induced by gas extraction in the Netherlands. *The Leading Edge*, *34*(6), 672–677. https://doi.org/10.1190/tle34060672.1

Muntendam-Bos, A. G., & De Waal, J. A. (2013). Reassessment of the probability of higher magnitude earthquakes in the Groningen gas field. State Supervision of Mines Publishing, The Hague-Leidschenveen.

Muntendam-Bos, A. G., Roest, J. P. A., & de Waal, J. A. (2015). A guideline for assessing seismic risk induced by gas extraction in the Netherlands. The Leading Edge, 34(6), 672–677. https://doi.org/10.1190/tle34060672.1

Muntendam-Bos, A. G. (2020). Clustering characteristics of gas-extraction induced seismicity in the Groningen gas field. *Geophysical Journal International*, *221*(2), 879–892. https://doi.org/10.1093/gji/ggaa038

Muntendam-Bos, A. G., Hoedeman, G., Polychronopoulou, K., Draganov, D., Weemstra, C., van der Zee, W., Bakker, R. R., & Roest, H. (2022). An overview of induced seismicity in the Netherlands. Netherlands Journal of Geosciences, 101, e1. https://doi.org/10.1017/njg.2021.14

Muntendam-Bos, A. G., Hoedeman, G., Polychronopoulou, K., Draganov, D., Weemstra, C., van der Zee, W., Bakker, R. R., & Roest, H. (2022). An overview of induced seismicity in the Netherlands. *Netherlands Journal of Geosciences*, *101*, e1. https://doi.org/10.1017/njg.2021.14

Muntendam-Bos, A. G., & Grobbe, N. (2022). Data-driven spatiotemporal assessment of the event-size distribution of the Groningen extraction-induced seismicity catalogue. Scientific Reports, 12.

Musson, R. M. W. (2007). British earthquakes. *Proceedings of the Geologists' Association*, *118*(4), 305–337. https://doi.org/10.1016/S0016-7878(07)80001-0

Nairn, A. E. M., & Alsharhan, A. S. (1997). Sedimentary basins and petroleum geology of the Middle East. Elsevier.

Nakamura, Y. (1989). A METHOD FOR DYNAMIC CHARACTERISTICS ESTIMATION OF SUBSURFACE USING MICROTREMOR ON THE GROUND SURFACE. Railway Technical Research Institute, Quarterly Reports, 30(1). https://trid.trb.org/view/294184

Nakamura, Y. (2019). What Is the Nakamura Method? Seismological Research Letters. https://doi.org/10.1785/0220180376

NAM (2021). Seismisch risico voor "kleine velden". NAM Rapport: EP201712203519. Version 2.1.

NAM. (2022). Report on the Second Workshop on Mmax for Seismic Hazard and Risk Analysis in the Groningen Gas Field. Main report (June).

Nantanoi, S., Rodríguez-Pradilla, G., & Verdon, J. (2022). 3D seismic interpretation and fault slip potential analysis from hydraulic fracturing in the Bowland Shale, UK. Petroleum Geoscience, 28(2), petgeo2021-057. https://doi.org/10.1144/petgeo2021-057

Natalya N. Mikhailova, Aidyn S. Mukambayev, Irina L. Aristova, Galina Kulikova, Shahid Ullah, Marco Pilz, & Dino Bindi. (2015). Central Asia earthquake catalogue from ancient time to 2009. *Annals of Geophysics*, *58*(1), 2. https://doi.org/10.4401/ag-6681

Nicholson, C., & Wesson, R. L. (1992). Triggered earthquakes and deep well activities. Pure and Applied Geophysics, 139(3–4), 561–578. https://doi.org/10.1007/BF00879951

Nicol, A., Gerstenberger, M., Bromley, C., Carne, R., Chardot, L., Ellis, S., Jenkins, C., Siggins, T., & Viskovic, P. (2013). Induced Seismicity; Observations, Risks and Mitigation Measures at CO2 Storage Sites. Energy Procedia, 37, 4749–4756. https://doi.org/10.1016/j.egypro.2013.06.384

Noorlandt, R., Kruiver, P. P., de Kleine, M. P. E., Karaoulis, M., de Lange, G., Di Matteo, A., von Ketelhodt, J., Ruigrok, E., Edwards, B., Rodriguez-Marek, A., Bommer, J. J., van Elk, J., & Doornhof, D. (2018). Characterisation of ground motion recording stations in the Groningen gas field. Journal of Seismology, 22(3), 605–623. https://doi.org/10.1007/s10950-017-9725-6

Novakovic M, Atkinson GM and Assatourians K (2018). Empirically calibrated ground-motion prediction equation for Oklahoma. Bulletin of the Seismological Society of America 108(5A): 2444–2461.

Novakovic M, Atkinson GM and Assatourians K (2020). Erratum to Empirically calibrated ground-motion prediction equation for Oklahoma. Bulletin of the Seismological Society of America. 110(4): 1996–1998.

NRC. (2013). Induced Seismicity Potential in Energy Technologies. National Academies Press. https://doi.org/10.17226/13355

Ntinalexis, M., Kruiver, P. P., Bommer, J. J., Ruigrok, E., Rodriguez-Marek, A., Edwards, B., Pinho, R., Spetzler, J., Hernandez, E. O., Pefkos, M., Bahrampouri, M., van Onselen, E. P., Dost, B., & van Elk, J. (2022). A database of ground motion recordings, site profiles, and amplification factors from the Groningen gas field in the Netherlands. Earthquake Spectra, 875529302211409. https://doi.org/10.1177/87552930221140926

Odonne, F. (2019). Analogue modeling of reservoir deflation and associated deformation. AAPG Bulletin, 103(1), 71-90.

Ognev, I., & Stepanov, A. (2021). Seismicity and development of Romashkino hydrocarbon field's Almetyevskaya area. *Georesursy*, *23*(4), 51–57. https://doi.org/10.18599/grs.2021.4.6

Olson, D. R., & Frohlich, C. (1992). Research Note: Felt Reports from the 20 July 1991 Falls City Earthquake, Karnes County, Texas. *Seismological Research Letters*, *63*(4), 603–604. https://doi.org/10.1785/gssrl.63.4.603

Orlic, B., & Wassing, B. B. T. (2012). Modeling stress development and fault slip in producing hydrocarbon reservoirs overlain by rock salt caprocks. In ARMA US Rock Mechanics/Geomechanics Symposium (pp. ARMA-2012). ARMA.

Ottemöller, L. (2005). The 7 May 2001 induced seismic event in the Ekofisk oil field, North Sea. *Journal of Geophysical Research*, *110*(B10), B10301. https://doi.org/10.1029/2004JB003374

Oumejjoud, S. (2023). An investigation into the reservoir parameters that control induced seismicity in small Dutch gas fields. Master thesis. TU Delft.

Ovens, J. E. V., Larsen, F. P., & Cowie, D. R. (1998). Making Sense of Water Injection Fractures in the Dan Field. *SPE Reservoir Evaluation & Engineering*, *1*(06), 556–566. https://doi.org/10.2118/52669-PA

Pagani, M., Monelli, D., Weatherill, G., Danciu, L., Crowley, H., Silva, V., Henshaw, P., Butler, L., Nastasi, M., Panzeri, L., Simionato, M., & Vigano, D. (2014). OpenQuake Engine: An Open Hazard (and Risk) Software for the Global Earthquake Model. Seismological Research Letters, 85(3), 692–702. https://doi.org/10.1785/0220130087

Paolucci, R., Mazzieri, I., Piunno, G., Smerzini, C., Vanini, M., & Özcebe, A. G. (2020). Earthquake ground motion modeling of induced seismicity in the Groningen gas field. Earthquake Engineering & Structural Dynamics, eqe.3367. https://doi.org/10.1002/eqe.3367

Papadopoulos, A. N., Bazzurro, P., & Marzocchi, W. (2020). Exploring probabilistic seismic risk assessment accounting for seismicity clustering and damage accumulation: Part I. Hazard analysis. Earthquake Spectra, 875529302095733. https://doi.org/10.1177/8755293020957338

Park, J., Bazzurro, P., & Baker, J. W. (2007). Modeling spatial correlation of ground motion Intensity Measures for regional seismic hazard and portfolio loss estimation. 9.

Pate-Cornell, E. (2002). Risk and Uncertainty Analysis in Government Safety Decisions. Risk Analysis, 22(3), 633–646. https://doi.org/10.1111/0272-4332.00043

Pawley, S., Schultz, R., Playter, T., Corlett, H., Shipman, T., Lyster, S., & Hauck, T. (2018). The Geological Susceptibility of Induced Earthquakes in the Duvernay Play. Geophysical Research Letters, 45(4), 1786–1793. https://doi.org/10.1002/2017GL076100

Pennington, W. D., Davis, S. D., Carlson', S. M., Dupree, J., & Ewing, T. E. (1986). *The evolution of seismic barriers and asperities caused by the depressuing of fault planes in oil and gas fields of south Texas*. 10.

Perron, V., Bergamo, P., & Fäh, D. (2022). Site Amplification at High Spatial Resolution from Combined Ambient Noise and Earthquake Recordings in Sion, Switzerland. Seismological Research Letters, 93(4), 2281–2298. https://doi.org/10.1785/0220210289

Petersen, M. D. (2008). *Documentation for the 2008 Update of the United States National Seismic Hazard Maps* (Open-File Report) [Open-File Report].

Petersen, M. D., Mueller, C. S., Moschetti, M. P., Hoover, S. M., Shumway, A. M., McNamara, D. E., ... & Rukstales, K. S. (2017). 2017 one-year seismic-hazard forecast for the central and eastern United States from induced and natural earthquakes. Seismological Research Letters, 88(3), 772-783.

Postma, T., & Jansen, J. D. (2018). The small effect of poroelastic pressure transients on triggering of production-induced earthquakes in the Groningen natural gas field. Journal of Geophysical Research: Solid Earth, 123(1), 401-417.

Pratt, W. E., & Johnson, D. W. (1926). Local Subsidence of the Goose Creek Oil Field. *The Journal of Geology*, *34*(7, Part 1), 577–590. https://doi.org/10.1086/623352

Richter, G., Hainzl, S., Dahm, T., & Zöller, G. (2020). Stress-based, statistical modeling of the induced seismicity at the Groningen gas field, The Netherlands. Environmental Earth Sciences, 79(11), 252.

Rodriguez-Marek, A., Kruiver, P. P., Meijers, P., Bommer, J. J., Dost, B., van Elk, J., & Doornhof, D. (2017). A Regional Site-Response Model for the Groningen Gas Field. Bulletin of the Seismological Society of America, 107(5), 2067–2077. https://doi.org/10.1785/0120160123

Roest, J. P. A., & Kuilman, W. (1994). Geomechanical analysis of small earthquakes at the Eleveld gas reservoir. *All Days*, SPE-28097-MS. https://doi.org/10.2118/28097-MS

Rogers, A. M., & Malkiel, A. (1979). *A study of earthquakes in the Permian basin of Texas—New Mexico*. 23.

Rothe, G. H., & Lui, C.-Y. (1983). Possibility of induced seismicity in the vicinity of the Sleepy Hollow oil Field, southwestern Nebraska. *Bulletin of the Seismological Society of America*, *73*(5), 1357–1367. https://doi.org/10.1785/BSSA0730051357

Roy, C., Nowacki, A., Zhang, X., Curtis, A., & Baptie, B. (2021). Accounting for Natural Uncertainty Within Monitoring Systems for Induced Seismicity Based on Earthquake Magnitudes. Frontiers in Earth Science, 9, 634688. https://doi.org/10.3389/feart.2021.634688

Ruigrok, E., Rodriguez-Marek, A., Edwards, B., Kruiver, P. P., Dost, B., & Bommer, J. (2022). Derivation of a near-surface damping model for the Groningen gas field. Geophysical Journal International, 230(2), 776–795. https://doi.org/10.1093/gji/ggac069

Rutledge, J. T., Phillips, W. S., & Schuessler, B. K. (1998). Reservoir characterization using oil-production-induced microseismicity, Clinton County, Kentucky. Tectonophysics, 289(1–3), 129–152. https://doi.org/10.1016/S0040-1951(97)00312-0

Sarhosis, V., Dais, D., Smyrou, E., & Bal, İ. E. (2019). Evaluation of modelling strategies for estimating cumulative damage on Groningen masonry buildings due to recursive induced earthquakes. Bulletin of Earthquake Engineering, 17(8), 4689–4710. https://doi.org/10.1007/s10518-018-00549-1

Sarkar, S., Kuleli, H. S., Toksöz, M. N., Zhang, H., Ibi, O., Al-Kindy, F., & Touqi, N. A. (2008). Eight years of passive seismic monitoring at a petroleum field in Oman: A case study. *SEG Technical Program Expanded Abstracts 2008*, 1397–1401. https://doi.org/10.1190/1.3059178

Scherbaum, F., Delavaud, E., & Riggelsen, C. (2009). Model selection in seismic hazard analysis: An information-theoretic perspective. Bulletin of the Seismological Society of America, 99(6), 3234-3247.

Schultz, R., Corlett, H., Haug, K., Kocon, K., MacCormack, K., Stern, V., & Shipman, T. (2016). Linking fossil reefs with earthquakes: Geologic insight to where induced seismicity occurs in Alberta. Geophysical Research Letters, 43(6), 2534–2542. https://doi.org/10.1002/2015GL067514

Schultz, R., & Wang, R. (2020a). Newly emerging cases of hydraulic fracturing induced seismicity in the Duvernay East Shale Basin. *Tectonophysics*, *779*, 228393. https://doi.org/10.1016/j.tecto.2020.228393

Schultz, R., Beroza, G., Ellsworth, W., & Baker, J. (2020b). Risk-Informed Recommendations for Managing Hydraulic Fracturing–Induced Seismicity via Traffic Light Protocols. Bulletin of the Seismological Society of America, 110(5), 2411–2422. https://doi.org/10.1785/0120200016

Schultz, R., Beroza, G. C., & Ellsworth, W. L. (2021a). A Strategy for Choosing Red-Light Thresholds to Manage Hydraulic Fracturing Induced Seismicity in North America. Journal of Geophysical Research: Solid Earth, 126(12). https://doi.org/10.1029/2021JB022340

Schultz, R., Beroza, G. C., & Ellsworth, W. L. (2021b). A risk-based approach for managing hydraulic fracturing–induced seismicity. Science, 372(6541), 504–507. https://doi.org/10.1126/science.abg5451

Schultz, R., Quitoriano, V., Wald, D. J., & Beroza, G. C. (2021c). Quantifying nuisance ground motion thresholds for induced earthquakes. Earthquake Spectra, 875529302098802. https://doi.org/10.1177/8755293020988025

Schultz, R., Ellsworth, W. L., & Beroza, G. C. (2022a). Statistical bounds on how induced seismicity stops. Scientific reports, 12(1), 1184. https://doi.org/10.1038/s41598-022-05216-9.

Schultz, R., Muntendam-Bos, A., Zhou, W., Beroza, G. C., & Ellsworth, W. L. (2022b). Induced seismicity red-light thresholds for enhanced geothermal prospects in the Netherlands. Geothermics, 106, 102580. https://doi.org/10.1016/j.geothermics.2022.102580

Schultz, R., Ellsworth, W. L., & Beroza, G. C. (2023). An Ensemble Approach to Characterizing Trailing-Induced Seismicity. Seismological Research Letters, 94(2A), 699–707. https://doi.org/10.1785/0220220352

Segall, P., Grasso, J.-R., & Mossop, A. (1994). Poroelastic stressing and induced seismicity near the Lacq gas field, southwestern France. *Journal of Geophysical Research*, *99*(B8), 15423. https://doi.org/10.1029/94JB00989

Segall, P., & Fitzgerald, S. D. (1998). A note on induced stress changes in hydrocarbon and geothermal reservoirs. Tectonophysics, 289(1-3), 117-128.

Selby, N. D., Eshun, E., Patton, H. J., & Douglas, A. (2005). Unusual long-period Rayleigh wave radiation from a vertical dip-slip source: The 7 May 2001 North Sea earthquake. *Journal of Geophysical Research*, *110*(B10), B10304. https://doi.org/10.1029/2005JB003721

Shalev, E., Wetzler, N., Shatanawi, A., Rödiger, T., Kurzon, I., Lyakhovsky, V., Salameh, E., & Siebert, C. (2023). Induced Seismicity by Groundwater Extraction at the Dead Sea Fault, Jordan. *Journal of Geophysical Research: Solid Earth*, *128*(1). https://doi.org/10.1029/2022JB025044

Shapiro, S. A. (2018). Seismogenic index of underground fluid injections and productions. Journal of Geophysical Research: Solid Earth, 123(9), 7983-7997.

Sharma, N., Convertito, V., Maercklin, N., & Zollo, A. (2013). Ground-Motion Prediction Equations for The Geysers Geothermal Area based on Induced Seismicity Records. Bulletin of the Seismological Society of America, 103(1), 117–130. https://doi.org/10.1785/0120120138

Sharma, N., Convertito, V., De Matteis, R., & Capuano, P. (2022). Strong ground-motion prediction equations from induced earthquakes in St. Gallen geothermal field, Switzerland. Journal of Geophysics and Engineering, 19(4), 820–832. https://doi.org/10.1093/jge/gxac044

SHFRP (2019). Scientific Review of Hydraulic Fracturing in British Columbia.

Shen, L. W., Schmitt, D. R., & Schultz, R. (2019). Frictional Stabilities on Induced Earthquake Fault Planes at Fox Creek, Alberta: A Pore Fluid Pressure Dilemma. Geophysical Research Letters, 46(15), 8753–8762. https://doi.org/10.1029/2019GL083566

Shipman, T., MacDonald, R., & Byrnes, T. (2018). Experiences and learnings from induced seismicity regulation in Alberta. Interpretation, 6(2), SE15–SE21. https://doi.org/10.1190/INT-2017-0164.1

Silva, V., Crowley, H., Pagani, M., Monelli, D., & Pinho, R. (2014). Development of the OpenQuake engine, the Global Earthquake Model's open-source software for seismic risk assessment. Natural Hazards, 72(3), 1409–1427. https://doi.org/10.1007/s11069-013-0618-x

Silva V, Yepes-Estrada C, Dabbeek J, Martins L and Brzev S (2018) GED4ALL: Global exposure database for multi-hazard risk analysis —Multi-hazard exposure taxonomy. GEM technical report 2018-01. Pavia: GEM Foundation.

Silva, V., Akkar, S., Baker, J., Bazzurro, P., Castro, J. M., Crowley, H., Dolsek, M., Galasso, C., Lagomarsino, S., Monteiro, R., Perrone, D., Pitilakis, K., & Vamvatsikos, D. (2019). Current Challenges and Future Trends in Analytical Fragility and Vulnerability Modelling. Earthquake Spectra, 042418EQS101O. https://doi.org/10.1193/042418EQS101O

Silva, V., Amo-Oduro, D., Calderon, A., Costa, C., Dabbeek, J., Despotaki, V., Martins, L., Pagani, M., Rao, A., Simionato, M., Viganò, D., Yepes-Estrada, C., Acevedo, A., Crowley, H., Horspool, N., Jaiswal, K., Journeay, M., & Pittore, M. (2020). Development of a global seismic risk model. Earthquake Spectra, 36(1_suppl), 372–394. https://doi.org/10.1177/8755293019899953

Simpson, D. W., & Leith, W. (1985). The 1976 and 1984 Gazli, USSR, Earthquakes--Were They Induced?

Skoumal, R. J., Brudzinski, M. R., & Currie, B. S. (2018). Proximity of Precambrian basement affects the likelihood of induced seismicity in the Appalachian, Illinois, and Williston Basins, central and eastern United States. Geosphere, 14(3), 1365–1379. https://doi.org/10.1130/GES01542.1

Stafleu, J., Maljers, D., Gunnink, J. L., Menkovic, A., & Busschers, F. S. (2011). 3D modelling of the shallow subsurface of Zeeland, the Netherlands. Netherlands Journal of Geosciences, 90(4), 293–310. https://doi.org/10.1017/S0016774600000597

Stafleu, J., D. Maljers, F. S. Busschers, J. Schokker, J. L. Gunnink, and R. M. Dambrink (2021), Models created as 3-d cellular voxel arrays, Applied Multidimensional Geological Modeling: Informing sustainable human interactions with the shallow subsurface, pp. 247–271.

SodM (State Supervision of Mines) (2016). Risk analysis methodology for induced earthquakes due to gas production: Interim guideline to address Article 24.1.p of the Mining Decree, version 1.2. PO Box 24037, 2490 AA The Hague.

Stein, S., & Wysession, M. (2009). An introduction to seismology, earthquakes, and earth structure. John Wiley & Sons.

Stewart, J., Afshari, K., & Hashash, Y. (2014). Guidelines for performing hazard-consistent one-dimensional ground response analysis for ground motion prediction.

Sousa L, Silva V, Marques M and Crowley H (2018). On the treatment of uncertainty in seismic vulnerability and portfolio risk assessment. Earthquake Engineering & Structural Dynamics 47(1): 87–104.

Sousa, R., Silva, V., & Rodrigues, H. (2022). The importance of indirect losses in the seismic risk assessment of industrial buildings–An application to precast RC buildings in Portugal. International Journal of Disaster Risk Reduction, 74, 102949.

Spetzler, J., & Dost, B. (2017). Hypocenter Estimation of Induced Earthquakes in Groningen. *Geophysical Journal International*, ggx020. https://doi.org/10.1093/gji/ggx020

Spica, Z. J., Perton, M., Nakata, N., Liu, X., & Beroza, G. C. (2018). Site characterization at Groningen gas field area through joint surface-borehole H/V analysis. Geophysical Journal International, 212(1), 412–421. https://doi.org/10.1093/gji/ggx426

Stern, V. H., Schultz, R. J., Shen, L., Gu, Y. J., & Eaton, D. W. (2013). Alberta Earthquake Catalogue, Version 1.0: September 2006 through December 2010. *AER/AGS Open File Report 2013-15*.

Suckale, J. (2009). Induced Seismicity in Hydrocarbon Fields. In *Advances in Geophysics* (Vol. 51, pp. 55–106). Elsevier. https://doi.org/10.1016/S0065-2687(09)05107-3

Suckale, J. (2010). Moderate-to-large seismicity induced by hydrocarbon production. *The Leading Edge*, *29*(3), 310–319. https://doi.org/10.1190/1.3353728

Tamburini-Beliveau, G., Grosso-Heredia, J. A., Béjar-Pizarro, M., Pérez-López, R., Portela, J., Cismondi-Duarte, M., & Monserrat, O. (2022). Assessment of ground deformation and seismicity in two areas of intense hydrocarbon production in the Argentinian Patagonia. *Scientific Reports*, *12*(1), 19198. https://doi.org/10.1038/s41598-022-23160-6

Tang, L., Lu, Z., Zhang, M., Sun, L., & Wen, L. (2018). Seismicity Induced by Simultaneous Abrupt Changes of Injection Rate and Well Pressure in Hutubi Gas Field. *Journal of Geophysical Research: Solid Earth*, *123*(7), 5929–5944. https://doi.org/10.1029/2018JB015863

Tasiopoulou, P., Giannakou, A., Drosos, V., Georgarakos, P., Chacko, J., De Wit, S., & Zuideveld-Venema, N. (2019). Numerical evaluation of dynamic levee performance due to induced seismicity. *Bulletin of Earthquake Engineering*, *17*(8), 4559–4574. https://doi.org/10.1007/s10518-018-0426-5

Templeton, D., Schoenball, M., Layland-Bachmann, C., Foxall, W., Guglielmi, Y., Kroll, K., Burghardt, J., Dilmore, R., & White, J. (2021). Recommended Practices for Managing Induced Seismicity Risk Associated with Geologic Carbon Storage (DOE/NETL-2021/2839, 1834402; p. DOE/NETL-2021/2839, 1834402). https://doi.org/10.2172/1834402

Templeton, D. C., Schoenball, M., Layland-Bachmann, C. E., Foxall, W., Guglielmi, Y., Kroll, K. A., Burghardt, J. A., Dilmore, R., & White, J. A. (2023). A Project Lifetime Approach to the Management of Induced Seismicity Risk at Geologic Carbon Storage Sites. Seismological Research Letters, 94(1), 113–122. https://doi.org/10.1785/0220210284

Teng, G., Baker, J. W., & Wald, D. J. (2021). Evaluation of Intensity Prediction Equations (IPEs) for Small-Magnitude Earthquakes. Bulletin of the Seismological Society of America. https://doi.org/10.1785/0120210150

Thomas, P., Bratvold, R. B., & Eric, B. J. (2013). The Risk of Using Risk Matrices. Day 1 Mon, September 30, 2013, D011S007R003. https://doi.org/10.2118/166269-MS

Tiwari, D. K., Jha, B., Kundu, B., Gahalaut, V. K., & Vissa, N. K. (2021). Groundwater extraction-induced seismicity around Delhi region, India. *Scientific Reports*, *11*(1), 10097. https://doi.org/10.1038/s41598-021-89527-3

TNO. (2012). Deterministische hazard analyse voor geïnduceerde seismiciteit in Nederland.

TNO. (2016). Seismicity in onshore gas fields in the Netherlands.

TNO (2021). Deterministic hazard analysis for induced seismicity (DHAIS), update 2021.

Toppozada, T., & Branum, D. (2004). *California earthquake history*.

Trutnevyte, E., & Wiemer, S. (2017). Tailor-made risk governance for induced seismicity of geothermal energy projects: An application to Switzerland. Geothermics, 65, 295–312. https://doi.org/10.1016/j.geothermics.2016.10.006

Turuntaev, S. B., & Razumnaya, O. A. (2002). An Application of Induced Seismicity Data Analysis for Detection of Spatial Structures and Temporal Regimes of Deformation Processes in Hydrocarbon Fields. In C. I. Trifu (Ed.), *The Mechanism of Induced Seismicity* (pp. 421–447). Birkhäuser Basel. https://doi.org/10.1007/978-3-0348-8179-1_18

Tutuarima, F. (2020). The impact of uncertainty on the probability of induced events in The Netherlands. Bachelor thesis. TU Delft.

van den Hoek, P. J., & Poessé, J. W. (2021). Assessment of Seismic Risk in Geothermal and Hydrocarbon Reservoirs Using an Exact Analytical Solution of Stress Change. *Day 3 Wed, October 20, 2021*, D031S007R002. https://doi.org/10.2118/205122-MS

van der Voort, N., & Vanclay, F. (2015). Social impacts of earthquakes caused by gas extraction in the Province of Groningen, The Netherlands. *Environmental Impact Assessment Review*, *50*, 1–15. https://doi.org/10.1016/j.eiar.2014.08.008

van Ginkel, J., Ruigrok, E., & Herber, R. (2019). Assessing soil amplifications in Groningen, the Netherlands. First Break, 37(10), 33–38. https://doi.org/10.3997/1365-2397.2019026

van Ginkel, J., Ruigrok, E., Stafleu, J., & Herber, R. (2022a). Development of a seismic site-response zonation map for the Netherlands. Natural Hazards and Earth System Sciences, 22(1), 41–63. https://doi.org/10.5194/nhess-22-41-2022

van Ginkel, J. (2022b). Seismic site response in the Netherlands: Impact of the shallow subsurface composition on earthquake ground motion amplification [Thesis fully internal (DIV), University of Groningen]. https://doi.org/10.33612/diss.211424759

van Ginkel, J., Ruigrok, E., Wentinck, R., & Herber, R. (2022c). Amplification Behaviour of Compressional Waves in Unconsolidated Sediments. Frontiers in Earth Science, 10. https://www.frontiersin.org/articles/10.3389/feart.2022.812658

van Eck, T., Goutbeek, F., Haak, H., & Dost, B. (2006). Seismic hazard due to small-magnitude, shallow-source, induced earthquakes in The Netherlands. *Engineering Geology*, *87*(1–2), 105–121. https://doi.org/10.1016/j.enggeo.2006.06.005

van Eijs, R. M. H. E., Mulders, F. M. M., Nepveu, M., Kenter, C. J., & Scheffers, B. C. (2006). Correlation between hydrocarbon reservoir properties and induced seismicity in the Netherlands. Engineering Geology, 84(3-4), 99-111.

van Elk, J., Doornhof, D., Bommer, J. J., Bourne, S. J., Oates, S. J., Pinho, R., & Crowley, H. (2017). Hazard and risk assessments for induced seismicity in Groningen. *Netherlands Journal of Geosciences*, *96*(05), s259–s269. https://doi.org/10.1017/njg.2017.37

van Elk, J., Bourne, S. J., Oates, S. J., Bommer, J. J., Pinho, R., & Crowley, H. (2019). A Probabilistic Model to Evaluate Options for Mitigating Induced Seismic Risk. Earthquake Spectra, 35(2), 537–564. https://doi.org/10.1193/050918EQS118M

van Noten, K., Lecocq, T., Goffin, C., Meyvis, B., Molron, J., Debacker, T. N., & Devleeschouwer, X. (2022). Brussels' bedrock paleorelief from borehole-controlled power laws linking polarised H/V resonance frequencies and sediment thickness. Journal of Seismology, 26(1), 35–55. https://doi.org/10.1007/s10950-021-10039-8

van Thienen-Visser, K., & Breunese, J. N. (2015). Induced seismicity of the Groningen gas field: History and recent developments. *The Leading Edge*, *June*, 664–671. https://doi.org/10.1190/tle34060664.1

van Thienen-Visser, K., Roholl, J. A., van Kempen, B. M. M., & Muntendam-Bos, A. G. (2018). Categorizing seismic risk for the onshore gas fields in the Netherlands. Engineering Geology, 237, 198–207. https://doi.org/10.1016/j.enggeo.2018.02.004

van Wees, J. D., Orlic, B., Van Eijs, R., Zijl, W., Jongerius, P., Schreppers, G. J., Hendriks, M., & Cornu, T. (2003). Integrated 3D geomechanical modelling for deep subsurface deformation: A case study of tectonic and human-induced deformation in the eastern Netherlands. *Geological Society, London, Special Publications*, *212*(1), 313–328. https://doi.org/10.1144/GSL.SP.2003.212.01.21

Verdon, J. P., & Bommer, J. J. (2020). Green, yellow, red, or out of the blue? An assessment of Traffic Light Schemes to mitigate the impact of hydraulic fracturing-induced seismicity. Journal of Seismology. https://doi.org/10.1007/s10950-020-09966-9

Verdoes, A., & Boin, A. (2021). Earthquakes in Groningen: Organized Suppression of a Creeping Crisis. In A. Boin, M. Ekengren, & M. Rhinard (Eds.), Understanding the Creeping Crisis (pp. 149–164). Springer International Publishing. https://doi.org/10.1007/978-3-030-70692-0_9

Vlek, C. (2018). Induced Earthquakes from Long-Term Gas Extraction in Groningen, the Netherlands: Statistical Analysis and Prognosis for Acceptable-Risk Regulation: Induced Earthquakes from Long-Term Gas Extraction in Groningen. Risk Analysis, 38(7), 1455–1473. https://doi.org/10.1111/risa.12967

Vlek, C. (2019). Rise and reduction of induced earthquakes in the Groningen gas field, 1991–2018: Statistical trends, social impacts, and policy change. Environmental Earth Sciences, 78(3), 59. https://doi.org/10.1007/s12665-019-8051-4

Walsh, F. R., & Zoback, M. D. (2016). Probabilistic assessment of potential fault slip related to injection-induced earthquakes: Application to north-central Oklahoma, USA. Geology, 44(12), 991–994. https://doi.org/10.1130/G38275.1

Walsh, F. R. I., Zoback, M. D., Pais, D., Weingartern, M., & Tyrell, T. (2017). FSP 1.0: A program for probabilistic estimation of fault slip potential resulting from fluid injection. User Guide from the Stanford Center for Induced and Triggered Seismicity.

Walter, J. I., Frohlich, C., & Borgfeldt, T. (2018). Natural and Induced Seismicity in the Texas and Oklahoma Panhandles. *Seismological Research Letters*, *89*(6), 2437–2446. https://doi.org/10.1785/0220180105

Walters, R. J., Zoback, M. D., Baker, J. W., & Beroza, G. C. (2015). Characterizing and Responding to Seismic Risk Associated with Earthquakes Potentially Triggered by Fluid Disposal and Hydraulic Fracturing. Seismological Research Letters, 86(4), 1110–1118. https://doi.org/10.1785/0220150048

Wang, C.-Y., & Manga, M. (2021). Earthquakes Influenced by Water. In C.-Y. Wang & M. Manga, *Water and Earthquakes* (pp. 61–82). Springer International Publishing. https://doi.org/10.1007/978-3-030-64308-9_4

Wang, L., Kwiatek, G., Rybacki, E., Bonnelye, A., Bohnhoff, M., & Dresen, G. (2020). Laboratory Study on Fluid-Induced Fault Slip Behavior: The Role of Fluid Pressurization Rate. Geophysical Research Letters, 47(6). https://doi.org/10.1029/2019GL086627

Wang, B., Kao, H., Dokht, R. M. H., Visser, R., & Yu, H. (2022). Delineating the Controlling Factors of Hydraulic Fracturing-Induced Seismicity in the Northern Montney Play, Northeastern British Columbia, Canada, With Machine Learning. Seismological Research Letters, 93(5), 2439–2450. https://doi.org/10.1785/0220220075

Wang, R., Gu, Y. J., Schultz, R., & Chen, Y. (2018). Faults and Non-Double-Couple Components for Induced Earthquakes. *Geophysical Research Letters*, *45*(17), 8966–8975. https://doi.org/10.1029/2018GL079027

Weatherill, G., Kotha, S. R., & Cotton, F. (2020). Re-thinking site amplification in regional seismic risk assessment. Earthquake Spectra, 36, 274–297. https://doi.org/10.1177/8755293019899956

Weatherill, G. (2022). Esrm20_sitemodel. https://gitlab.seismo.ethz.ch/efehr/esrm20_sitemodel

Weatherill, G., Crowley, H., Roullé, A., Tourlière, B., Lemoine, A., Gracianne, C., Kotha, S. R., & Cotton, F. (2023). Modelling site response at regional scale for the 2020 European Seismic Risk Model (ESRM20). Bulletin of Earthquake Engineering, 21(2), 665–714. https://doi.org/10.1007/s10518-022-01526-5

Westaway, R. (2020). *Seismicity at Newdigate, Surrey, during 2018-2019: A candidate mechanism indicating causation by nearby oil production* [Preprint]. Geophysics. https://doi.org/10.1002/essoar.10502953.1

Wetmiller, R. J. (1986). Earthquakes near Rocky Mountain House, Alberta, and their relationship to gas production facilities. *Canadian Journal of Earth Sciences*, *23*(2), 172–181. https://doi.org/10.1139/e86-020

Wetzler, N., Shalev, E., Göbel, T., Amelung, F., Kurzon, I., Lyakhovsky, V., & Brodsky, E. E. (2019). Earthquake Swarms Triggered by Groundwater Extraction Near the Dead Sea Fault. *Geophysical Research Letters*, *46*(14), 8056–8063. https://doi.org/10.1029/2019GL083491

Wiemer, S., Kraft, T., & Landtwing, D. (2015). Seismic Risk (p. 38 p.) [Application/pdf]. ETH Zurich. https://doi.org/10.3929/ETHZ-B-000254177

Wiemer, S., Kraft, T., Trutnevyte, E., & Philippe, R. (2017). "Good Practice" Guide for Managing Induced Seismicity in Deep Geothermal Energy Projects in Switzerland.

Willacy, C., Van Dedem, E., Minisini, S., Li, J., Blokland, J.-W., Das, I., & Droujinine, A. (2019). Full-waveform event location and moment tensor inversion for induced seismicity. *GEOPHYSICS*, *84*(2), KS39–KS57. https://doi.org/10.1190/geo2018-0212.1

Wilson, M. P., Davies, R. J., Foulger, G. R., Julian, B. R., Styles, P., Gluyas, J. G., & Almond, S. (2015). Anthropogenic earthquakes in the UK: A national baseline prior to shale exploitation. *Marine and Petroleum Geology*, *68*, 1–17. https://doi.org/10.1016/j.marpetgeo.2015.08.023

White, J. A., & Foxall, W. (2016). Assessing induced seismicity risk at CO2 storage projects: Recent progress and remaining challenges. International Journal of Greenhouse Gas Control, 49, 413–424. https://doi.org/10.1016/j.ijggc.2016.03.021

Wilson, M. P., Foulger, G. R., Gluyas, J. G., Davies, R. J., & Julian, B. R. (2017). HiQuake: The Human-Induced Earthquake Database. Seismological Research Letters, 88(6), 1560–1565. https://doi.org/10.1785/0220170112

Wiprut, D., & Zoback, M. D. (2000). Fault reactivation and fluid flow along a previously dormant normal fault in the northern North Sea. *Geology*, *28*(7), 595. https://doi.org/10.1130/0091-7613(2000)28<595:FRAFFA>2.0.CO;2

Woessner, J., Laurentiu, D., Giardini, D., Crowley, H., Cotton, F., Grünthal, G., Valensise, G., Arvidsson, R., Basili, R., Demircioglu, M. B., Hiemer, S., Meletti, C., Musson, R. W., Rovida, A. N., Sesetyan, K., Stucchi, M., & The SHARE Consortium. (2015). The 2013 European Seismic Hazard Model: Key components and results. *Bulletin of Earthquake Engineering*, *13*(12), 3553–3596. https://doi.org/10.1007/s10518-015-9795-1

Wood, H. O., & Neumann, F. (1931). Modified Mercalli intensity scale of 1931. Bulletin of the Seismological Society of America, 21(4), 277-283.

Wozniakowska, P., & Eaton, D. W. (2020). Machine Learning-Based Analysis of Geological Susceptibility to Induced Seismicity in the Montney Formation, Canada. Geophysical Research Letters, 47(22). https://doi.org/10.1029/2020GL089651

Yeck, W. L., Hayes, G. P., McNamara, D. E., Rubinstein, J. L., Barnhart, W. D., Earle, P. S., & Benz, H. M. (2017). Oklahoma experiences largest earthquake during ongoing regional wastewater injection hazard mitigation efforts. Geophysical Research Letters, 44(2), 711–717. https://doi.org/10.1002/2016GL071685

Yerkes, R. F., & Castle, R. O. (1976). *Seismicity and faulting attributable to fluid extraction*. 17.

You, T., Wang, W., Chen, Y., & Tesfamariam, S. (2022). Gaussian random field based correlation model of building seismic performance for regional loss assessment. Soil Dynamics and Earthquake Engineering, 162, 107501. https://doi.org/10.1016/j.soildyn.2022.107501

Zalachoris G and Rathje EM (2019). Ground motion model for small-to-moderate earthquakes in Texas, Oklahoma, and Kansas. Earthquake Spectra 35(1): 1–20.

Zang, A., Yoon, J. S., Stephansson, O., & Heidbach, O. (2013). Fatigue hydraulic fracturing by cyclic reservoir treatment enhances permeability and reduces induced seismicity. Geophysical Journal International, 195(2), 1282–1287. https://doi.org/10.1093/gji/ggt301

Zbinden, D., Rinaldi, A. P., Urpi, L., & Wiemer, S. (2017). On the physics-based processes behind production-induced seismicity in natural gas fields. Journal of Geophysical Research: Solid Earth, 122(5), 3792–3812. https://doi.org/10.1002/2017JB014003

Zhang, H., Sarkar, S., Toksöz, M. N., Kuleli, H. S., & Al-Kindy, F. (2009). Passive seismic tomography using induced seismicity at a petroleum field in Oman. *GEOPHYSICS*, *74*(6), WCB57–WCB69. https://doi.org/10.1190/1.3253059

Zhang, Y., Fung, J. F., Johnson, K. J., & Sattar, S. (2022). Review of Seismic Risk Mitigation Policies in Earthquake-Prone Countries: Lessons for Earthquake Resilience in the United States. Journal of Earthquake Engineering, 26(12), 6208–6235. https://doi.org/10.1080/13632469.2021.1911889

Zhou, P., Yang, H., Wang, B., & Zhuang, J. (2019). Seismological Investigations of Induced Earthquakes Near the Hutubi Underground Gas Storage Facility. *Journal of Geophysical Research: Solid Earth*, *124*(8), 8753–8770. https://doi.org/10.1029/2019JB017360

Zhu, S., Feng, C., Xing, L., Ren, Y., Qi, B., Zhang, P., & Tan, C. (2022). Changes in Fault Slip Potential Due to Water Injection in the Rongcheng Deep Geothermal Reservoir, Xiong'an New Area, North China. Water, 14(3), 410. https://doi.org/10.3390/w14030410

Zhu, C., Pilz, M., & Cotton, F. (2020). Evaluation of a novel application of earthquake HVSR in site-specific amplification estimation. Soil Dynamics and Earthquake Engineering, 139, 106301. https://doi.org/10.1016/j.soildyn.2020.106301

Zoback, M. D., & Zinke, J. C. (2002). Production-induced Normal Faulting in the Valhall and Ekofisk Oil Fields. In C. I. Trifu (Ed.), *The Mechanism of Induced Seismicity* (pp. 403–420). Birkhäuser Basel. https://doi.org/10.1007/978-3-0348-8179-1_17

Zoback, M. D. (2012). Managing the Seismic Risk Posed by Wastewater Disposal.

Zöller, G., & Hainzl, S. (2022). Seismicity Scenarios for the Remaining Operating Period of the Gas Field in Groningen, Netherlands. Seismological Society of America, 94(2A), 805-812. doi: 10.1785/0220220308

7 External reviews

We benefitted three external reviews from three experts with background either in the private sector (oil and gas industry), or in regulatory/policy frameworks, or in both. They reviewed an earlier version of this report and provided their written feedback which we have incorporated in the final version. Their comments, together with our brief responses, are listed below.

7.1 External review #1

Dr. Shawn Maxwell [Geophysical and Geomechanical Advisor at Ovintiv]:

The report is a comprehensive analysis of relevant publications and includes a critical review of current protocols as implemented by the Dutch State Supervision of Mines. Recommendations are provided intended to improve the science-based protocols using additional research publications.

Generally, the report is well written with a logical format. However, the work uses numerous acronyms which are often undefined and so should include a glossary. One underlying issue that stands out with the numerous publications that are reviewed and cited in the report, is that it is often unclear what statements relate to the actual publication versus editorial opinions of the authors. It is obviously important to distinguish what are finding and conclusions in a particular publication from any editorial commentary.

In a few places through the document, there are holding places obviously intended for inclusion of additional material and references.

The following provides specific comments on various sections of the report.

- Section 2.

Section 2 begins with an extensive literature review of global cases of hydrocarbon production induced seismicity, along with additional cases which may have a combined mechanism associated with simultaneous injection. While the review is a very helpful summary of extensive research database representing an exhaustive literature search, it contains a lot of detailed information and not always clear how it relates to the Dutch production issue. I would recommend focusing the case studies to the Netherlands and immediate surrounding areas and move the remaining sections (2.1.5 onwards) to an Appendix. A table could be included in the main body of the text summarizing the case studies and tabulating key observations such as maximum observed magnitude.

The report would also benefit from a more extensive discussion of mechanism of production induced seismicity and perhaps a cartoon depiction of mechanisms that could be compiled using the Groningen example.

The case study review tends to cite examples as being quiet or aseismic at various points in the report, without providing details of the minimum detectable magnitude. Since quiescence will in many cases be controlled by monitoring sensitivity, this context is important to the discussion. In section 2.1.2, for example, it is stated that "38 or 450 gas fields are now associated with induced seismicity" but it is important with such a statement to clarify the associated magnitude basis. Another example of the importance of

seismic sensitivity is the Clinton County, Kentucky USA example which describes essential a microseismic monitoring (Mw<1) in contrast to other cases.

The authors cite a relatively large number of Texas cases, in context of the rest of the section. Perhaps the authors have been more rigorous in the case of Texas or leveraged material from previous reviews? It would be helpful to the reader to clarify if the number of cases have some sort of review bias or if indeed relatively more cases are readily available through internet searches.

Finally, perhaps the Castor example should be included for completeness. While the case could well be classified as injection induced, the proximity to the Netherlands and associated with a depleted reservoir would appear comparable to other examples cited in the report.

- Section 3.

The review of guidelines for induced seismicity risk assessment, comprehensively covers key elements. However, it would be helpful for the reader to insert some of the material currently covered in section 5 (or perhaps a high level summary of detailed discussion of the current Dutch protocol discussed in section 5) prior to a more general discussion of induced seismicity risk. There are several aspects of risk discussion that could more pointedly describe implications to the Dutch protocol and provide critical contrasts with other protocols.

Regarding the discussion of "traffic light system" (TLS) it would be helpful to provide context of the role of TLS and monitoring in relation to the interplay with the screening and risk assessment steps. More generally, the section would benefit from a critical discussion of seismic monitoring performance aspects for induced seismicity (magnitude of completeness, hypocentral accuracy). The role of monitoring to calibrate and ground truth risk assessments is an important aspect that does not stand out currently in Section 3. The role of TLS in protocols and risk management could be more directly described along with the importance of a robust monitoring framework. One specific editorial comment related to the bottom of page 20 describing research associated with "properly defining" thresholds but should consider rewording and perhaps using the term rigorously defining.

In terms of section 3.4 and real-time monitoring it would be helpful to also describe the need for timely operational data.

Section 3.6 covering mitigation would be helpful to separately described scenarios for injection from extraction, the mechanisms and operational considerations are obviously significantly different.

- Section 4

The discussion of geomechanical models in section 4.2.1. covers several diverse studies including various methods from finite element simulations of deformation to analytically solutions to statistical methods associated with seismicity catalogs to investigate causation. The section is part of a section on Seismicity Rates and hence is likely intended to describe a variety of techniques that attempt to investigate such. It would be helpful if the scope of the review were explained, specifically targeting what operational scenarios

and how it ties to induced seismicity protocols. A critical review of advantages and limitations of the various techniques would be helpful at the start. Part way through the section there is a detailed discussion of Groningen and a review paper by Kuhn, which could be moved to the start of the section and used to introduce the range of techniques and discuss the more general requirements for the Dutch protocols.

The remainder of the section provides a useful and comprehensive discussions of other aspects of hazard and risk assessments.

- Sections 5 and 6

Details of the current Dutch protocol as described in Section 5 is obviously key to the report objectives and would benefit with being introduced much earlier in the document. The discussion includes both a description and in the text is interlaced with a critique of various points. It would be helpful in Figure 12, to define the classifications of I, II and III as shown.

Throughout the document, the authors focus on aspects of the hazard and risk assessment. However, the seismic monitoring details are also clearly an important aspect but are not critically reviewed. Perhaps the topic is outside the scope of the report, but it would seem prudent to discuss in the document. On page 48 with the discussion of magnitude of completeness requirements depending on the classification level. It would be helpful to critically discuss these, particularly in terms of the recommended protocol changes. For example, would a lower magnitude of completeness be beneficial to probably estimates of various magnitudes above Mmin and is there a requirement to have some practical monitoring level below Mmin. It would also seem that monitoring could help calibrate or ground truth assumptions associated with the hazard assessments and ground motion models.

The three recommended changes to Step 1 screening potential appear sound. However, it is unclear what the process would be, for example it should be clarified if the authors are proposing a follow-up project to evaluate various machine learning options and customize an approach for an improved screening system. Apparently, there are numerous current fields where the seismicity state is known and as the authors point out there are numerous performance metrics that could be assessed and compared to current observations. Similarly, the details of the input data and associated uncertainties could be further explored. Perhaps a 'roadmap' of implementing the proposed changes would be useful including a conceptual statement of the revised screening tool functionality in context of the skill set of the intended users.

The proposed changes to Step 2 of the process appear sound. The suggestion appears to incorporate the most recent data available and leveraging the previous work on Groningen ground motion is pragmatic as discussed by the authors. Additional discussion could be included describing potential issues associated with a broader application of Groningen and particularly how it could be assessed if monitoring data is available. As previously discussed, I recommend including a discussion of seismic monitoring and in this part of the report specifically in context of potentially validating or recalibrating the Groningen model.

Finally, the authors' suggestion of precomputed risk tables that could be used to populate risk tables with different magnitude scenarios appears technically sound. The authors claim that the location of gas

fields has already been identified, but scenarios could likely be encountered pushing the spatial extents of known fields, finding new fields or generalizing the approach to other activities. Furthermore, ground motion data could be recorded in the future that would require an update to risk tables. It would seem important that such contingency scenarios be considered to ensure reproducibility of consistent results in the future.

In conclusion, the report is a comprehensive review of relevant information and sound technical recommendations to improve aspects of the current protocol. Suggestions have been made to improve the format of the report and relatively minor technical aspects of the proposed protocol changes. Whatever pre-screening recommendations the authors make, and the Dutch State Supervision of Mines ultimately implement, the probabilistic forecasting will not be perfect and susceptible to both missed cases and false positives. Therefore, it is critical that the actual seismic performance of these fields be closely monitored and timely actions taken dependent on the risk tolerance for induced seismicity at the discretion and accountability of the operators and regulators. The comments and suggestions of this review are not meant to comment on the effectiveness or accuracy of the screening process itself or any implied responsibility associated with the implementation.

Authors' response:

We greatly appreciate Dr. Maxwell's constructive feedback on an earlier version of the current report. We are glad to hear that "the report is a comprehensive review of relevant information and [includes] sound technical recommendations to improve aspects of the current protocol". Below we clarify a few points that were raised by the external reviewer.

- There were indeed a few instances where the exact citation for a study was missing. This issue has been resolved now.
- Information from section 2 is used in section 4.2.2 and helped us have a broad understanding of the triggering mechanisms, aiding sections 5.1, 5.2 and 6.1
- It is true that high M_c might mask some seismicity in the field we list in the literature review. We have added a sentence to reflect that now.
- We believe that we cite a relatively large number of cases from Texas because this area is better covered by the scientific and historical records, not because we are more familiar with that part of the world.
- Now monitoring requirements are an essential part of the proposed TLS (risk management plan)
- We have now rearranged section 4.2.1
- The cited references at the end of section 3.4 [e.g. Templeton et al., 2021] include a lot of details for the monitoring requirements, both in terms of instrumentation and data-availability.
- In section 3.6, we have now clarified which mitigation measures apply to fluid extraction.

- The minimum value of M_1 is the M_c (section 6.2.1), so the operators are incentivized to lower M_c as much as possible.
- The caption of Figure 12 has been now updated.
- Yes, we envision that SoDM will commission a follow-up project that will conduct quantitative studies based on our recommendations and eventually provide implementation details for a revised protocol.
- This report is focused more on the protocol used for the permitting process and less so on the protocol used during the production-phase (because the latter is very loosely defined in the current guidelines). That said, now in section 6.3 we do propose a new "risk management plan" and there we have now added more information regarding the M_c and the uncertainty behind the magnitude solutions.
- We agree that the risk tables might require updates if new fields are found (or existing ones are extended) and if new strong-motion data become available. We added that to the text now.

7.1 External review #2

Anonymous:

My comments come from the perspective as a scientist that works for a regulator, plus some direct comments on the seismology of the problems proposed.

- General Comments

This is a very well written report. The literature review is outstanding and forms the basis of the recommendations. The literature review illustrates the challenges faced with regulating for induced earthquakes that have yet to occur but are based on past events. Furthermore, as stated in the report, recent literature has focused on the role of water injection for induced seismicity. Regardless, the literature review and the proposed recommendations are based on what is currently know and is likely to change in the future. I can appreciate having to form policy based on imperfect information. This report does well to point out the current state of knowledge and to propose changes to the current system. I will point out a few points that the author may consider for this report. My comments are suggestions based on my experience and knowledge; there is no correct answer.

You might consider mechanisms for industry involvement in sharing information with the regulating agency, academics, and other industry members, even creating operator teams. This model, although not ideal, has provided a change in the culture of sharing in the state of Texas, and is termed Operator-Led Response Plan (ORLP) (https://www.rrc.texas.gov/oil-and-gas/applications-and-permits/injection-storage-permits/oil-and-gas-waste-disposal/injection-disposal-permit-procedures/seismicity-review/seismicity-response/). In the state of Texas, we struggle to get information from industry, but have found this mechanism to work well to get companies to share information. We have a carrot/stick approach for this. We propose strict regulations based on the information that we have, and encourage industry to "prove us wrong" by providing information, to be shared with other industry working in the impact region.

Another aspect that many studies fail to address is the nature of changing injection/extraction that occurs in an active reservoir. A maximum magnitude estimation can be completely off given the changing conditions of faults in response to fluctuation in operations. The level of regulation required to monitor these changes may be virtually impossible to achieve. The framework proposed need to consider these changing conditions, especially in regards to maximum magnitudes.

One of the challenges is to make sure that a response to induced seismicity can be standardized, yet, remain flexible enough such that experts can modify given the situation. I know that the point here is to automate as much as possible, however, there may be a situation not quite with a scenario, and experts should weight in heavily. The framework needs to incorporate expert opinion and have points of entry for this to occur. For example, in Texas, the state seismology only reviews permits that are high risk, or warrant special consideration. This allows the automation to move forward for lower risk wells. In my opinion,

experts should be reviewing the response when warranted (higher than expect event magnitudes; changing seismicity rates; improved monitoring, etc.)

There is a substantial need to continue to research mechanisms because of extraction of natural gas. There are many times the report highlights some of these outstanding research questions. I suggest placing these questions in a table, and having the report serve as a foundation for a research plan.

Finally, I cannot emphasize enough that all of these recommendations work on the assumption of a stable and robust seismic network. This is foundational, and improvements in the network can improve the understanding of these gas fields.

I am not going to provide comments for each section, as some of this is out of my expertise. I am providing comments that I hope are helpful to focus the report such that a regulator can implement immediately. In the end, I support all of the recommendations proposed, and provide these comments for consideration for improvement and clarification.

- Specific Comments

- Broken link- Geological Survey of the Netherlands (GDN; https://www.dinoloket.nl/en/subsurface- models)
- Missing Ref: Simpson & Leith [1984], Hicks et al., 2021
- Page 17: Pre-screening of anticipated hazards/risks: Might be good to have an illustration of this approach (risk/likelihood).
- Page 56, bottom of page: "Finally, a recent study by _____ concluded that industrial facilities and critical infrastructure in the country can sustain moderate earthquakes of magnitude around 5, a level that we do not expect to be exceeded under normal circumstances in any of the small gas fields. Similar conclusions have been drawn for the dikes (_____)." . Needs reference.
- Page 60: "Studies should explore alternative models, using performance metrics to both assess validity and quantify improvements." "For similar reasons, the epicentral uncertainty behind the earthquake solutions might be much larger than currently foreseen (3km), something that should be also taken into account in an explicit way. Furthermore, the classification data is biased temporally, in the sense that events above the M_c will only be recorded after sufficient reservoir changes have occurred. ". The ugly truth about seismology is that earthquake location depends mainly on your station coverage. Even with a decent network and what appears to be small, the depth determination trades off with origin time. Depth can be off significantly due to model uncertainties, and you need to have a station within a focal depth to have a chance at getting at this number. As also mentioned, these uncertainties change as a result of a changing seismic network. This dictates that regular updates need to be made on any system assessing hazard/risk.
- Page 61 "For the lower bound, M_1 is defined as the largest observed magnitude thus far. To be on the conservative side, if no magnitudes above Mc have been recorded around the field, then M_1 is set equal to M_c." "Assuming a binning of 0.1 for the range of magnitudes…". Magnitudes are even

more uncertain than the depth of an earthquake. This is the result of different geology at different seismic stations that can result in significant variation of magnitude at each location. It is not uncommon to have a 0.5 difference in magnitude estimation at different stations for each event. This highlights the need to incorporate errors in the complete framework.

Authors' response:

We thank the anonymous reviewer for reviewing our work. We are glad to hear that "this report does well to point out the current state of knowledge and to propose changes to the current system". Below we clarify a few points that were raised by the external reviewer.

- It is true that in some cases found in the literature some of the wells in the producing field are injecting fluids to aid the extraction process. We did not have data to confirm this for the small onshore Dutch gas fields we were focusing on. Our guidelines assume that any generated seismicity is only linked to fluid-extraction and that injection volumes are either negligible or preferably zero. We have now stated that in section 6.
- Our framework does incorporate points of entry for expert opinion given that if a field is labelled as Category III, then Step 3 becomes mandatory. Step 3 employs a detailed (yet purposefully loosely defined) quantitative risk analysis conducted by experts.
- The GDN broken web-link has been now fixed.
- There are no missing references anymore.
- Although accurate depths can be difficult to obtain, this is not a huge issue for the production-only fields in the Netherlands, given that the depth of the reservoir bounds is well known and seismicity is expected to occur only within those constraints. Depth becomes more important if there are overlapping injection activities within the field, something that is outside the scope of this report.
- We agree with the reviewer that the uncertainty behind magnitude solutions can be significant. Now in sections 6.2.1 and 6.3 we have accounted for this uncertainty in an explicit way.

7.3 External review #3

Dr. Gunter Siddiqi [conim ag]:

I found the report extremely interesting and informative, and I thoroughly enjoyed reading and thinking about it. Allow me to make a few summary comments that capture a large part of my detailed comments.

(1) It is my opinion that you should explain your preferred regulatory approach to the reader of the report. I have sketched an introductory passage in chapter 3 where I suggest an approach to outlining your preferred approach to regulations. Regulations might span a spectrum from prescriptive to performance-based on the one hand, and from deterministic to probabilistic on the other hand. I have indicated in my textual comments, particularly in chapter 3-5, passages of your text where I have interpreted a strong penchant for a prescriptive approach to regulations. If you identified your preferred style of regulation, the reader would very much understand, for example, a number of your passages that I have commented on in the document itself. Some of the passages include not only fact-based arguments but also judgements that are not supported by references to scientific facts.

(2) I suggest that you emphasize the point that a number of your recommendations derive from recent research and innovation – a substantial amount of which has not been tried and tested yet in an operational environment. In my experience, the arrival at scientific and technological consensus regarding the effectiveness and utility of new technologies, processes and procedures is a lengthy process which requires a lot of testing and verification between origination of ideas and routine application in the field. Once there is ample field observational evidence that new or modified processes, technologies, procedures etc. work, then comes the time to adjust industry standards that will be subsequently subject of regulatory scrutiny and rule-setting.

(3) Along those lines, I suggest that you explicitly state that have you not provided an analysis of the effectiveness and outcomes of the existing Dutch (binding) guideline (DHAIS); you are undoubtedly aware of the cost-benefit analysis of regulations that need to be undertaken. Recommendations are particularly welcome if – to give a few examples – regulations have proven to be ineffective, desired outcomes not achieved, costly to the extent that industry has scaled back or withdrawn, or if regulations pose significant difficulties to be implemented. As you are undoubtedly keenly aware, proposed changes to regulations trigger intricate processes where all parties involved have to discuss and ultimately agree on proposed changes.

(4) I also suggest that you acknowledge very clearly that you have not consulted industry or industrial practices when it comes to managing induced seismicity. In my professional experience, policies and practices of highly performing companies view regulatory guidance as a "minimum" to be complied with and that actual procedures and processes are significantly more sophisticated than what regulators expect.

(5) I very much appreciate the long list of interesting case studies that you have provided. I could not help, however, wonder about the relevance to the problem at hand. I have suggested a minimalistic approach to addressing the relevance at the outset of chapter 2. This chapter would benefit greatly from a summary of kinematic and dynamic features of the small natural gas fields in The Netherlands; features that makes them susceptible to induced seismicity (e.g. fault architecture, fault rheology, initial pressures in natural gas bearing formations, information regarding the state of stress and its inhomogeneity, ...). I have also mentioned a number of references that might be useful to bridge the gap between relevance of the case studies that you cite and their applicability/relevance to small Dutch natural gas field. The subsequent case studies would then benefit from additional sentences that describe the relevance of a case study to Dutch small natural gas fields in terms of geological and operational hazards that have caused unwanted earthquakes.

(6) Overall, I see the merit of your recommendations. I suggest, however, that you improve the quality of the justification by drawing much more explicitly on chapters 3 and, particularly 4 as well as basing your justification on scientific facts alone. Again, I have provided ample comments in the text to this effect.

Authors' response:

We thank the reviewer for reviewing our work. Below we clarify a few points.

- We were tasked with critically reviewing the existing regulatory protocol, and in particular with rendering it more quantitative and up-to-date with the latest scientific literature. We do not consider the proposed changes materially less or more prescriptive than the existing protocol. The proposed changes simply enable the protocol to be more data-driven and in line with the state-of-knowledge.
- We were assigned this task because of our expertise in the topic under investigation. For transparency reasons, we always aimed at citing all relevant literature, regardless of it being in line with our expert-opinions or not. Given that the topics under review were often at the cutting edge of scientific research, well-established methods and opinions were not always available to us. In those infrequent cases, we had both the expertise and the assigned discretion to express our own well-informed opinions and recommendations.
- We were tasked with critically reviewing the existing regulatory protocol because it was deemed to be likely outdated and not rigorous enough given the latest quantitative trends. We made great efforts in greatly reducing the added cost of our recommendations (section 6.2.7). We believe that the operators will face negligible additional costs when it comes to the permitting phase and minimal additional costs when it comes to the monitoring phase. The proposed increased computational costs to aid the permitting phase will burden only the regulator and are essentially a one-off non-recurring relatively low-level expense. In any case, these costs are extremely small

when compared to both the value of the extracted energy and the potential mitigated economic losses.

- We purposefully targeted people from the industry as external reviewers to gather feedback decoupled from the academic domain.